JAERI-M
90-171

NEANDC (J)-154/U
INDC (JPN)-140/L

MEASUREMENT OF FORMATION CROSS SECTIONS OF SHORT-LIVED NUCLEI BY 14 MEV NEUTRONS

—Mg, Si, S, Cl, Cr, Zn, Ga, Y, In—

October 1990

Kiyoshi KAWADE*, Hiroshi YAMAMOTO*, Takashi YAMADA*
Toshio KATOH*, Toshiyuki IIDA** and
Akito TAKAHASHI**

日本原子力研究所
Japan Atomic Energy Research Institute

JAERI-Mレポートは，日本原子力研究所が不定期に公刊している研究報告書です。
入手の問合わせは，日本原子力研究所技術情報部情報資料課（〒319-11茨城県那珂郡東海村）あて，お申しこしください。なお，このほかに財団法人原子力弘済会資料センター（〒319-11 茨城県那珂郡東海村日本原子力研究所内）で複写による実費頒布をおこなっております。

JAERI-M reports are issued irregularly.
Inquiries about availability of the reports should be addressed to Information Division Department of Technical Information, Japan Atomic Energy Research Institute, Tokai-mura, Naka-gun, Ibaraki-ken 319-11, Japan.

編集兼発行　日本原子力研究所
印　　刷　いばらき印刷㈱

JAERI-M 90-171

Measurement of Formation Cross Sections of Short-lived Nuclei by 14 MeV Neutrons - Mg, Si, S, Cl, Cr, Zn, Ga, Y, In -

Kiyoshi KAWADE*, Hiroshi YAMAMOTO*, Takashi YAMADA*, Toshio KATOH*
Toshiyuki IIDA** and Akito TAKAHASHI**

Department of Physics
Tokai Research Establishment
Japan Atomic Energy Research Institute
Tokai-mura, Naka-gun, Ibaraki-ken

(Received September 7, 1990)

Sixteen neutron activation cross sections for (n,2n), (n,p), (n,n'p), (n,t) and (n,α) reactions producing short-lived nuclei with half-lives between 0.5 and 20 m have been measured in the energy range of 13.4 to 14.9 MeV for Mg, Si, S, Cl, Cr, Zn, Ga, Y and In.

Five half-lives of short-lived nuclei produced by 14 MeV or thermal neutron bombardments were measured with Ge detectors for ^{66}Cu, ^{89m}Zr, ^{91m}Mo, ^{97m}Nb and ^{104m}Rh in the spectrum multi-scaling mode.

Keywords: Activation, Cross Section, 14 MeV Neutron, Short-lived Nucleus, Half-life, Measurement, Ge-detector

---

This work was performed under the contract between Japan Atomic Energy Research Institute and Nagoya University.

* Nagoya University

** Osaka University

JAERI－M 90－171

短寿命核生成断面積の測定－Mg, Si, S, Cl, Cr, Zn, Ga, Y, In－

日本原子力研究所東海研究所物理部
河出　清*・山本　洋*・山田　隆志*
加藤　敏郎*・飯田　敏行**・高橋　亮人**

（1990年9月7日受理）

半減期が0.5分から20分程度の短寿命核生成断面積の測定を，中性子エネルギー13.4から14.9 MeVの範囲にわたり，Mg, Si, S, Cl, Cr, Zn, Ga, Y, In試料に対し（n, 2n），（n, p），（n, n′p），（n, t），（n, α）反応，16断面積を測定した。

14 MeVまたは熱中性子照射で生成される短寿命核の半減期の測定を，^{66}Cu, ^{89m}Zr, ^{91m}Mo, ^{97m}Nb, ^{104m}Rhの5核種について，Ge検出器を用いてスペクトルマルチスケーリングモードで行なった。

本報告書は，日本原子力研究所が名古屋大学に委託して行なった研究の成果である。

東海研究所：〒319－11　茨城県那珂郡東海村白方字白根2－4
* 名古屋大学
** 大阪大学

Contents

目　　次

1. Introduction

Neutron activation cross section data around 14 MeV have become important from the viewpoint of fusion reactor technology, especially for calculations on radiation damage, nuclear transmutation, induced activity and so on. A lot of experimental data have been reported and great efforts have been given to compilations and evaluations, but there are often unexplained inconsistencies among the existing experimental data.

Recently activation cross sections have been measured systematically and in good accuracy for 110 reactions on 26 elements by Ikeda et al.[1] to provide more reliable data. However, formation cross sections of short-lived nuclei have often not been measured in a reasonable accuracy or there are no available data on some reactions, because of difficulty in measuring short-lived nuclei. In the present work, 16 cross sections for the (n,2n), (n,p), (n,n'p), (n,t) and (n,α) reactions leading to short-lived nuclei with half-lives between 0.5 and 20 m were measured at neutron energies of 13.4 to 14.9 MeV by the activation method.

The half-life is one of the most fundamental constants of the radioactive isotopes. In the activation cross section measurements, the uncertainty of the half-life brings a strong effect on the results. Five half-lives of short-lived nuclei were measured with Ge detectors in the spectrum multi-scaling mode. Measured reactions and half-lives are shown in Table 1 and Table 2, respectively.

2. Measurement of Activation Cross Sections

2.1 Experimental

2.1.1 Neutron irradiation and fluence monitoring

The d-T neutrons were generated by an intense 14 MeV neutron source facility (OKTAVIAN) at Osaka University. Incident d^+ beam energy and intensity were 300 keV and about 5 mA, respectively. A pneumatic sample transport system was used for the irradiation of samples. Transfer time was about 2 s. The angle of the irradiation position to the d^+ beam were 0°, 45°, 75°, 95°, 120° and 155°, which covered the neutron energies ranging from 14.9 to 13.4 MeV. Another pneumatic tube was also set at -95° to examine the arrangement of the pneumatic tubes. The distance

1. Introduction

Neutron activation cross section data around 14 MeV have become important from the viewpoint of fusion reactor technology, especially for calculations on radiation damage, nuclear transmutation, induced activity and so on. A lot of experimental data have been reported and great efforts have been given to compilations and evaluations, but there are often unexplained inconsistencies among the existing experimental data.

Recently activation cross sections have been measured systematically and in good accuracy for 110 reactions on 26 elements by Ikeda et al.[1] to provide more reliable data. However, formation cross sections of short-lived nuclei have often not been measured in a reasonable accuracy or there are no available data on some reactions, because of difficulty in measuring short-lived nuclei. In the present work, 16 cross sections for the (n,2n), (n,p), (n,n'p), (n,t) and (n,α) reactions leading to short-lived nuclei with half-lives between 0.5 and 20 m were measured at neutron energies of 13.4 to 14.9 MeV by the activation method.

The half-life is one of the most fundamental constants of the radioactive isotopes. In the activation cross section measurements, the uncertainty of the half-life brings a strong effect on the results. Five half-lives of short-lived nuclei were measured with Ge detectors in the spectrum multi-scaling mode. Measured reactions and half-lives are shown in Table 1 and Table 2, respectively.

2. Measurement of Activation Cross Sections

2.1 Experimental

2.1.1 Neutron irradiation and fluence monitoring

The d-T neutrons were generated by an intense 14 MeV neutron source facility (OKTAVIAN) at Osaka University. Incident d^+ beam energy and intensity were 300 keV and about 5 mA, respectively. A pneumatic sample transport system was used for the irradiation of samples. Transfer time was about 2 s. The angle of the irradiation position to the d^+ beam were 0°, 45°, 75°, 95°, 120° and 155°, which covered the neutron energies ranging from 14.9 to 13.4 MeV. Another pneumatic tube was also set at -95° to examine the arrangement of the pneumatic tubes. The distance

between the T-target and the irradiation position was 15 cm. The typical neutron flux was about 5×10^7 n/cm^2•s at the irradiation position. The sample cartrige and the pneumatic sample transport system are shown in Fig. 1. When strongly induced activities are required, an additional tube set at 22.5° and at 5 cm from the neutron source was used. In Appendix 1, the neutron flux is shown as a function of T-target-to-sample distance.

The neutron flux at the sample position was measured with use of the $^{27}Al(n,p)^{27}Mg(T_{1/2}=9.46\ m)$ reaction, whose cross sections were determined by referring to the standard $^{27}Al(n,\alpha)^{24}Na$ reaction (ENDF/B-V).[2] The samples were sandwiched between two aluminum foils of 10 mm × 10 mm × 0.2 mm thick. The standard cross section of $^{27}Al(n,\alpha)$ is shown in Table 3. Good statistics for fluence monitoring could be achieved in reasonably short measuring time by using $^{27}Al(n,p)$ reaction instead of $^{27}Al(n,\alpha)$. The use of the (n,p) reaction brought an additional statistical uncertainty of 0.5% to final results.

The effective reaction energy of incident neutrons at each irradiation position was determined by the ratio of the $^{90}Zr(n,2n)^{89}Zr(3.27d)$[3] and $^{93}Nb(n,2n)^{92m}Nb(10.15d)$[4] cross sections (Zr/Nb method[5]). Since each position of the pneumatic tubes is mutually arranged in good accuracy, the effective d^+ energy was chosen as a fitting parameter in the relativistic calculation of d-T neutron energy. A fitting result obtained for E_d=130 keV is shown in Fig. 2. The uncertainty in the neutron energy is estimated to be ±50 keV.

Separated isotopes and samples of natural abundance were used. Foil samples were rectangular-shaped 10 mm×10 mm and 0.1~0.2 mm thick. Powder samples were wrapped in powder papers (each sample size : 10 mm×10 mm and about 1 mm thick, sample masses : 10~70 mg). The abundance of the separated isotopes and the purity of natural abundance samples used are shown in Table 4 and Table 5, respectively.

2.1.2 Activity measurement

Gamma-rays emitted from the irradiated sample and monitor aluminum foils were measured with 12% HpGe (1.75 keV FWHM at 1333 keV) and 16% HpGe (2.00 keV), respectively. Each detector was covered with a 5 mm thick acrylic absorber in order to reduce β-rays. The peak efficiency calibration at 5 cm was accomplished by using sources of ^{24}Na, ^{56}Co, ^{133}Ba, ^{152}Eu and ^{154}Eu. Corrections for true coincidence sums were

applied. The errors in the efficiency curves are estimated to be 1.5% above 300 keV, 3% between 300 and 80 keV, and 5% below 80 keV. The germanium detectors used are shown in Table 6. The full-energy-peak detection efficiency of the 12% Ge detector is shown in Fig. 3.

To measure efficiently the weakly induced activities, the samples were put on the absorber surface (source-to-detector distance is 5 mm). To convert the efficiency at 5 mm to the one at 5 cm, calibration measurements were carried out at both distances by using extra samples irradiated with rather strong neutron flux. The ratios of the efficiencies at 5 mm and 5 cm are shown in Fig. 4. Single γ-ray emitters (open circle) are on a smooth curve, while cascade γ-ray emitters (closed circle) are below the curve owing to a sum effect. This method improved the detection efficiency by a factor of about 7. This calibration procedure brought an additional error of 1.0% to the results.

Radial dependence of the detection efficiency of the off-axis distance on the absorber surface was examined by using a source of ^{85}Sr (514 keV). It was shown that an uncertainty of ± 0.3 mm in the sample position brought an error less than 0.3%.

The β^+ activities of radionuclides emitting almost no γ-rays were measured by detecting 511 keV annihilation γ-rays. The irradiated sample was set between two 10 mm thick acrylic plates. The efficiencies for the 511 keV γ-rays arising from annihilations in the acrylic plates were measured as a function of thickness of the rear acrylic plate. Beta-rays with energies less than about 3.4 MeV were fully stopped by the 10 mm thick plate. Effect of diffused annihilation positions of β^+ particles in the absorber on the detection efficiencies was observed to be negligible with an accuracy of 1.0%. Namely, the β^+ sources with maximum energies up to about 3.4 MeV can be regarded as 511 keV point γ sources, if the sources are set between two 10 mm thick acrylic plates.

Peak areas of γ-rays are evaluated by summing all recorded counts in the channel interval $\{C-3\sigma, C+3\sigma\}$ and subtracting the background counts (N_B), where C is the position of the peak center and σ is FWHM. N_B is given by $(6\sigma)\times(N_L+N_H)/2$, where N_L and N_H are the average count of 5 channels in the vicity of $C-3\sigma$ and that in the vicinity of $C+3\sigma$, respectively. This summing method is similar to that by Debertin and Schötzig[6]. The uncertainty from the peak area evaluation is estimated to be 0.5%.

2.1.3 Decay data

In Table 7, measured reactions and associated decay data[7] of the half-life ($T_{1/2}$), the γ-ray energy (E_γ), the absolute intensity in photons per disintegration (I_γ) are listed together with the Q values (MeV) and the fractional contribution of low energy neutrons (FC) discussed later.

2.1.4 Corrections

The following principle corrections in deducing cross sections were made :

1) fluctuation of the neutron flux,
2) fractional contribution of low energy neutrons,
3) sum effect,
4) thickness of sample,
5) self-absorption of γ-ray in the sample material,
6) interfering reaction.

Details of the corrections are given below.

(1) Fluctuation of the neutron flux

A multi-channel scaling measurement (MCS) was carried out at intervals of 3 s or 6 s with a fission counter to monitor the fluctuation of the neutron flux. As seen in Fig. 5, the corrections for activities with half-lives of about 10 m almost cancelled out, since the reaction of $^{27}Al(n,p)^{27}Mg$ ($T_{1/2}$=9.46 m) was used as the flux monitor.

(2) Fractional contribution of low energy neutrons

The incident neutron spectrum is not monoenergetic, but it shows low energy components below the d-T neutron peak owing to scattering as shown in Fig. 6. The spectrum was taken at 70° with respect to d^+ beam direction by two crystal method ($^{12}C(n,n')$ peak was removed in the spectrum).

To determine the cross sections around 14 MeV accurately, contributions of the low energy neutrons should be taken into account. Especially (n,p) or (n,α) cross sections are strongly affected, because such reactions have low Q values. A cut-off energy (E_c) was set on 10 MeV. The low-energy components were about 15%. The fractional contribution of low energy neutrons to total reaction rates (FC) was calculated by

$$FC = \sum_{E_i=0}^{E_c} \phi(E_i)\cdot\sigma(E_i) \Big/ \left\{ \sum_{E_i=0}^{E_c} \phi(E_i)\cdot\sigma(E_i) + \phi_x\cdot\phi_x \right\}$$

where $\phi(E_i)$ and ϕ_x are neutron flux at E_i and E_x, respectively and $\sigma(E_i)$ and σ_x are cross sections at E_i and E_x. Here we assumed that neutrons above E_c are nearly monoenergetic with an energy E_x. A correction factor (f_s) for the FC is given by

$$f_s = \{1-FC(n,x)\}/\{1-FC(n,\alpha)\} ,$$

where FC(n,x) and FC(n,α) are FCs for the (n,x) reaction of interest and the standard $^{27}Al(n,\alpha)^{24}Na$ reaction, respectively. The FCs were calculated by using excitation functions of JENDL-3[8] and Yamamuro's calculations.[9] The results are listed in Table 7 and are shown in Fig. 7 as a function of Q-values. The FCs are greatly scattered. Then they were plotted as a function of the slope of the excitation function at 14 MeV ($[\Delta\sigma/\Delta E)/\sigma]$ at 14 MeV) for the Q-values. They are reasonably on a smooth curve as seen in Fig. 8. Hence, this curve serves to estimate FC when the excitation function is not known.

(3) Sum effect

When activities decay by emitting γ-rays, true coincidence summing may happen. The total efficiency at 5 cm was measured by using calibrated sources of ^{54}Mn, ^{57}Co, ^{65}Zn and ^{137}Cs. The sum effect is still of order of 1 to 2%.

When counting rate is over 10^3 s^{-1}, pile-up losses due to random coincidence summing are not negligible. Since the counting rates are usually less than 10^3 s^{-1}, the corrections are small.

(4) Thickness of sample

When a sample has a thickness of t(mm), the correction factor (f_d) is given by

$$f_d = (4.90+0.5t+x_o)^2/(4.90+x_o)^2 ,$$

where 4.90 is the accurate thickness of the 5 mm thick absorber and x_o (mm) is an effective length[10] determined from the ratio of the efficiencies at 0.5 cm and 5 cm. Here, it is assumed that the detector efficiency is inversely proportional to the square of the distance. In Fig. 9 the effective interaction depth (x_o) for single-line nuclides is shown.

(5) Self-absorption of γ-ray in the sample material

Since the source-to-detector distance is 5 cm, and the thickness of the sample is usually less than 100 mg/cm^2, the one-dimensional treatment is reasonably accepted. The correction factor (f_a) is given by

$$f_a = 1/(1-0.5\rho\mu t)$$

where ρ is the density (g/cm^3) of the sample, t is the thickness (cm) of the sample and μ is the mass absorption coefficient (cm^2/g)[11].

(6) Interfering reaction

When the same activity is produced in the sample by two different reactions or more than two activities emitting γ-rays of the same energy are produced, the interfering contribution should be removed.

In the case of the β^+ activity measurement by detecting the 511 keV annihilation γ-rays, another attention should be paid. If there are some other activities emitting γ-rays of energies greater than the electron-positron-pair production energy (1.022 MeV) in the β^+ source, the photons produce the electron-positron pairs in the surrounding materials around the Ge detector and consequently the annihilation γ-rays are emitted. To estimate these contributions, detection efficiencies of the annihilation γ-rays were measured in the shielding box by using ^{60}Co, ^{88}Y and ^{24}Na sources. The γ-sources were set between the absorber just as the β^+ activity measurements. Obtained efficiency curves shown in Fig. 10 are roughly fitted by pair production cross section for iron (in arbitrary units)[11]. Since the efficiencies depend on the source position, detector volume and shielding, those should be measured for individual detector arrangements. Since the powder paper (about 40 mg) used for powder samples contains a small amount of nitrogen (0.1%) as an impurity, the contribution of β^+ annihilation from $^{14}N(n,2n)^{13}N$ ($T_{1/2}$=9.96 m) should be subtracted (see Fig. 11).

The corrected cross sections can be obtained by multiplying these correction factors.

2.1.5 Error estimation

The total errors (δ_t) were derived by combining the experimental error (δ_e) and the error of nuclear data (δ_r) in quadratic :

$$\delta_t^2 = \delta_e^2 + \delta_r^2 .$$

Estimated major sources of the errors are listed in Table 8. When good counting statistics were achieved, the experimental error and the total error were 2.0% and 3.6%, respectively.

2.2 Results

Numerical data tables of cross sections are given in Table 9 and graphs are given in Fig. 12. In the figures experimental errors (δ_e) are only shown. In Appendix 3, the singles γ-ray spectra of samples irradiated by 14 MeV neutrons are shown.

3. Measurement of Half-Lives

In the procedure to deduce the cross sections, the half-life value is one of the important decay data. It is required that the half-life values are precise and reliable. Most of the values previously published have been obtained with GM counters, ionization chambers, proportional counters and scintillation counters. Recently the Ge detectors have been widely used for measuring the intensity and energy of γ-rays because of their excellent energy resolution. However during last 10 years works with the Ge detectors are scarce. In order to improve the precision and the reliability of the half-life values, the Ge detectors were used.

3.1 Experimental

The γ-rays were measured with the Ge detector in the spectrum multi-scaling mode. Decay was followed for about 10 times the half-life at equal intervals of 1/3 to 1/6 of the half-life. The ^{133}Ba (or ^{137}Cs, ^{170}Tm) source was simultaneously measured together with the short-lived activity for the correction of the pile-up loss and the dead time (source method). A constant-pulser with a rate of 60 cps was also connected to the preamplifier (constant-pulser method). During the measuring time the counting rate greatly changes. For the correction of the pile-up loss and the dead time the source method seems most reliable. But statistical fluctuations of the reference source happen and the peak area evaluation might be affected by the decaying Compton backgrounds. On the other hand the constant-pulser method gives good statistics and no effect to the γ-ray spectrum. However the peak shape of the pulser is different from that of the γ-radiation and the constant-pulser produces no random pile-up pulse by itself. Hence there might be some difference between both the methods at the high counting rates. The variation of the peak intensity ratios of the ^{133}Ba (or ^{137}Cs, ^{170}Tm) and the pulser was examined. If both the methods are reasonable, the ratios should be constant. In the high counting rate region they showed a clear deviation. When the initial counting rates were less than 9×10^3 cps, no deviation was always observed. Data points in the constant ratio region were only used in the least-squares analysis.

3.2 Source Preparation

Sources of ^{89m}Zr, ^{91m}Mo and ^{97m}Nb were produced by 14 MeV neutron

bombardments. Sources of ^{66}Cu and ^{104m}Rh were produced by thermal neutron irradiation at the TRIGA-II reactor of Rikkyo University (100 kW).

3.3 Results

The results are summarized in Table 10 together with production reactions, γ-rays followed, reference sources for corrections and previous works[7]. As an example, singles γ-ray spectrum and the decay curve in the decay of 4.3 m ^{104}Rh are shown in Fig. 13 and Fig. 14, respectively. The results are shown in Fig. 15 togehter with previous works taken from ref. 7. Present results show somewhat shorter half-lives in general.

4. Summary

The activation cross sections were measured on 16 reactions producing short-lived nuclei in the neutron energy range of 13.4 to 14.9 MeV for Mg, Si, S, Cl, Cr, Zn, Ga, Y and In. The reliability and precesion of the data were improved. The new estimation method of corrections for low energy neutrons was proposed. Five half-lives of short-lived nuclei were measured by applying both the source and pulser methods, which showed somewhat smaller values than the previous ones as a whole.

Acknowledgements

This work was performed under the contract between Nagoya University and Japan Atomic Energy Research Institute.

The authors wish to express their sincere thanks to Drs. S. Igarashi, T. Asami, T. Nakagawa and other members of the JAERI Nuclear Data Center. They are also grateful to Prof. K. Sumita for his support to this work and Messrs. H. Sugimoto, M. Datemichi, and S. Yoshida for the operation of the OKTAVIAN accelerator. We wish to thank Prof. N. Yamamuro for his calculations of the cross sections. Messrs. M. Shibata and A. Osa are appreciated for help in this experiment. The data analysis was done by using FACOMM-380 computer at the Institute of Plasma Physics, Nagoya University. Mrs. S. Okazaki is also thanked for typing the manuscript.

bombardments. Sources of ^{66}Cu and ^{104m}Rh were produced by thermal neutron irradiation at the TRIGA-II reactor of Rikkyo University (100 kW).

3.3 Results

The results are summarized in Table 10 together with production reactions, γ-rays followed, reference sources for corrections and previous works[7]. As an example, singles γ-ray spectrum and the decay curve in the decay of 4.3 m ^{104}Rh are shown in Fig. 13 and Fig. 14, respectively. The results are shown in Fig. 15 togehter with previous works taken from ref. 7. Present results show somewhat shorter half-lives in general.

4. Summary

The activation cross sections were measured on 16 reactions producing short-lived nuclei in the neutron energy range of 13.4 to 14.9 MeV for Mg, Si, S, Cl, Cr, Zn, Ga, Y and In. The reliability and precesion of the data were improved. The new estimation method of corrections for low energy neutrons was proposed. Five half-lives of short-lived nuclei were measured by applying both the source and pulser methods, which showed somewhat smaller values than the previous ones as a whole.

Acknowledgements

This work was performed under the contract between Nagoya University and Japan Atomic Energy Research Institute.

The authors wish to express their sincere thanks to Drs. S. Igarashi, T. Asami, T. Nakagawa and other members of the JAERI Nuclear Data Center. They are also grateful to Prof. K. Sumita for his support to this work and Messrs. H. Sugimoto, M. Datemichi, and S. Yoshida for the operation of the OKTAVIAN accelerator. We wish to thank Prof. N. Yamamuro for his calculations of the cross sections. Messrs. M. Shibata and A. Osa are appreciated for help in this experiment. The data analysis was done by using FACOMM-380 computer at the Institute of Plasma Physics, Nagoya University. Mrs. S. Okazaki is also thanked for typing the manuscript.

bombardments. Sources of ^{66}Cu and ^{104m}Rh were produced by thermal neutron irradiation at the TRIGA-II reactor of Rikkyo University (100 kW).

3.3 Results

The results are summarized in Table 10 together with production reactions, γ-rays followed, reference sources for corrections and previous works[7]. As an example, singles γ-ray spectrum and the decay curve in the decay of 4.3 m ^{104}Rh are shown in Fig. 13 and Fig. 14, respectively. The results are shown in Fig. 15 togehter with previous works taken from ref. 7. Present results show somewhat shorter half-lives in general.

4. Summary

The activation cross sections were measured on 16 reactions producing short-lived nuclei in the neutron energy range of 13.4 to 14.9 MeV for Mg, Si, S, Cl, Cr, Zn, Ga, Y and In. The reliability and precesion of the data were improved. The new estimation method of corrections for low energy neutrons was proposed. Five half-lives of short-lived nuclei were measured by applying both the source and pulser methods, which showed somewhat smaller values than the previous ones as a whole.

Acknowledgements

This work was performed under the contract between Nagoya University and Japan Atomic Energy Research Institute.

The authors wish to express their sincere thanks to Drs. S. Igarashi, T. Asami, T. Nakagawa and other members of the JAERI Nuclear Data Center. They are also grateful to Prof. K. Sumita for his support to this work and Messrs. H. Sugimoto, M. Datemichi, and S. Yoshida for the operation of the OKTAVIAN accelerator. We wish to thank Prof. N. Yamamuro for his calculations of the cross sections. Messrs. M. Shibata and A. Osa are appreciated for help in this experiment. The data analysis was done by using FACOMM-380 computer at the Institute of Plasma Physics, Nagoya University. Mrs. S. Okazaki is also thanked for typing the manuscript.

References

1) Y. Ikeda, C. Konno, K. Oishi, T. Nakamura, H. Miyade, K. Kawade, H. Yamamoto and T. Katoh: JAERI, 1312 (1988).
2) "Evaluated Neutron Data File, ENDF/B-V" ENDF/B Summary Documentation, compiled by R. Kinsey, ENDF-201, 3rd edition, Brookhaven Laboratory (1979).
3) A. Pavlik, G. Winkler, H. Vonach, A. Paulsen and H. Linskien: J. Phys. G; Nucl. Phys. 8, 1283 (1982).
4) D.R. Nethaway: J. Inorg. Nucl. Chem. 40, 1285 (1978).
5) V.E. Lewis and K.J. Zieba: Nucl. Instr. Meth. 174, 141 (1980).
6) K. Debertin and U. Schötzig: Nucl. Instr. Meth. 140, 337 (1977).
7) E. Browne, R.B. Firestore and V.S. Shirley: "Table of Radioactive Isotopes", John Wiley & Sons, New York (1986).
8) JAERI Nuclear Data Center: "JENDL-3", Private Communication (1989).
9) N. Yamamuro: JAERI-M 88-140 (1988) (in Japanese).
10) K. Kawade, M. Ezuka, H. Yamamoto, K. Sugioka and T. Katoh: Nucl. Instr. Meth. 190, 101 (1981).
11) L. Strom and H.I. Israel: Nucl. Data Tables A7 565 (1970).

Table 1 Measured activation cross sections

Reaction[a]	$T_{1/2}$	Reaction[a]	$T_{1/2}$
$^{26}Mg(n,\alpha)^{23}Ne$	37.6s	$^{53}Cr(n,p)^{53}V$	1.61m
$(n,np)^{25}Na$	59.6s	$(n,np)^{52}V$	3.75m
$^{28}Si(n,p)^{28}Al$	2.241m	$^{66}Zn(n,p)^{66}Cu$	5.10m
$^{30}Si(n,\alpha)^{27}Mg$	9.46m	$^{67}Zn(n,np)^{66}Cu$	5.10m
$(n,np)^{29}Al$	6.56m	$^{68}Zn(n,np)^{68m}Cu$	3.75m
$^{32}S(n,t)^{30}P$	2.50m	$^{71}Ga(n,\alpha)^{68m}Cu$	3.75m
$^{37}Cl(n,p)^{37}S$	5.05m	$^{89}Y(n,\alpha)^{86m}Rb$	1.017m
$^{52}Cr(n,p)^{52}V$	3.75m	$^{113}In(n,2n)^{112g}In$	14.4m

[a] (n,np) means [(n,d) + (n,n'p) + (n,pn)].

Table 2 Measured half-lives

Nuclide				
^{66}Cu	^{89m}Zr	^{91m}Mo	^{97m}Nb	^{104m}Rh
(5.1m)	(4.2m)	(65s)	(60s)	(4.3m)

Table 3 Cross section of $^{27}Al(n,\alpha)^{24}Na$ reaction[a)]

En(MeV)	Cross section(mb)
14.96	113.42
14.92	113.93
14.84	114.97
14.71	116.65
14.53	118.97
14.32	121.28
14.10	123.63
13.95	125.02
13.81	125.93
13.68	126.77
13.55	127.62
13.33	128.60

a) taken from ENDF/B-V[2)]
Uncertainty is ±3% for all values.

Table 4 Samples of separated isotope

Sample	Chemical form	Enrichment (%)	Weight (mg)	Reaction	Impurity[a)] (%)
^{26}Mg	MgO	99.55	50	$^{26}Mg(n,\alpha)$ (n,np)	24(0.35) , 25(0.10)
^{30}Si	SiO_2	95.28	40	$^{30}Si(n,\alpha)$ (n,np)	28(4.40) , 29(0.32)
^{53}Cr	Cr_2O_3	98.23	50	$^{53}Cr(n,p)$ (n,np)	50(0.027), 52(1.665) 54(0.077)
^{66}Zn	ZnO	98.41	80	$^{66}Zn(n,p)$	64(0.86) , 67(0.20) 68(0.53) , 70(<0.005)
^{67}Zn	ZnO	94.60	60	$^{67}Zn(n,np)$	64(1.113), 66(1.95) 68(2.23) , 70(0.054)
^{113}In	In	89.76	10	$^{113}In(n,2n)^{g}$	115(10.24)

a) A(x) means mass nummber A with atomic percent x.

Table 5 Samples of natural abundance

Sample	Chemical form	Purity (%)	Weight (%)	Reaction	Abundance (%)
Si	Si	99.99	70	$^{28}Si(n,p)$	28(92.23), 29(4.67), 30(3.10)
S	S	99.999	100	$^{32}S(n,t)$	32(95.23), 33(0.75), 34(4.21), 36(0.017)
Cl	C_2H_3Cl	99.99	50	$^{37}Cl(n,p)$	35(75.77), 37(24.23)
Cr	Cr	99.99	85	$^{52}Cr(n,p)$	50(4.35), 52(83.79), 53(9.50), 54(2.36)
Zn	Zn	99.99	370	$^{68}Zn(n,p)^{m}$	64(48.6), 66(27.9) 67(4.1), 68(18.8), 70(0.62)
Ga	Ga_2O_3	99.99	220	$^{71}Ga(n,\alpha)^{m}$	69(60.1), 71(39.9)
Y	Y_2O_3	99.999	210	$^{89}Y(n,\alpha)^{m}$	89(100)

Table 6 Ge detectors used for cross section measurement

Detector	Volume (cm^3)	Efficiency (%)	FWHM (keV)	Object of measurement
Vertical HPGe	60	12	1.75	short-lived nuclei
Horizontal HPGe	89	16	2.00	Al monitor foil (^{27}Mg)
Horizontal HPGe	113	23	2.00	^{92m}Nb, ^{89}Zr for En

Table 7 Reactions and decay parameters

Reaction[a]	$T_{1/2}$	E_γ(keV)	I_γ(%)	Q(MeV)[b]	FC[c]
$^{26}Mg(n,\alpha)^{23}Ne$	37.6s	439.9	32.9(10)	-5.41	2.1
$(n,np)^{25}Na$	59.6s	389.7	12.65(22)	-14.144	0
$^{28}Si(n,p)^{28}Al$	2.241m	1779.0	100	-3.86	4.4
$^{30}Si(n,\alpha)^{27}Mg$	9.46m	843.8	73(1)	-4.20	1.9
$(n,np)^{29}Al$	6.56m	1273.4	91.3	-13.51	0
$^{32}S(n,t)^{30}P$	2.50m	511[d]	200	-12.687	0
$^{37}Cl(n,p)^{37}S$	5.05m	3104.0	94.2(6)	-4.08	3.2
$^{52}Cr(n,p)^{52}V$	3.75m	1434.1	100	-3.19	3.2
$^{53}Cr(n,p)^{53}V$	1.61m	1006.2	90(2)	-2.65	0.8
$(n,np)^{52}V$	3.75m	1434.1	100	-11.13	0
$^{66}Zn(n,p)^{66}Cu$	5.10m	1039.4	7.4(1.8)	-1.86	3.0
$^{67}Zn(n,np)^{66}Cu$	5.10m	1039.4	7.4(1.8)	-8.91	0
$^{68}Zn(n,np)^{68m}Cu$	3.75m	525.7	75(15)	-4.56	0.2
$^{71}Ga(n,\alpha)^{68m}Cu$	3.75m	525.7	75(15)	1.065	
$^{89}Y(n,\alpha)^{86m}Rb$	1.017m	556.1	98.19(10)	0.688	
$^{113}In(n,2n)^{112g}In$	14.4m	511[d]	44	-9.44	0
$^{27}Al(n,\alpha)^{24}Na$[e]	14.959h	1368.6	99.994(3)	-3.13	2.1
$^{27}Al(n,p)^{27}Mg$[f]	9.46m	843.8	73(1)	-1.83	6.2

a) (n,np) means [(n,d) + (n,n'p) + (n,pn)].

b) Q(n,n'p) is given here. Q(n,d) = Q(n,n'p) + 2.225 MeV.

c) Fractional contribution of low energy neutrons, see the text.

d) Annihilation γ-ray from β^+.

e) Standard reaction (ENDF/B-V) used for cross section measurements.

f) Secondary conventional reaction used for short-lived nuclei.

Table 8 Principal sources of uncertainty in the measured cross sections

Experimental error (δ_e)	
Source of error	Uncertainty (%)
Counting statistics	0.3 ~ 40
Sample mass including purity	0.1
Neutron flux fluctuation	< 0.1
Gamma-peak area evaluation	0.5
Detector efficiency	1.5(E_γ>300 keV), 3(300 ~ 80 keV), 5(E_γ:80<keV)
Efficiency calibration at 0.5 and 5 cm	1.0
Correction for true coincidence sum	< 0.3
Correction for random coincidence sum	< 0.4
Correction for sample thickness	0.2 ~ 0.6
Correction for self-absorption of γ-rays	0 ~ 0.2
Correction for low energy neutrons	0 ~ 5
Secondary reference cross section for	
$^{27}Al(n,p)^{27}Mg$	0.5 (only statistics)

Error of nuclear data (δ_r)	
Source of error	Uncertainty (%)
Reference cross section for	
$^{27}Al(n,\alpha)^{24}Na$(ENDF/B-V)	3.0
Absolute γ-ray intensity	0 ~ 20
Half-life	0 ~ 5

Table 9(a) Activation cross section of short-lived nuclei

$^{26}Mg(n,\alpha)^{23}Ne(37.6s)$					$^{26}Mg(n,np)^{25}Na(59.6S)$			
En(MeV)	σ(mb)	δ_e(%)	δ_r(%)	δ_t(%)	σ(mb)	δ_e(%)	δ_r(%)	δ_t(%)
14.87	29.7	6.5	4.3	7.8	3.9	27	3.5	27
14.64	32.6	9.7	4.3	11				
14.35	32.2	9.0	4.3	10				
14.02	29.2	6.0	4.3	7.4				
13.70	26.7	12.0	4.3	13				
13.40	32.7	7.1	4.3	8.3				

$^{28}Si(n,p)^{28}Al(2.241m)$					$^{30}Si(n,\alpha)^{25}Na(9.46m)$			
En(MeV)	σ(mb)	δ_e(%)	δ_r(%)	δ_t(%)	σ(mb)	δ_e(%)	δ_r(%)	δ_t(%)
14.87	219	4.5	3.0	5.4	63.6	2.5	3.3	4.1
14.64	229	4.3	3.0	5.2	68.4	3.6	3.3	4.9
14.35	229	4.2	3.0	5.2	64.3	3.3	3.3	4.7
14.02	254	4.2	3.0	5.2	60.2	4.0	3.3	5.2
13.70	265	4.4	3.0	5.3	60.0	3.5	3.3	4.8
13.40	254	3.9	3.0	4.9	66.4	2.3	3.3	4.0

$^{30}Si(n,np)^{29}Al(6.56m)$					$^{37}Cl(n,p)^{37}S(5.05m)$			
En(MeV)	σ(mb)	δ_e(%)	δ_r(%)	δ_t(%)	σ(mb)	δ_e(%)	δ_r(%)	δ_t(%)
14.87	6.1	6.7	3.1	7.4	24.8	8.4	3.0	8.9
14.64	5.8	10.9	3.1	11	22.3	8.3	3.0	8.8
14.35	4.9	9.7	3.1	10	22.4	7.9	3.0	8.5
14.02	3.8	13.8	3.1	14	24.9	11.4	3.0	12
13.70	0.8	43	3.1	43	25.9	10.2	3.0	11
3.40	0.4	52	3.1	52	25.6	7.7	3.0	8.3

* δ_e : experimental error , δ_r : error of nuclear data , $\delta_t^2 = \delta_e^2 + \delta_r^2$
* Error of neutron energy is estimated as about 50 keV.

Table 9(b) Activation cross section of short-lived nuclei

$^{52}Cr(n,\alpha)^{52}V(3.75m)$					$^{53}Cr(n,p)^{53}V(1.61m)$			
En(MeV)	σ(mb)	δ_e(%)	δ_r(%)	δ_t(%)	σ(mb)	δ_e(%)	δ_r(%)	δ_t(%)
14.87	74.4	3.8	3.0	4.8	42.8	4.6	3.7	5.9
14.64	73.6	3.6	3.0	4.7	45.6	6.2	3.7	7.2
14.35	79.1	3.4	3.0	4.5	44.4	6.4	3.7	7.4
14.02	80.4	3.4	3.0	4.5	41.2	6.7	3.7	7.7
13.70	78.3	3.6	3.0	4.7	44.9	7.2	3.7	8.1
13.40	85.6	3.2	3.0	4.4	39.4	3.7	3.7	5.2

$^{53}Cr(n,np)^{52}V(3.75m)$					$^{66}Zn(n,p)^{66}Cu(5.10m)$			
En(MeV)	σ(mb)	δ_e(%)	δ_r(%)	δ_t(%)	σ(mb)	δ_e(%)	δ_r(%)	δ_t(%)
14.87	13.2	7.3	3.0	7.9	73.9	9.2	24.2	26
14.64	9.5	12.5	3.0	13	70.1	8.4	24.2	26
14.35	6.8	14.9	3.0	15	67.1	7.8	24.2	25
14.02	4.9	19.4	3.0	20	72.0	7.7	24.2	25
13.70	3.7	25	3.0	25	62.0	9.4	24.2	30
13.40	2.7	13.7	3.0	14	74.0	5.4	24.2	25

$^{67}Zn(n,np)^{66}Cu(5.10m)$					$^{68}Zn(n,p)^{68m}Cu(3.75m)$			
En(MeV)	σ(mb)	δ_e(%)	δ_r(%)	δ_t(%)	σ(mb)	δ_e(%)	δ_r(%)	δ_t(%)
14.87	35.9	7.5	24.2	25	5.5	12.0	20.2	24
14.64	30.9	13.0	24.2	28	4.6	8.5	20.2	22
14.35	24.9	12.6	24.2	27	4.9	7.5	20.2	22
14.02	19.0	9.9	24.2	26	4.2	8.0	20.2	22
13.70	12.9	22	24.2	33	4.2	8.4	20.2	22
13.40	11.5	14.6	24.2	28	3.0	12.0	20.2	24

* δ_e : experimental error , δ_r : error of nuclear data , $\delta_t^2 = \delta_e^2 + \delta_r^2$
* Error of neutron energy is estimated as about 50 keV.

Table 9(c) Activation cross section of short-lived nuclei

$^{113}In(n,2n)^{112g}In(14.4m)$				
En(MeV)	σ(mb)	δ_e(%)	δ_r(%)	δ_t(%)
14.87	279	13.5	3.0	14
14.64	293	11.2	3.0	12
14.35	275	9.0	3.0	9.5
14.02	297	10.9	3.0	11
13.70	286	9.8	3.0	10
13.40	293	9.9	3.0	10

* δ_e : experimental error , $\delta_t^2 = \delta_e^2 + \delta_r^2$
  δ_r : error of nuclear data
* Error of neutron energy is estimated as, about 50 keV.

Table 9(d) Activation cross section of short-lived nuclei

$^{32}S(n,t)^{30}Cu(2.50m)$					$^{71}Ga(n,\alpha)^{68m}Cu(3.75m)$			
En(MeV)	σ(mb)	δ_e(%)	δ_r(%)	δ_t(%)	σ(mb)	δ_e(%)	δ_r(%)	δ_t(%)
14.8[a)]	0.016	50	3.0	50	1.5	21	20	29

$^{89}Y(n,\alpha)^{86m}Rb(1.017m)$				
En(MeV)	σ(mb)	δ_e(%)	δ_r(%)	δ_t(%)
14.8[a)]	1.8	21	3.0	22

a) Irradiations were done at 5cm by using the calibration tube at 22.5°. The error of neutron energy is estimated as about 0.2 MeV.

Table 10 Results of half-life measurement

Nuclide	Production reaction	Eγ (keV)	Reference[a] (Eγ in keV)	Half-life Present	Reference[b]
^{66}Cu	^{65}Cu(n, γ)	1039.4	^{137}Cs (611.7)	5.063(20)m	5.10(2)m
^{89m}Zr	^{90}Zr(n,2n)^{m}	587.8	^{133}Ba (356.0)	4.148(20)m	4.18(1)m
^{91m}Mo	^{92}Mo(n,2n)^{m}	652.9	^{133}Ba (356.0)	63.5(10)s	65.2(8)s
^{97m}Nb	^{97}Mo(n,p)^{m}	743.4	^{137}Cs (661.7)	52.7(18)s	60(8)s
^{104m}Rh	^{103}Rh(n, γ)^{m}	555.8	^{170}Tm (84.3)	4.256(20)m	4.34(5)m

[a] These sources were used for corrections of dead-time and pile-up losses.

[b] taken from ref.7.

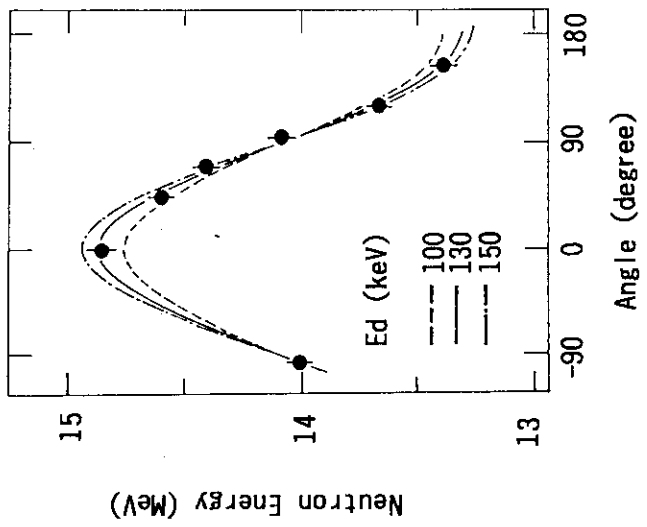

Fig. 2 Angular dependence of d-T neutron enegy.

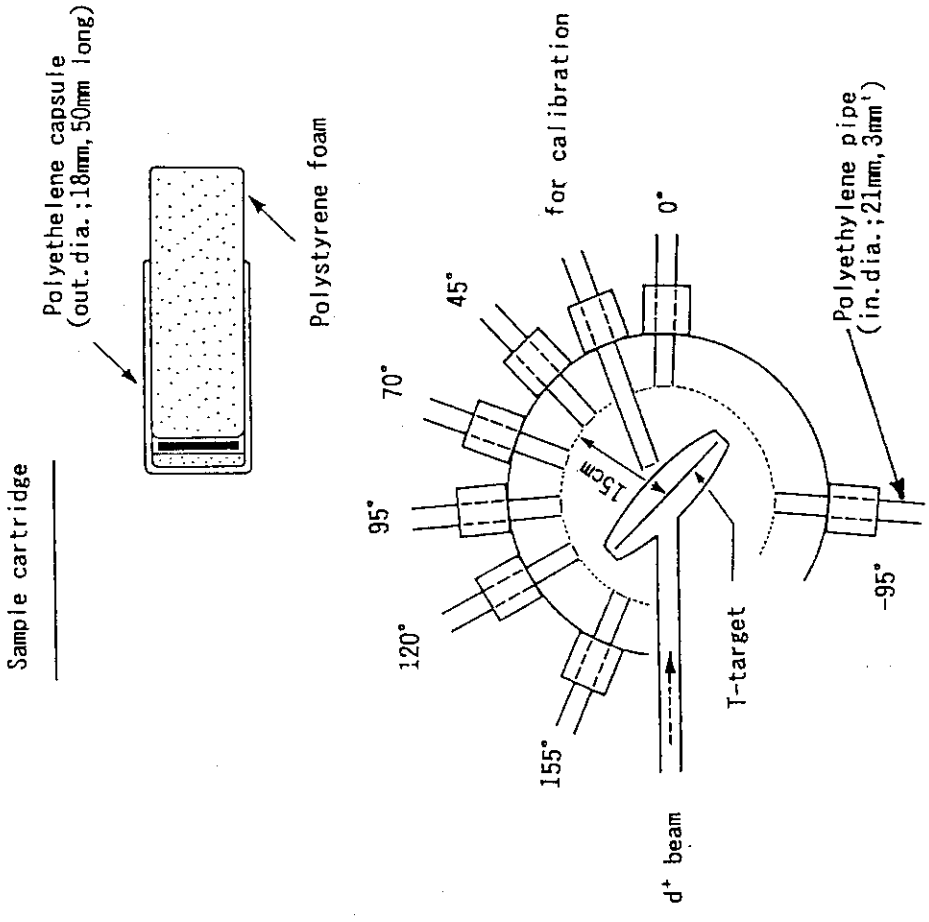

Fig. 1 Pneumatic sample transport system.

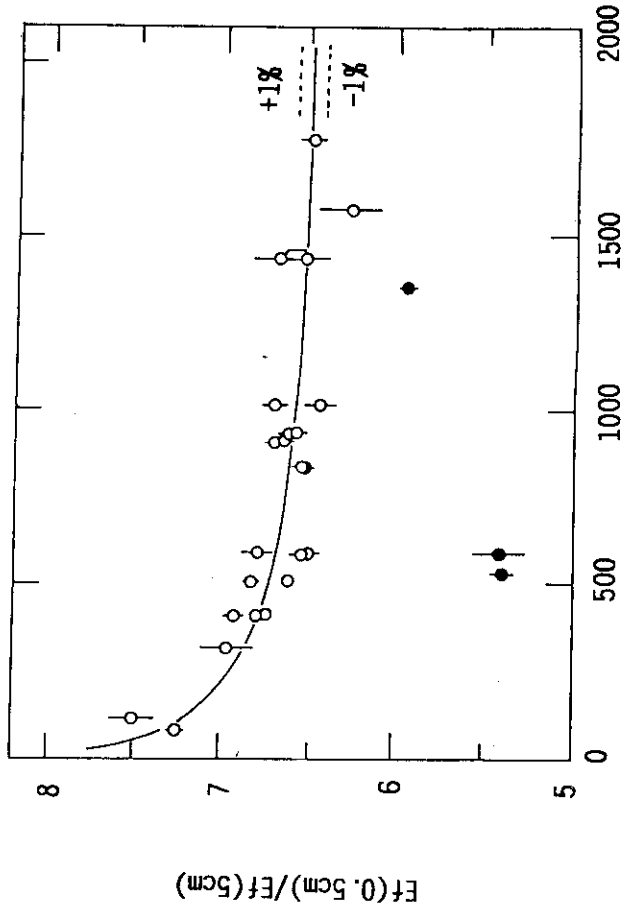

Fig. 4 Ratio of detection efficiencies at 0.5cm and at 5cm. Open circles show single γ-ray emitters and closed ones show cascade γ-ray emitters.

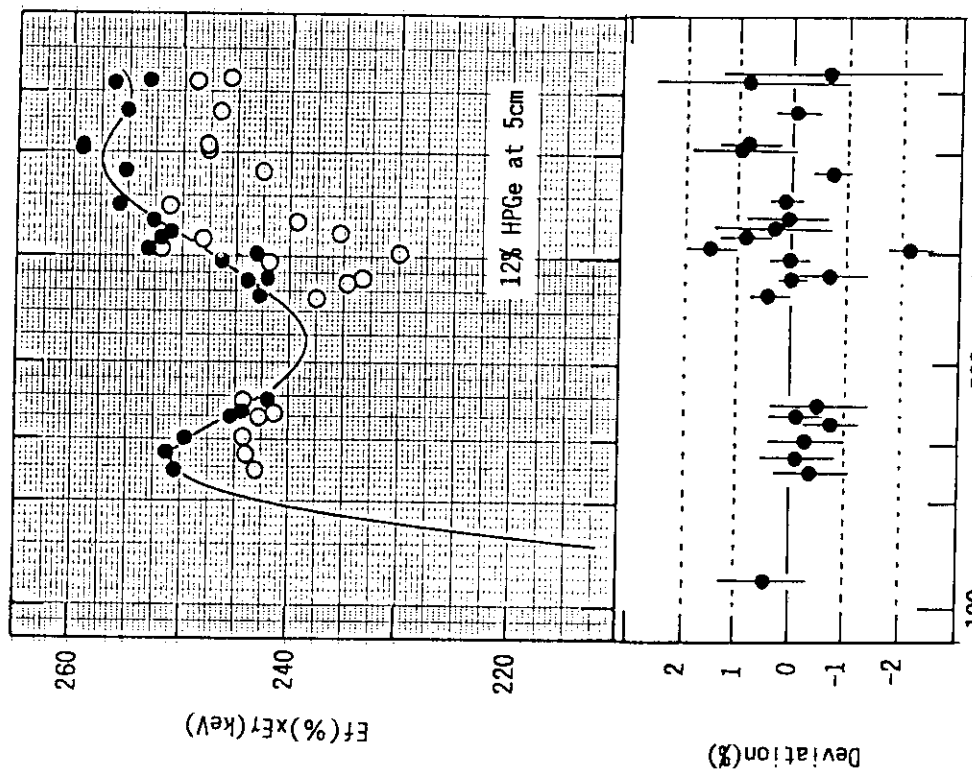

Fig. 3 Full-energy-peak detection efficiency of 12% HPGe with a 5mm acrylic absorber at 5cm. Closed circles are corrected for sum effects. Open circles are not. The fitted line was calculated from equations given in Appendix 2.

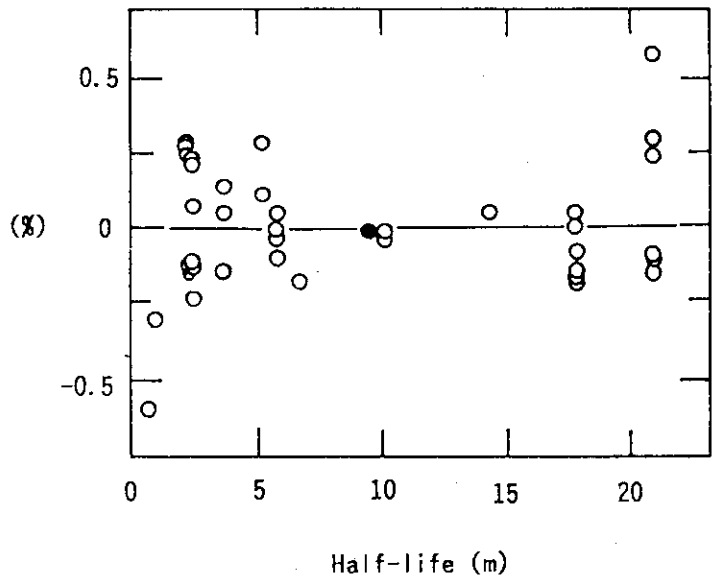

Fig. 5 An example of correction for the fluctuation of the neutron flux. $^{27}Mg(T_{1/2}=9.46m)$ was used as a flux monitor.

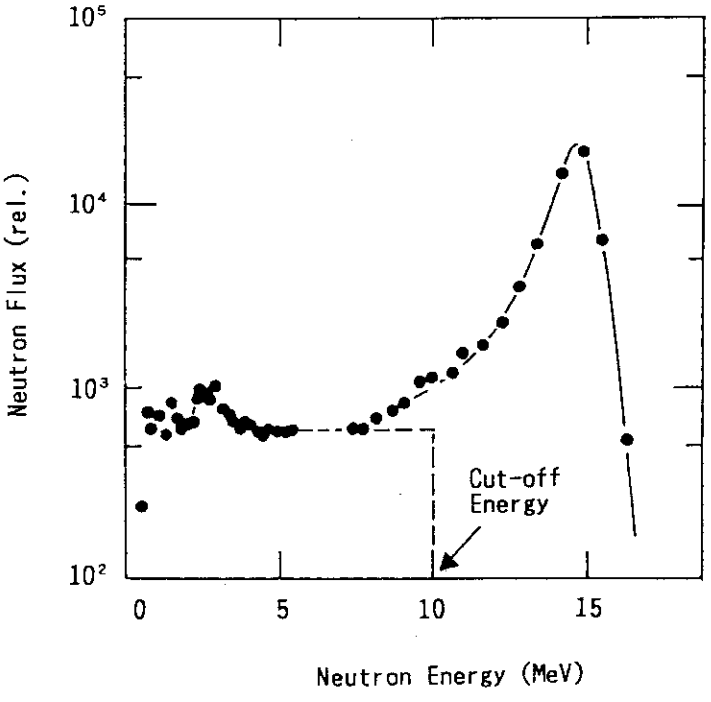

Fig. 6 Neutron spectrum at OKTAVIAN measured at 70° with respect to d^+ beam direction by two-crystal method.

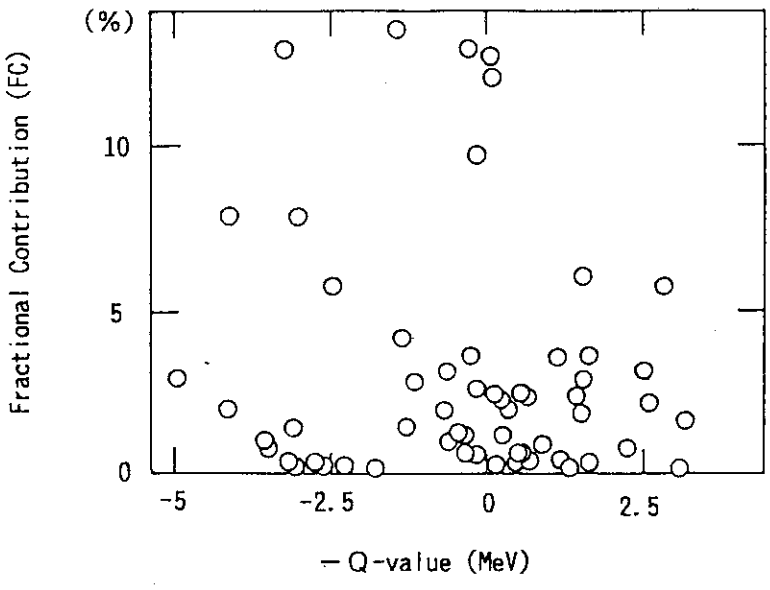

Fig. 7 Fractional contributions (FC) of low energy neutrons as a function of reaction Q-values. FCs were calculated by using excitation functions from JENDL-3[8] and Yamamuro's calculations[9].

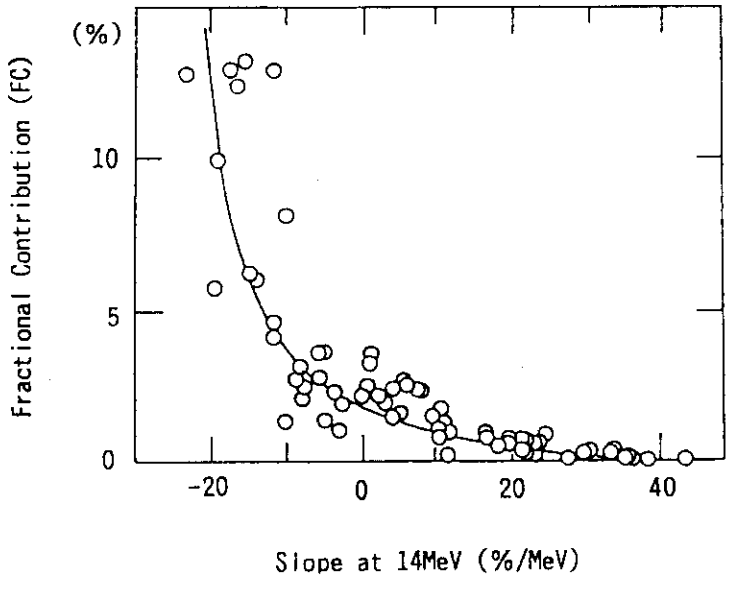

Fig. 8 Fractional contributions (FC) of low energy neutrons as a function of the slope $[(\Delta\sigma/\Delta E)/\sigma]$ of excitation functions at 14 MeV.

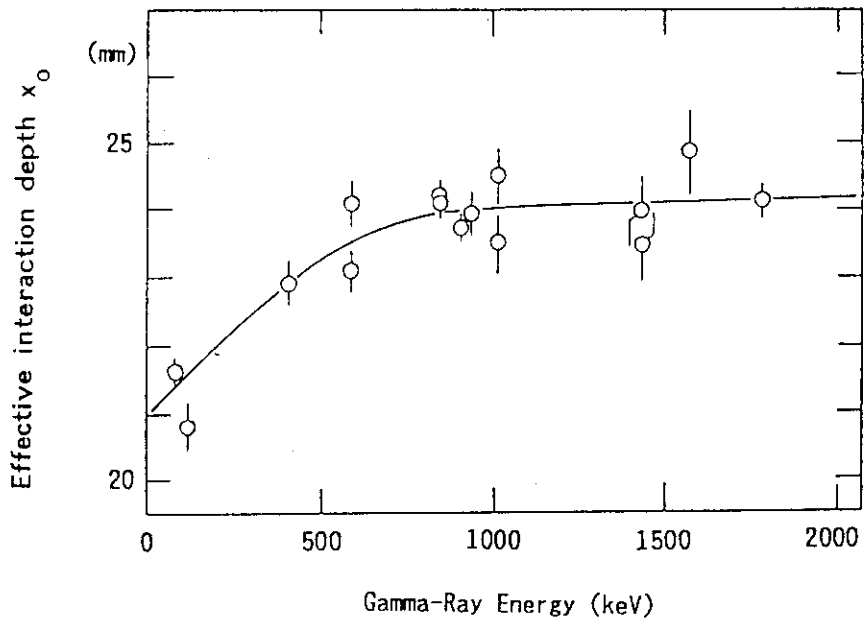

Fig. 9 Effective interaction depth x_o versus γ-ray energy for 12% HPGe detector.

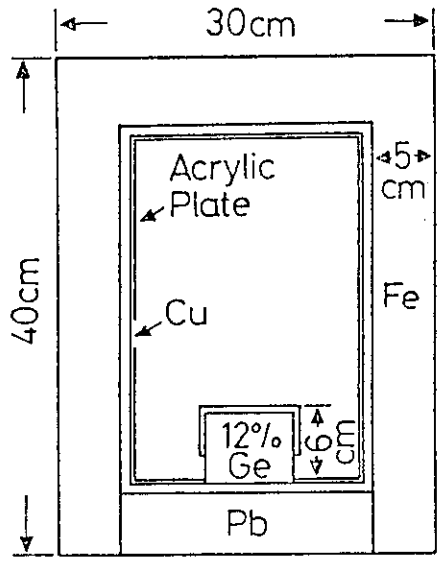

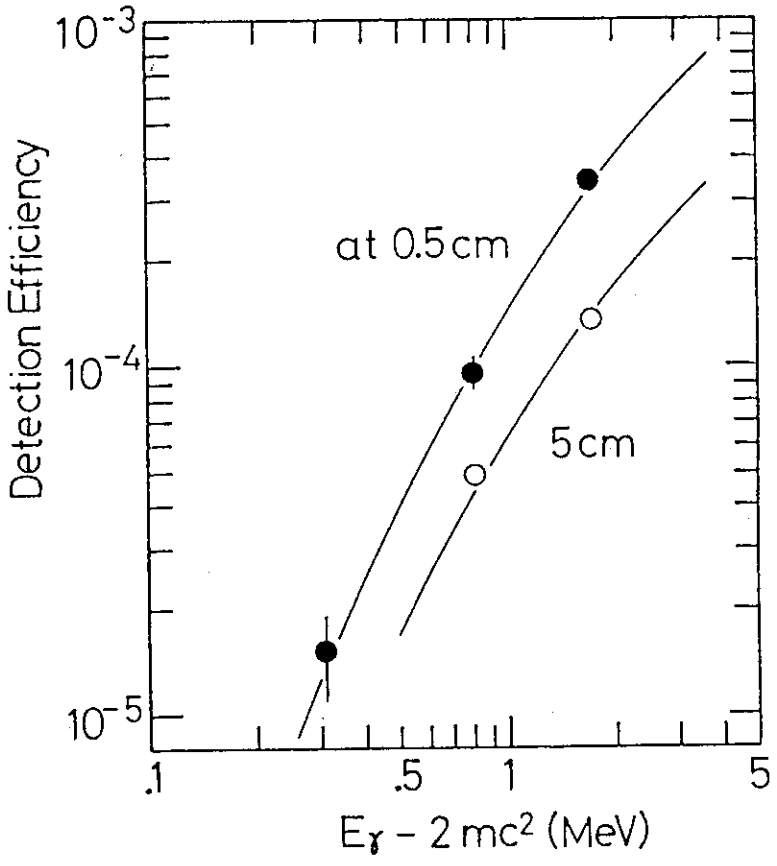

Fig. 10 Detection efficiency of a 12% high-purity Ge detector for 511 keV annihilation γ-rays due to electron-positron-pair production in the shielding box. The fitted lines show pair production cross section for iron in arbitrary units[11].

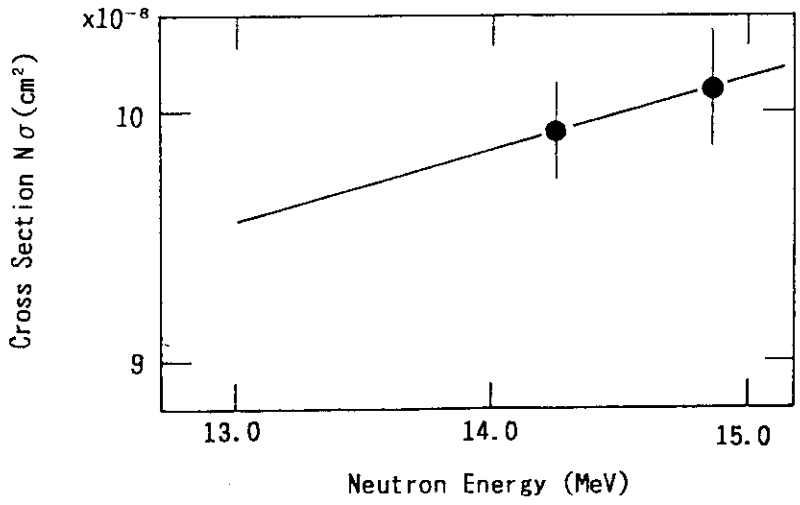

Fig. 11 Effective cross section of a wrapping powder paper (about 40mg) producing 511 keV annihilation γ-ray through $^{13}N(n,2n)^{12}N$ reaction.

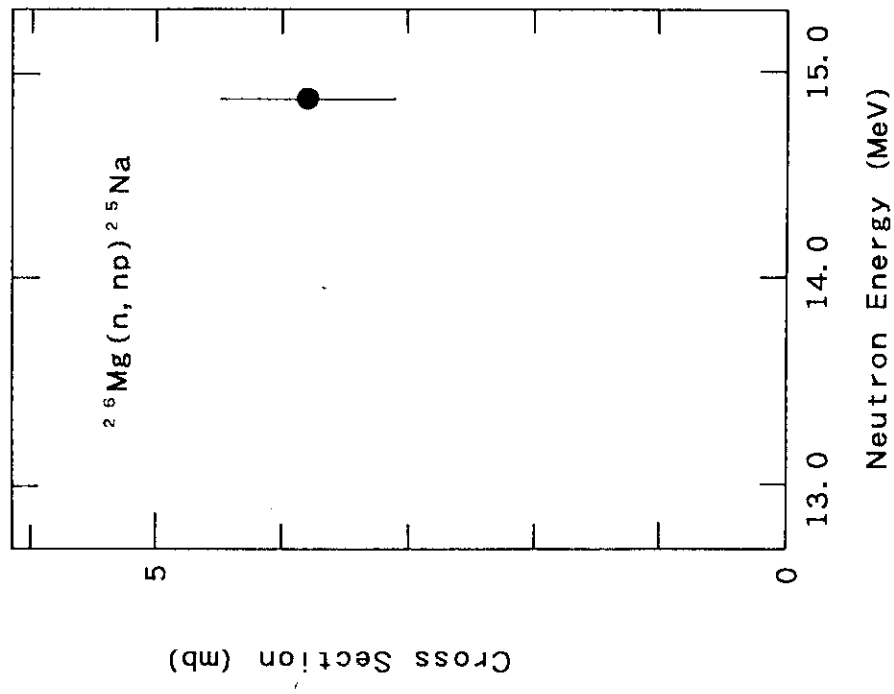

Fig. 12.2 Cross section of ^{26}Mg(n,np)^{25}Na.

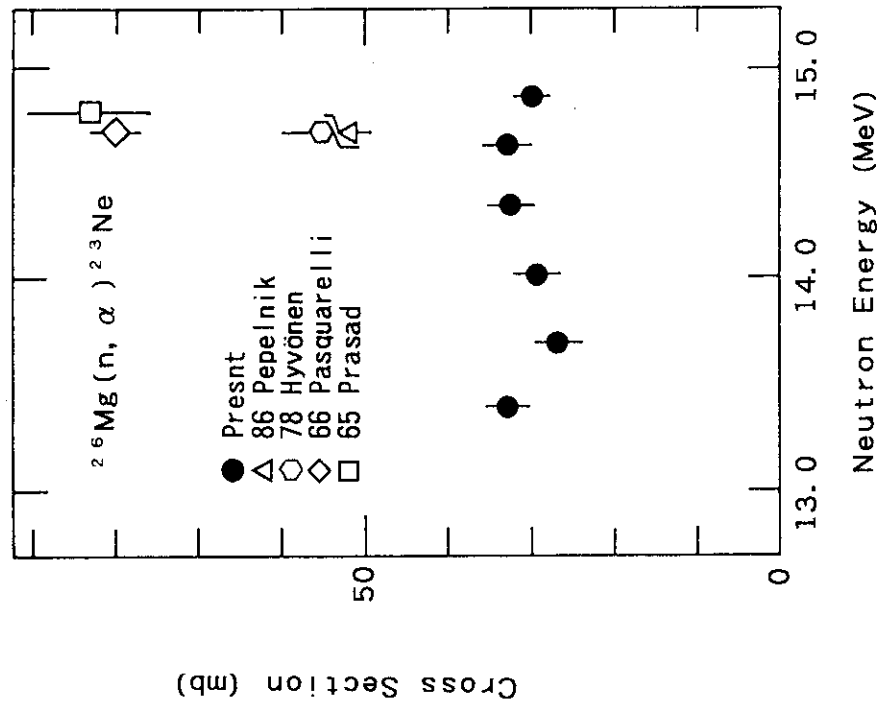

Fig. 12.1 Cross section of ^{26}Mg(n,α)^{23}Ne.

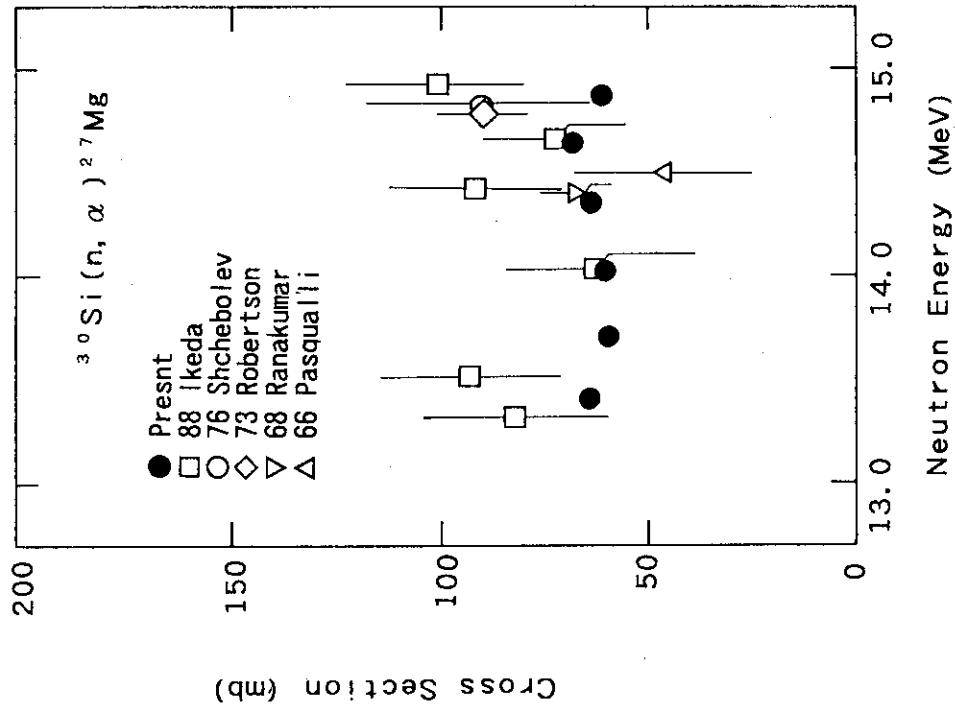

Fig. 12.4 Cross section of $^{30}Si(n,\alpha)^{27}Mg$.

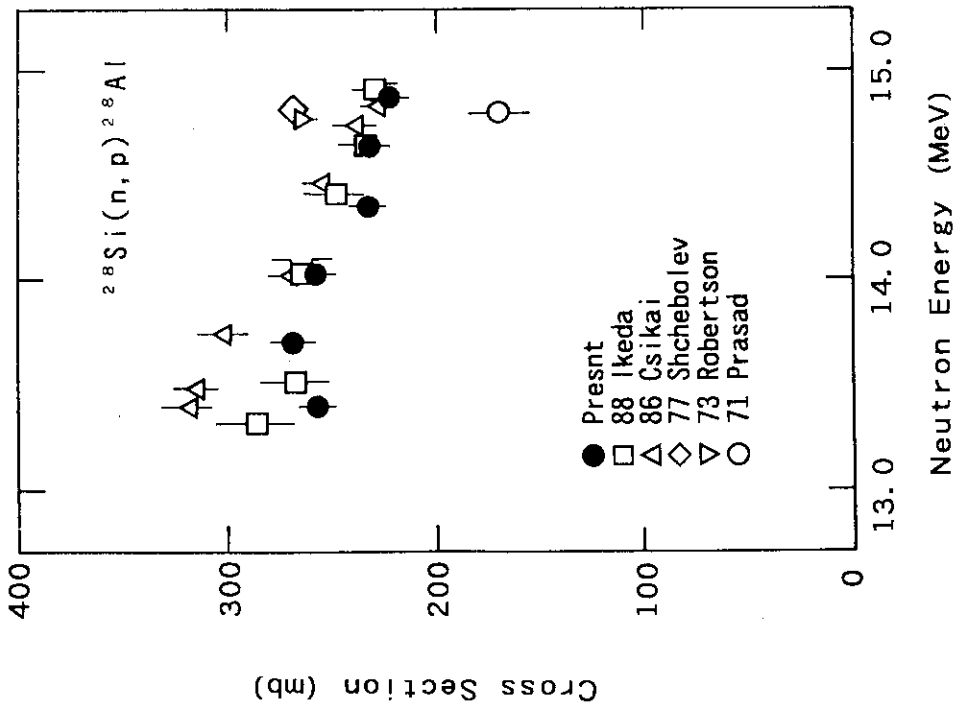

Fig. 12.3 Cross section of $^{28}Si(n,p)^{28}Al$.

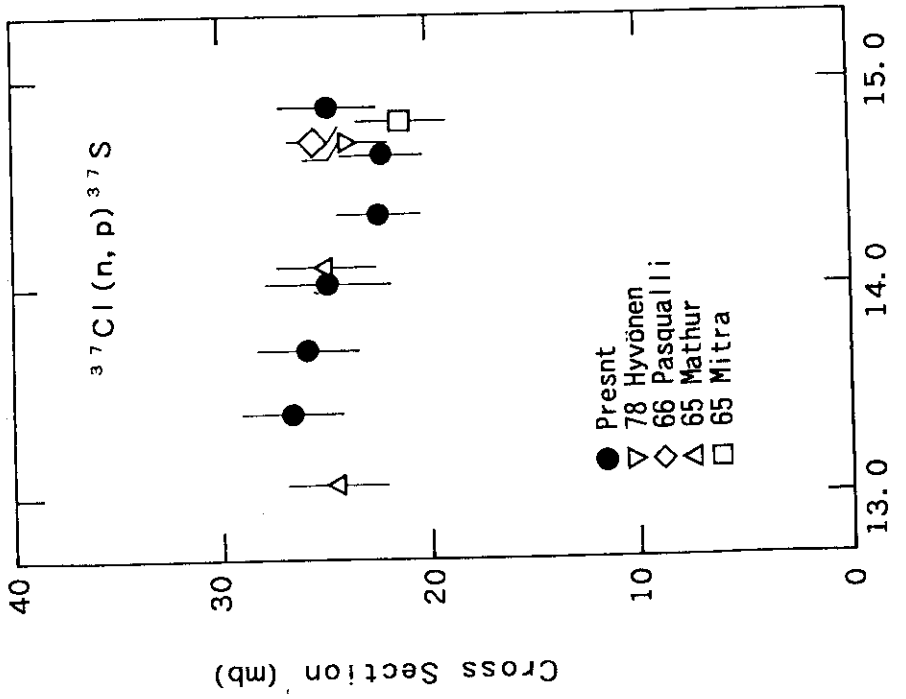

Fig. 12.6 Cross section of ^{37}Cl(n,p)^{37}S.

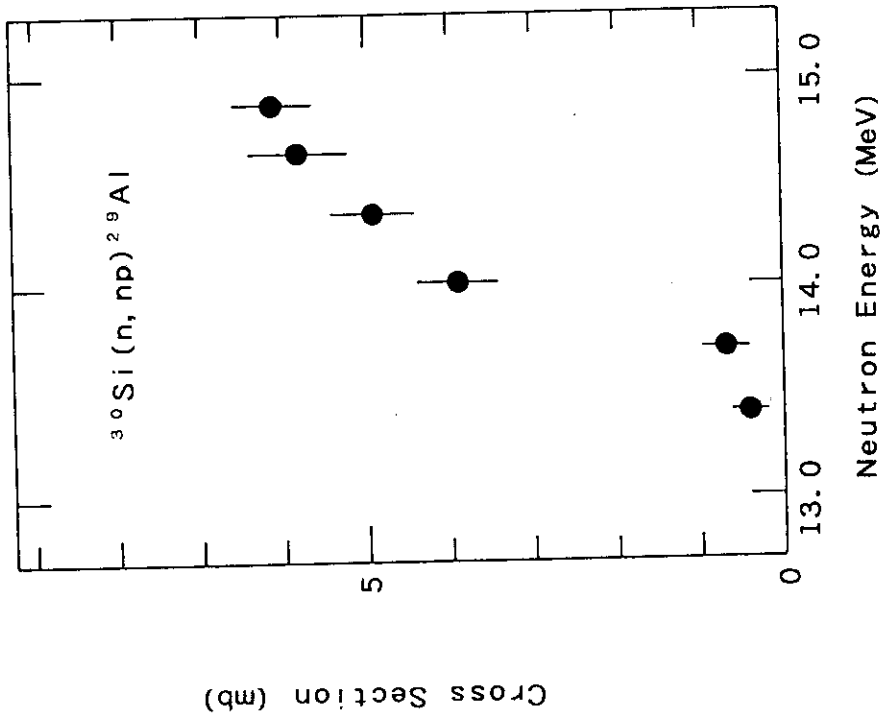

Fig. 12.5 Cross section of ^{30}Si(n,np)^{29}Al.

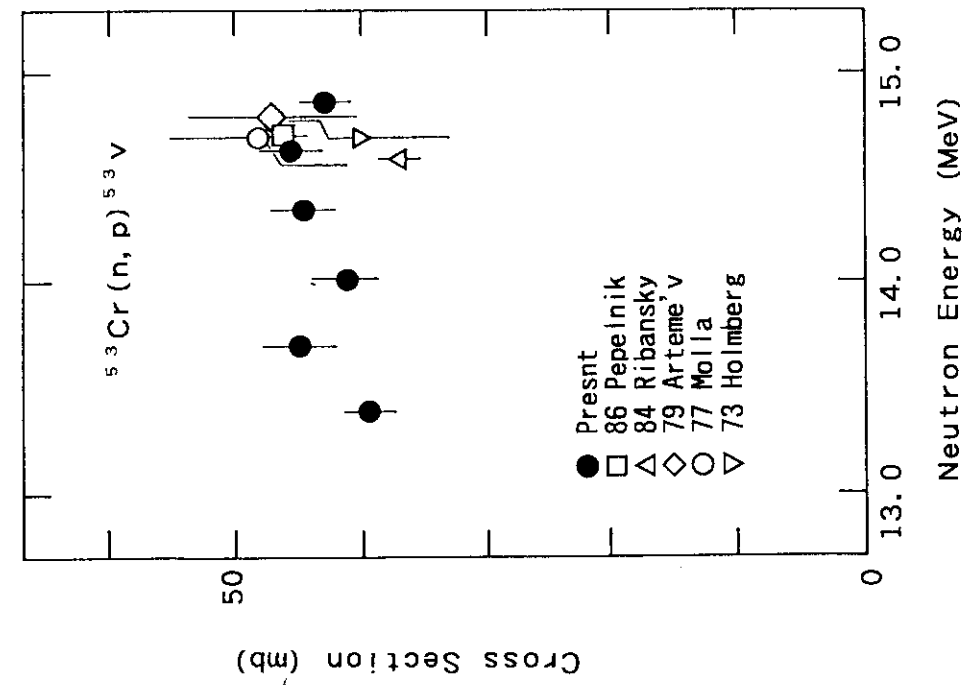

Fig. 12.8 Cross section of ^{53}Cr(n,p)^{53}V.

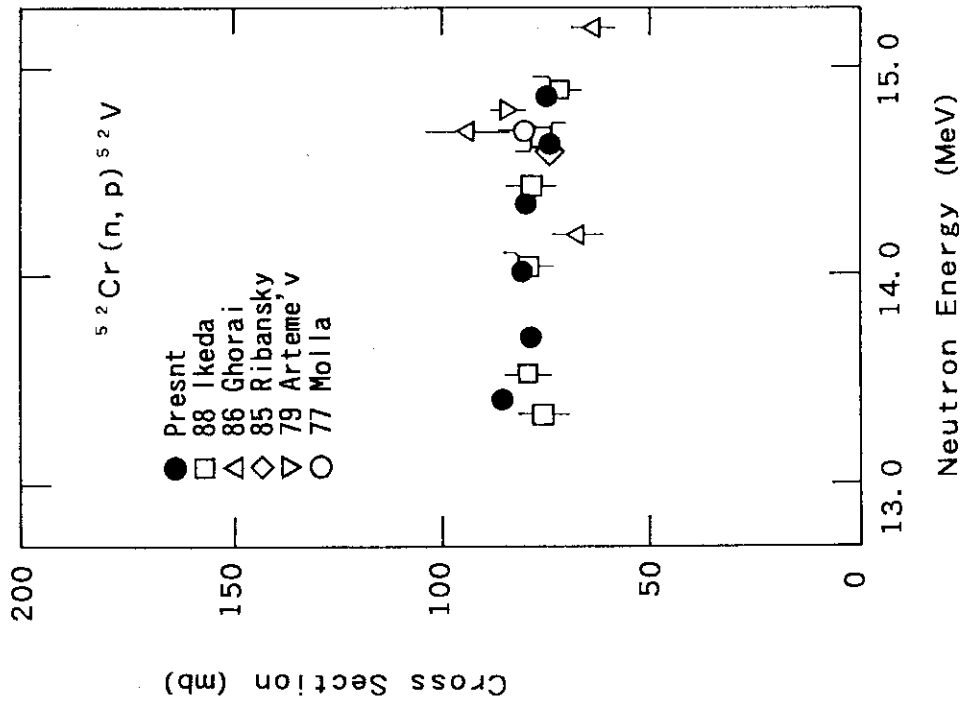

Fig. 12.7 Cross section of ^{52}Cr(n,p)^{52}V.

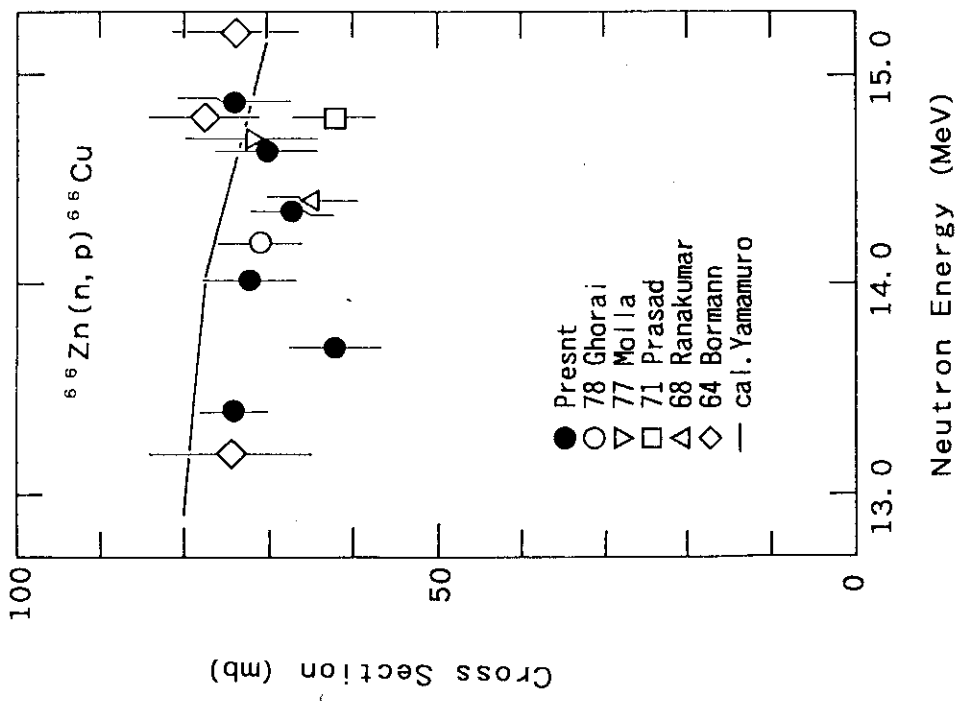

Fig. 12.10 Cross section of ^{66}Zn(n,p)^{66}Cu.

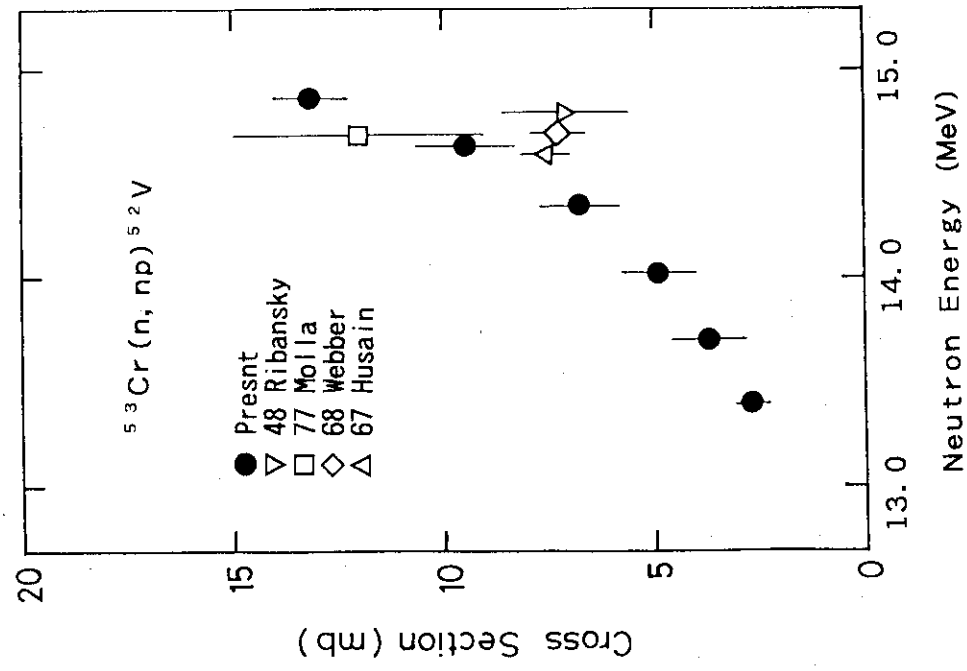

Fig. 12.9 Cross section of ^{53}Cr(n,np)^{52}V.

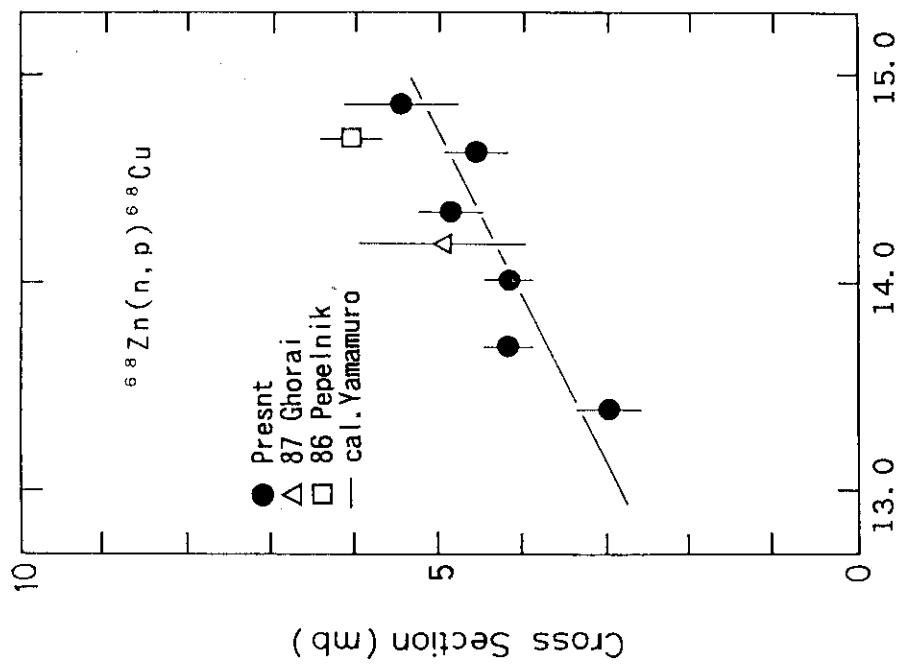

Fig. 12.12 Cross section of ^{68}Zn(n,p)^{68}Cu.

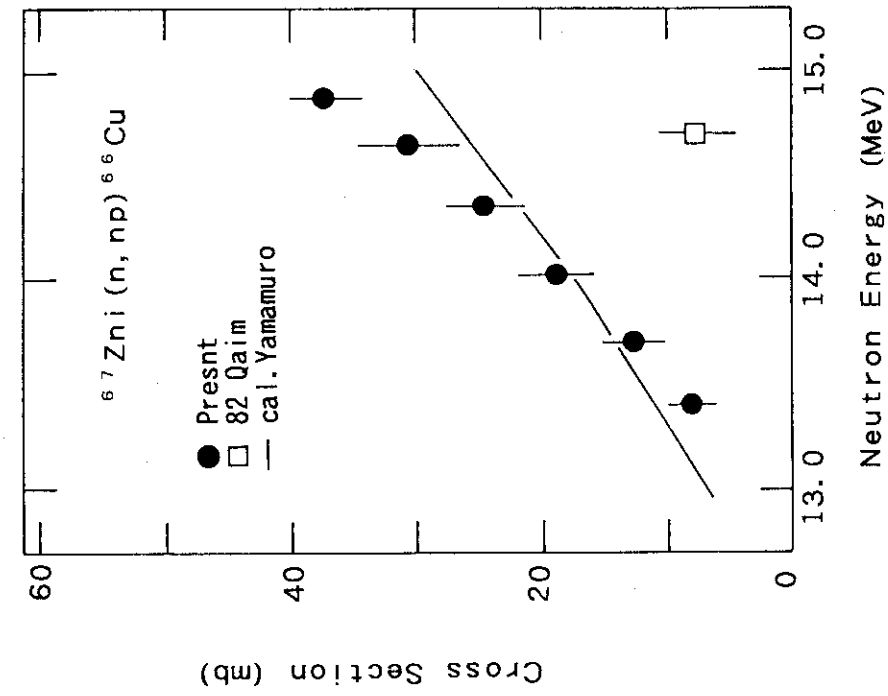

Fig. 12.11 Cross section of ^{67}Zn(n,np)^{66}Cu.

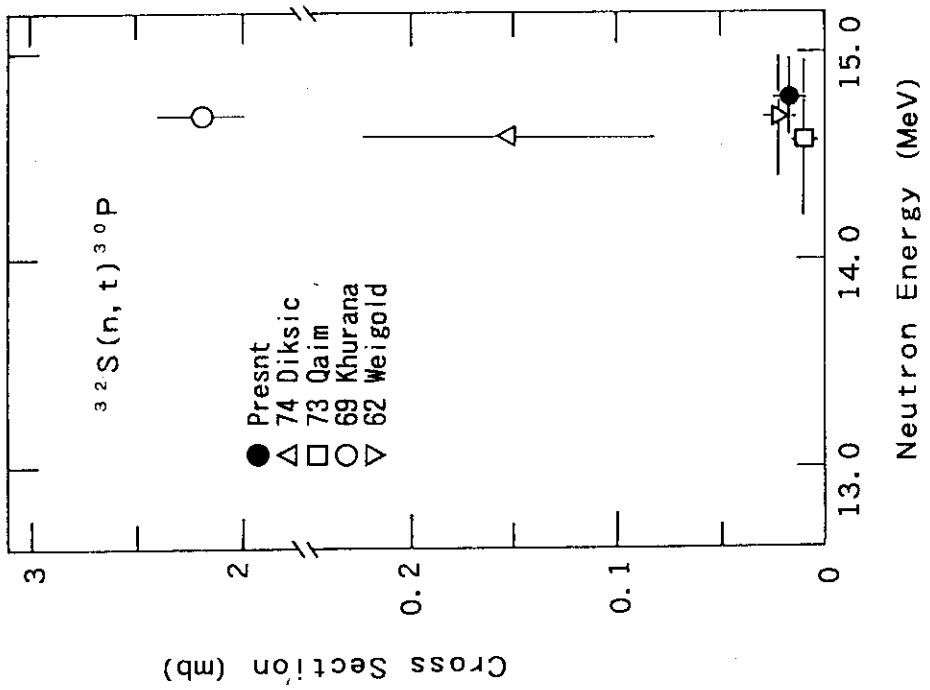

Fig. 12.14 Cross section of $^{32}S(n,t)^{30}P$.

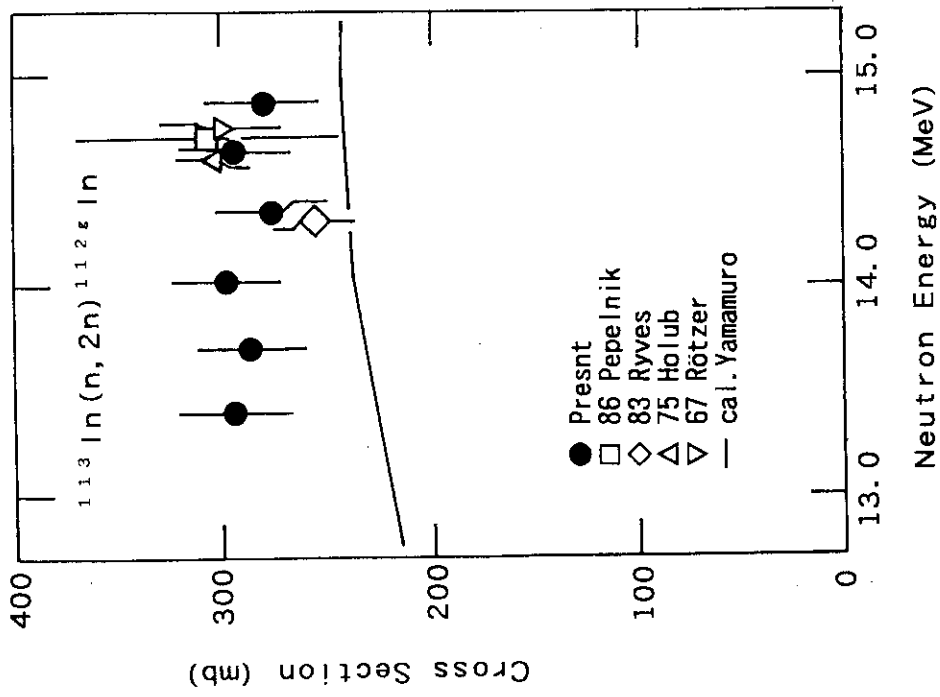

Fig. 12.13 Cross section of $^{113}In(n,2n)^{112g}In$.

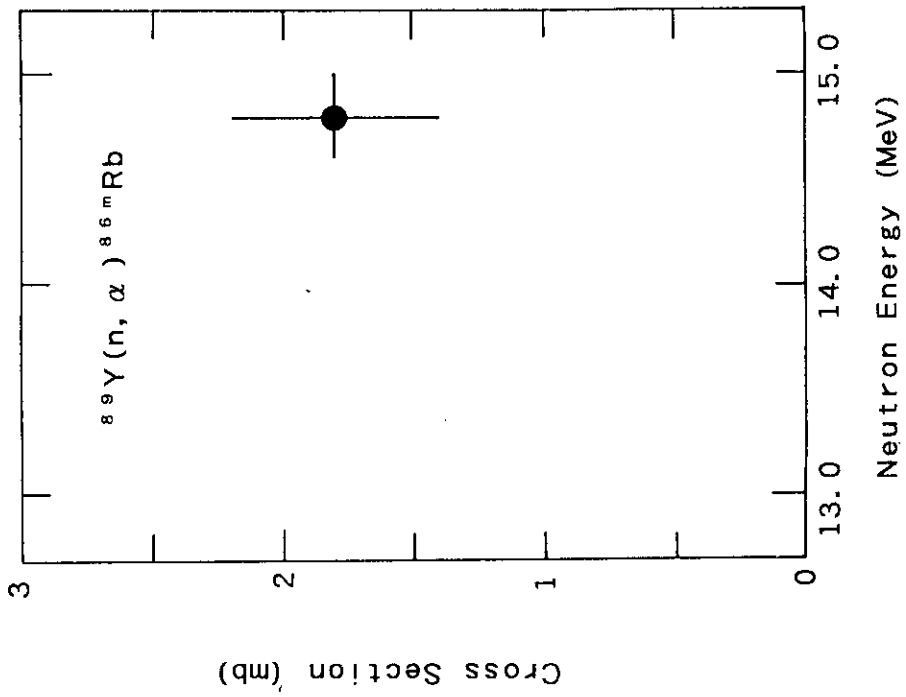

Fig. 12.16 Cross section of $^{89}Y(n,\alpha)^{86m}Rb$.

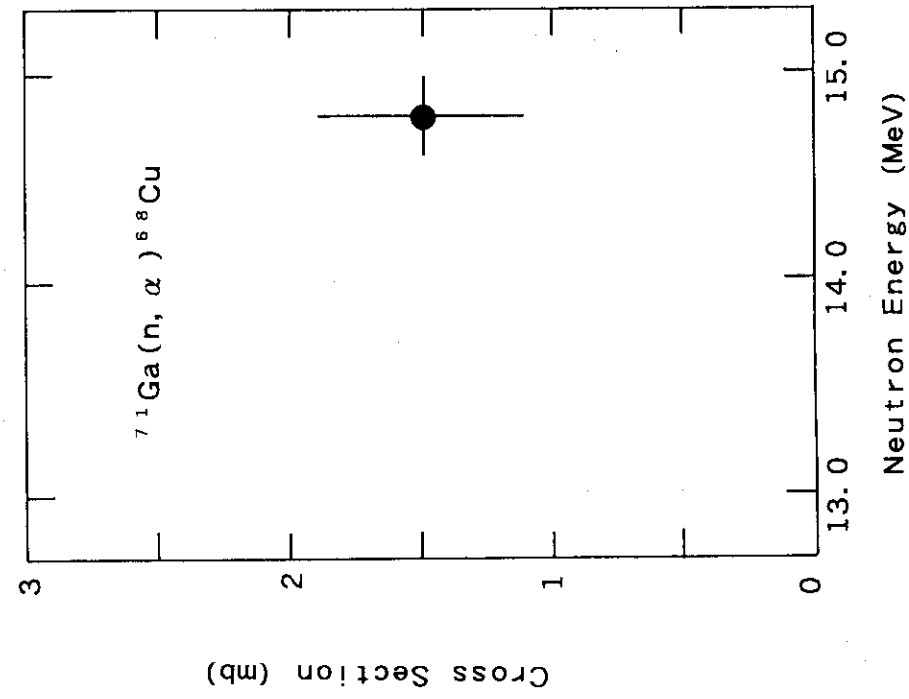

Fig. 12.15 Cross section of $^{71}Ga(n,\alpha)^{68}Cu$.

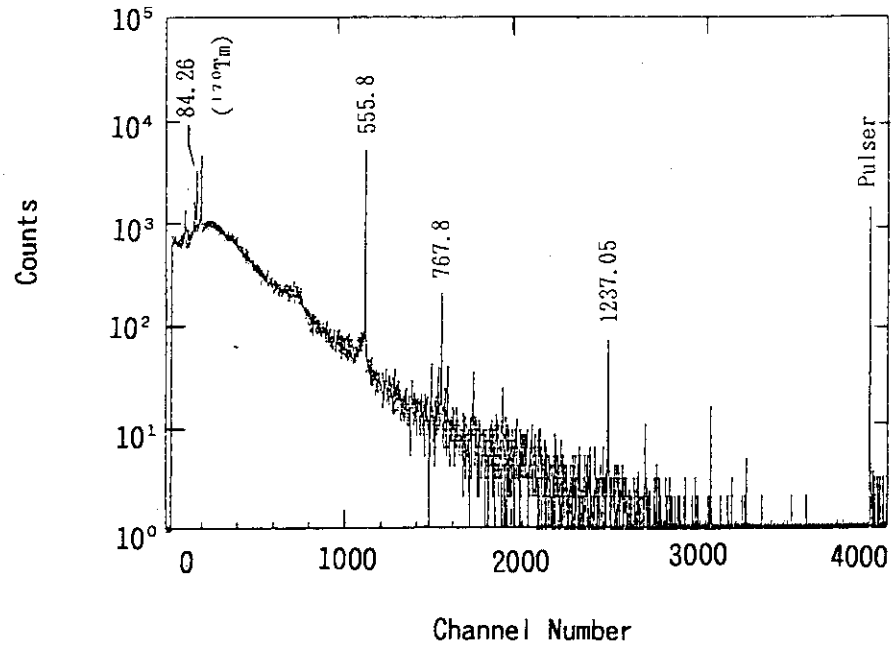

Fig. 13 Gamma-ray spectrum in the decay of ^{104m}Rh. Gamma-rays from ^{170}Tm and pulses were simultaneously measured for the correction of pile-up losses.

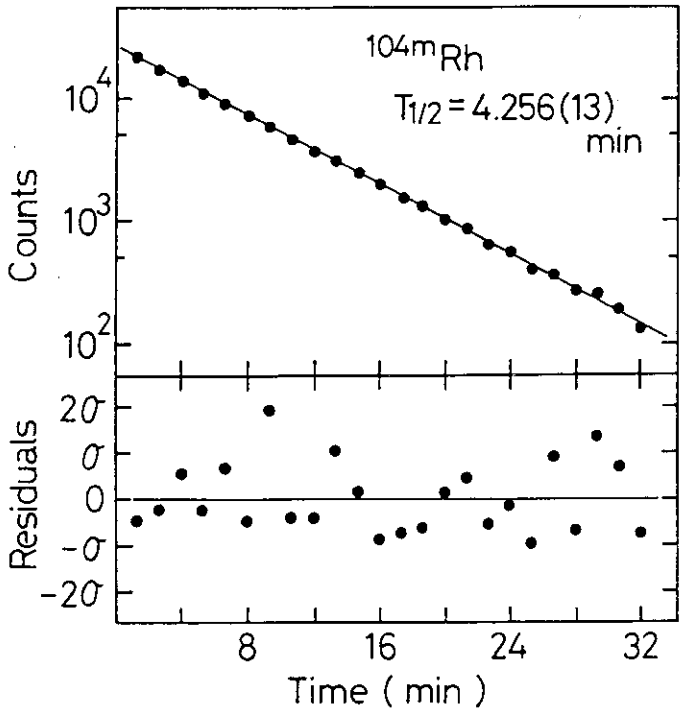

Fig. 14 Decay curve of 4.3m ^{104}Rh and residuals obtained from a least quares fitting analysis.

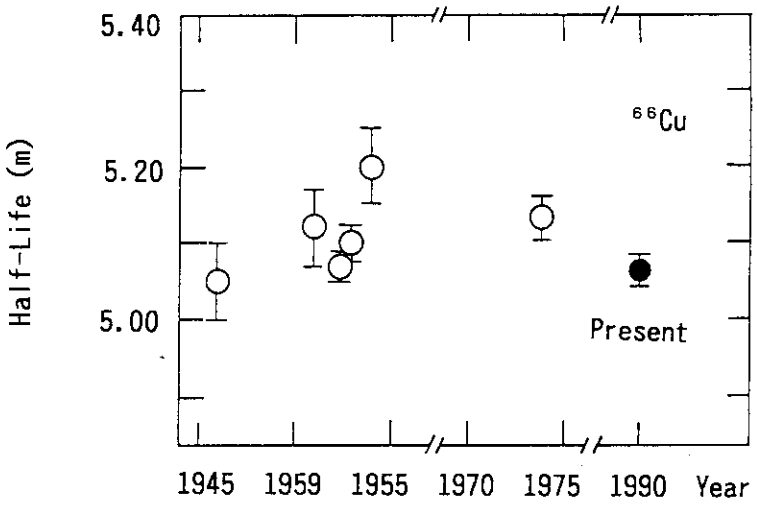

Fig. 15.1 Half-life of ^{66}Cu. Previous works are taken from ref. 7.

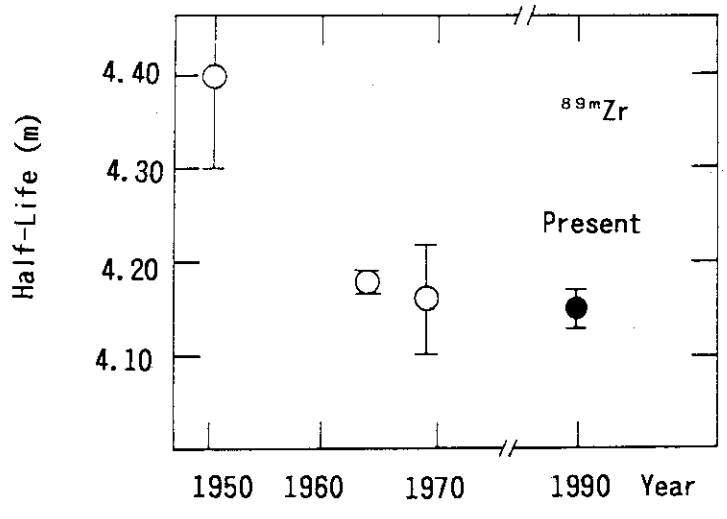

Fig. 15.2 Half-life of ^{89m}Zr.

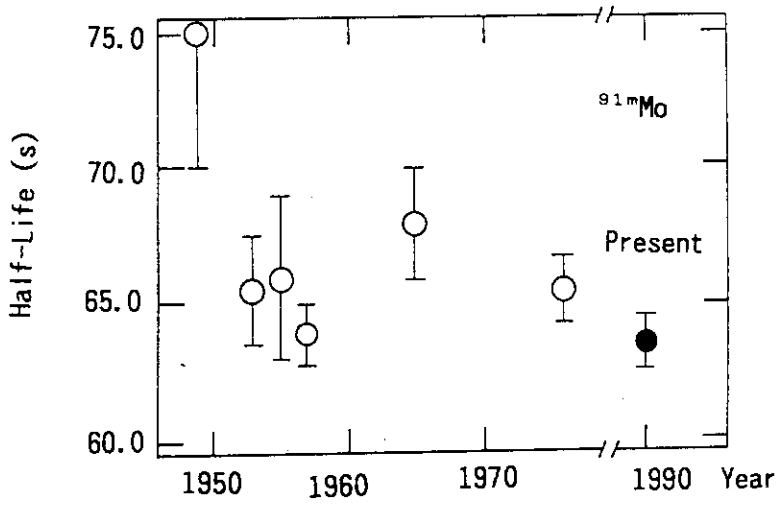

Fig. 15.3 Half-life of ^{91m}Mo.

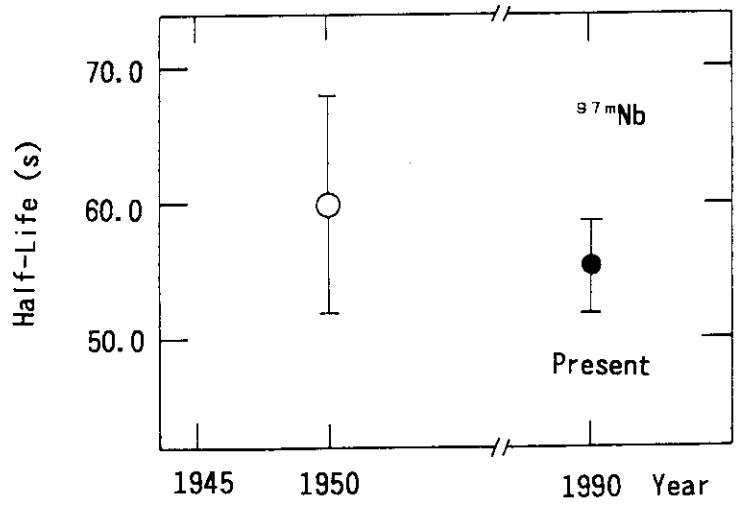

Fig. 15.4 Half-life of ^{97m}Nb.

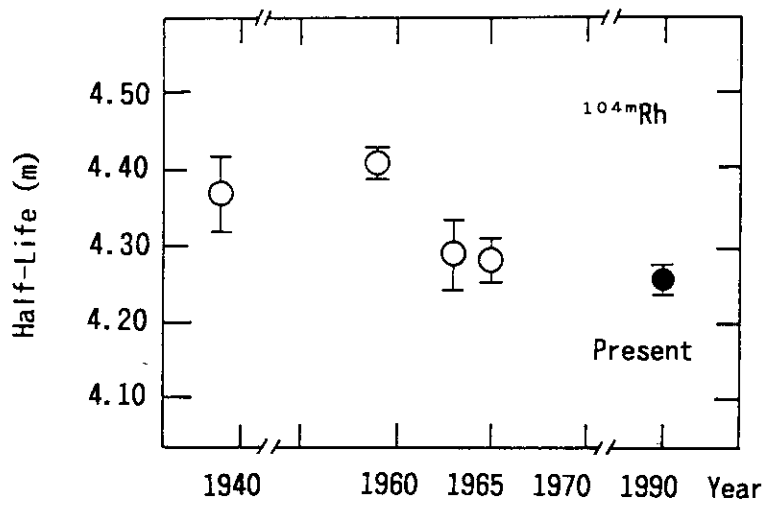

Fig. 15.5 Half-life of ^{104m}Rh.

Appendix 1 Neutron Flux as a Function of Target-to-Sample Distance

Neutron flux as a function of T-target-to-sample distance at OKTAVIAN. Fluxes were measured by using Al-foil of 10mm×10mm via $^{27}Al(n,\alpha)^{24}Na$ reaction. Calculations as a parameter of d^+-beam diameter are shown.

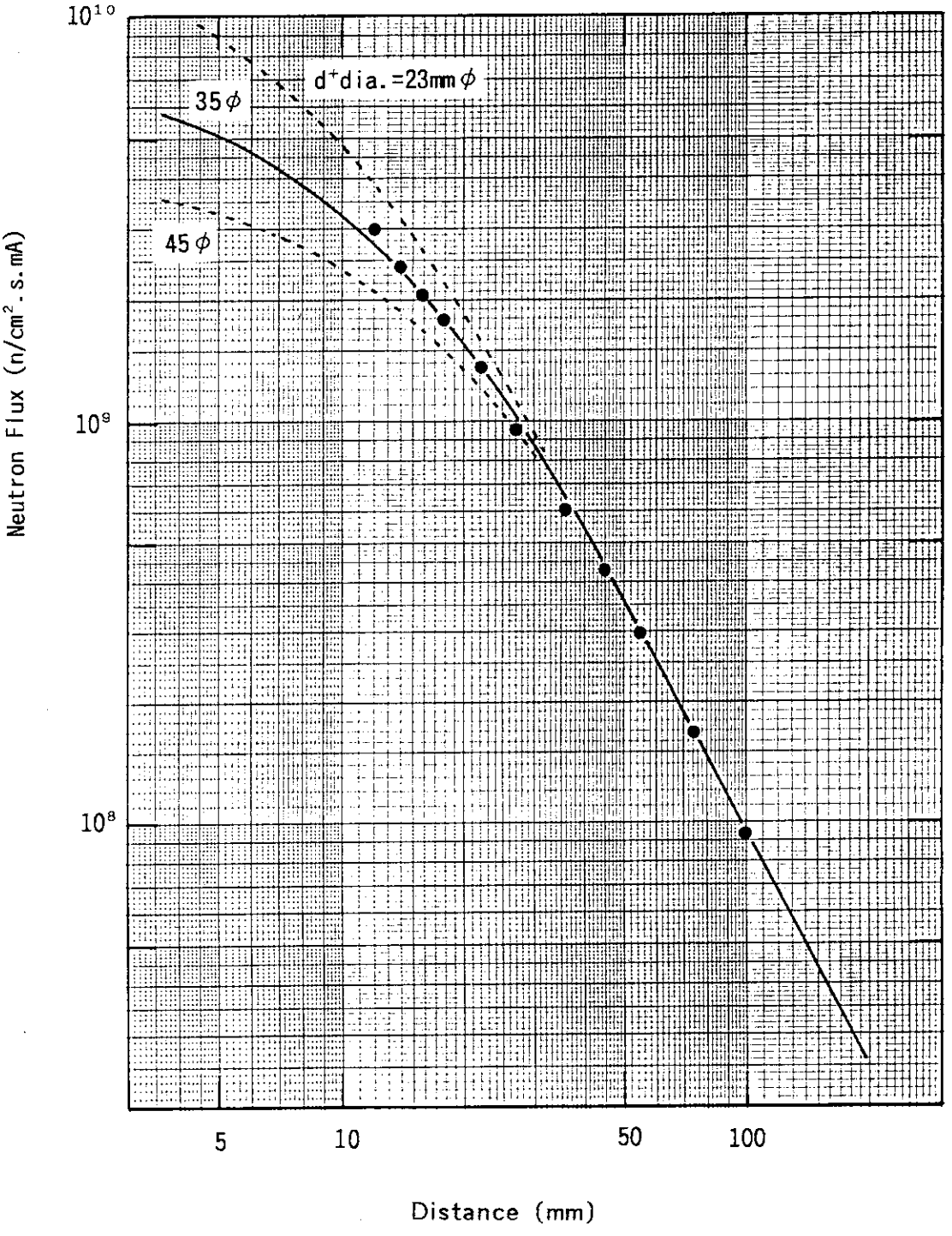

Appendix 2 Detection Efficiency of Ge Detector

Full-energy-peak detection efficiency of 12% HPGe detector with 10mm acrylic absorber at 5cm.

Fitting function

(1) 50 ~ 340 keV region ;

$$F_1 = A_1 + A_2 \cdot \{1-\exp(-A_3 \cdot E)\}\exp(-A_4 \cdot E) + A_5 \cdot \exp(-A_6 \cdot E)$$

$A_1 = -0.101071$, $A_2 = 0.105648$, $A_3 = 28.7187$

$A_4 = 0.0205795$, $A_5 = 0.030281$, $A_6 = 6.43981$

(2) 340 ~ 3000 keV region ;

$$F_2 = A_1 + A_2 \cdot \exp(-A_3 \cdot E) + A_4 \cdot \exp(-A_5 \cdot E) + A_6 \cdot \exp(-A_7 \cdot E)$$

$A_1 = 4.97202 \times 10^{-4}$, $A_2 = 3.86987 \times 10^{-3}$, $A_3 = 0.799341$,

$A_4 = 2.82847 \times 10^{-2}$, $A_5 = 8.62519$, $A_6 = 7.4166 \times 10^{-3}$

$A_7 = 3.47737$

Gamma-ray energy(E) in MeV , Efficiency(F) in % .

Appendix 3 Gamma-ray Spectra of Samples Irradiated by 14.9 MeV Neutrons

Gamma-ray spectra of samples irradiated by 14.9 MeV neutrons are given in Figs. A.3.1 ~ 30.

EXPLANATION

Sample: ^{26}MgO(99.55%)	⇒ ①
Time: 180s-28s-180s	⇒ ②
●: ^{26}Mg(n, α)^{23}Ne	⇒ ③
Det.: 12% HPGe	⇒ ④
Distance: 0.5cm	⇒ ⑤

① Sample(enrichment % for separated isotope, nat.:sample of natural abundance)
② Irradiation time, cooling time, measurement time
③ Reaction
④ Detector. Usually Ge detectors are covered with 5mm acrylic absorber.
⑤ Source-to-detector distance.

* Gamma-ray energies are in keV. 511γ; 511keV annihilation γ-ray,
S.E.P.; single escape peak, D.E.P.; double escape peak.

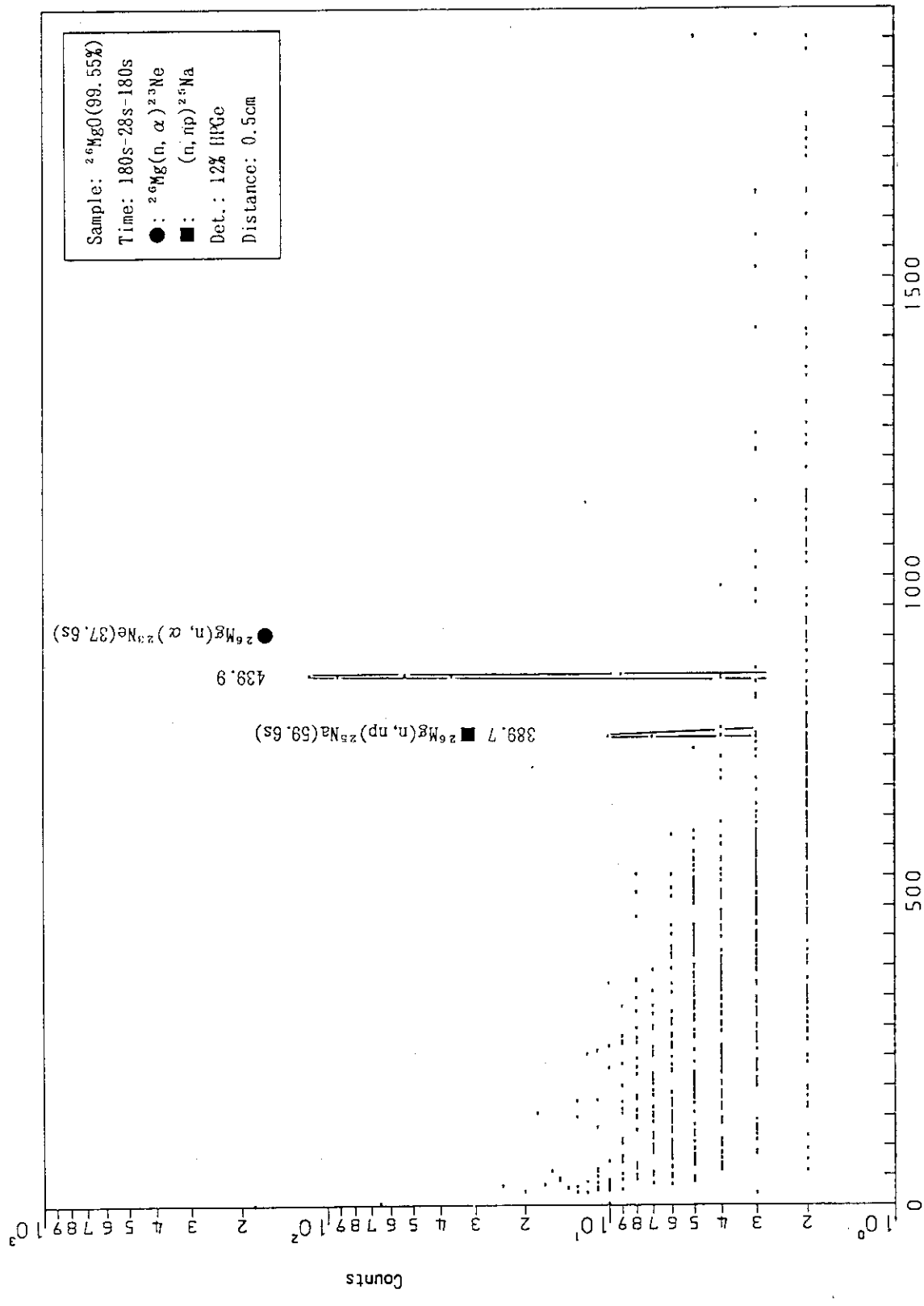
Sample: ^{26}MgO(99.55%)
Time: 180s-28s-180s
●: ^{26}Mg(n, α)^{23}Ne
■: (n, np)^{25}Na
Det.: 12% HPGe
Distance: 0.5cm
●^{26}Mg(n, α)^{23}Ne(37.6s)
439.9
389.7 ■^{26}Mg(n, np)^{25}Na(59.6s)
Counts
Channel Number
0
500
1000
1500

Fig. A.3.1

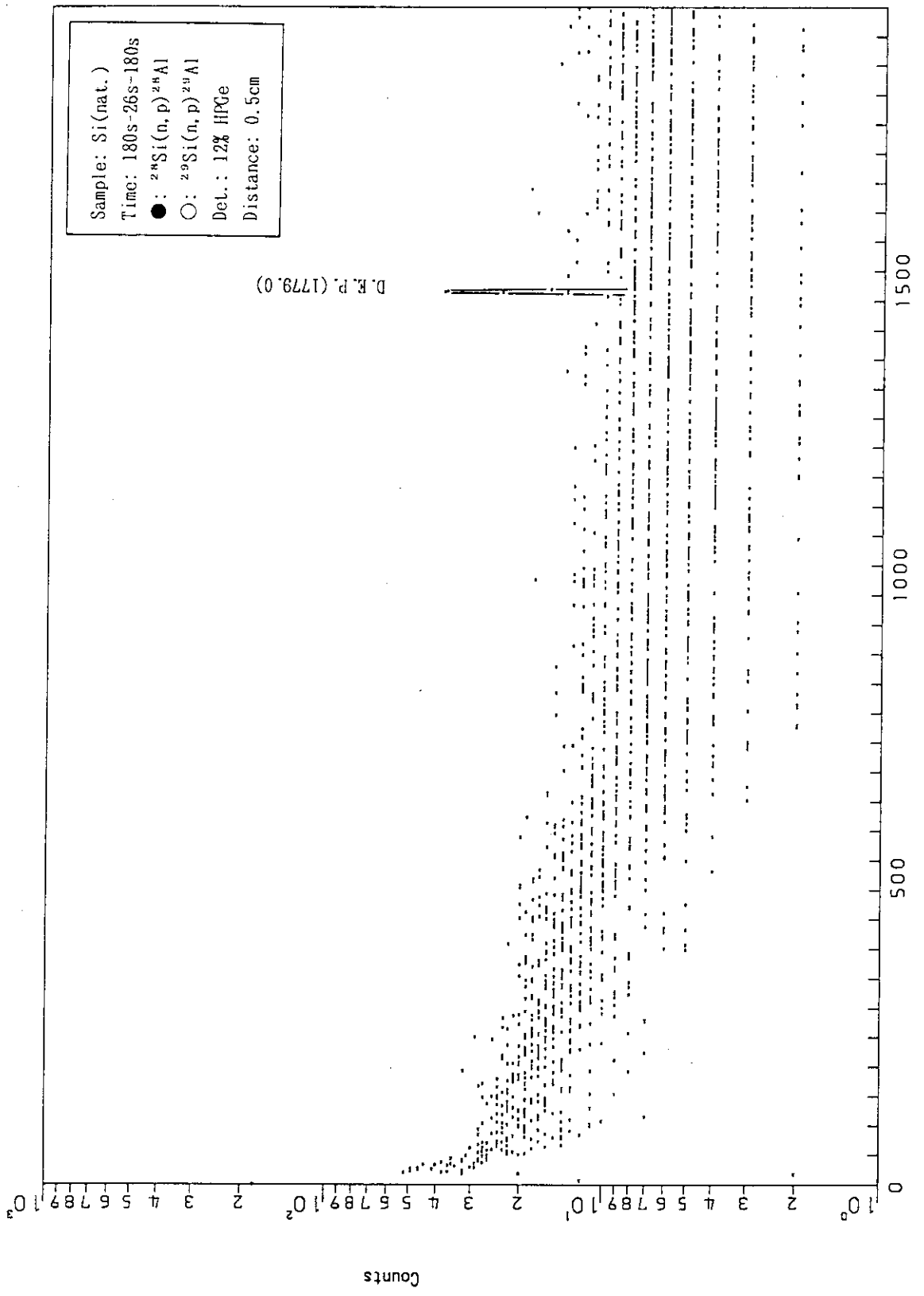
Sample: Si(nat.)
Time: 180s-26s-180s
●: $^{28}Si(n,p)^{28}Al$
○: $^{29}Si(n,p)^{29}Al$
Det.: 12% HPGe
Distance: 0.5cm
D.E.P.(1779.0)
Counts
Channel Number
0
500
1000
1500

Fig. A.3.2

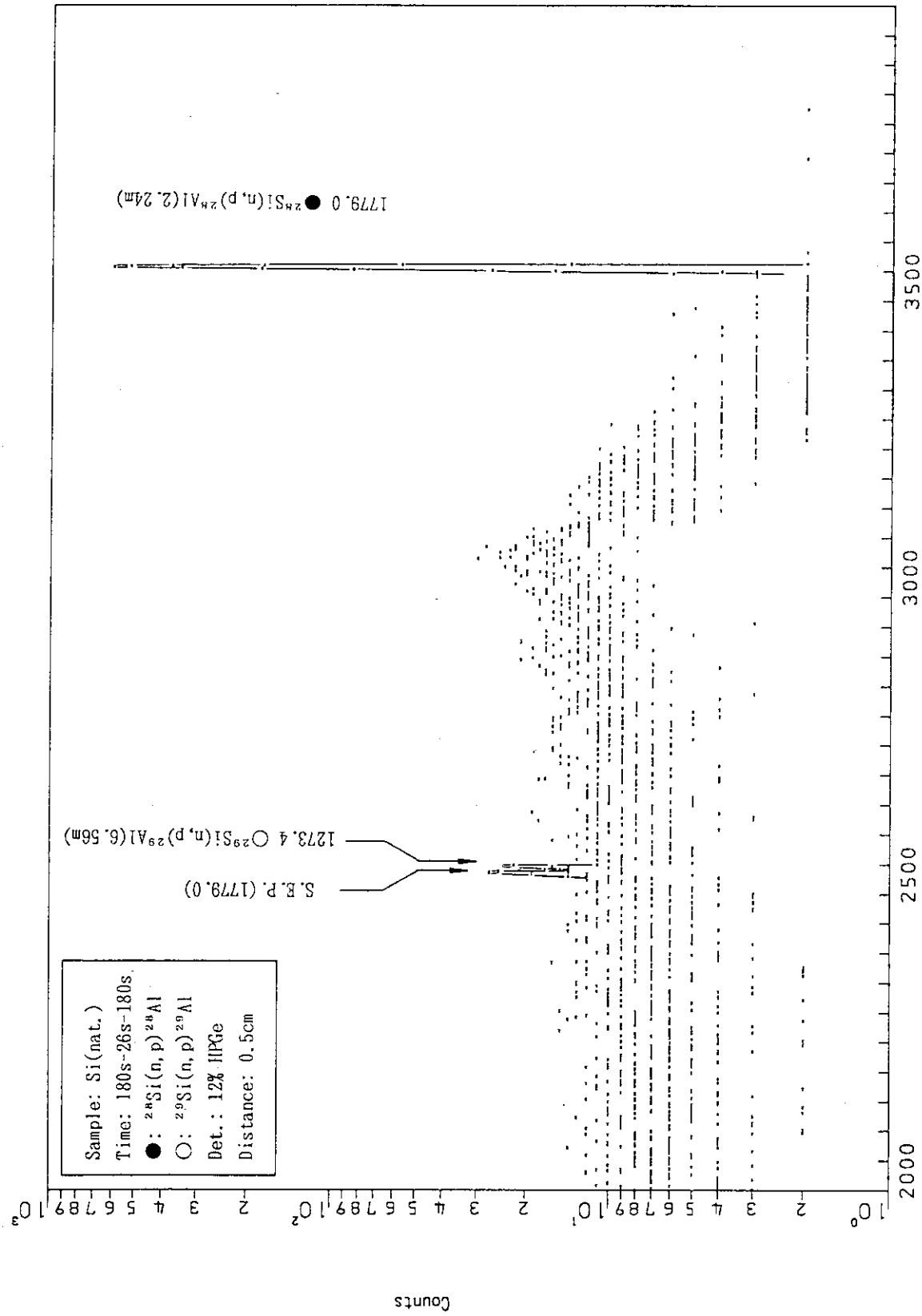
Sample: Si(nat.)
Time: 180s-26s-180s
●: ²⁸Si(n,p)²⁸Al
○: ²⁹Si(n,p)²⁹Al
Det.: 12% HPGe
Distance: 0.5cm
S.E.P.(1779.0)
1273.4 ○²⁹Si(n,p)²⁹Al(6.56m)
1779.0 ●²⁸Si(n,p)²⁸Al(2.24m)
Counts
Channel Number

Fig. A.3.3

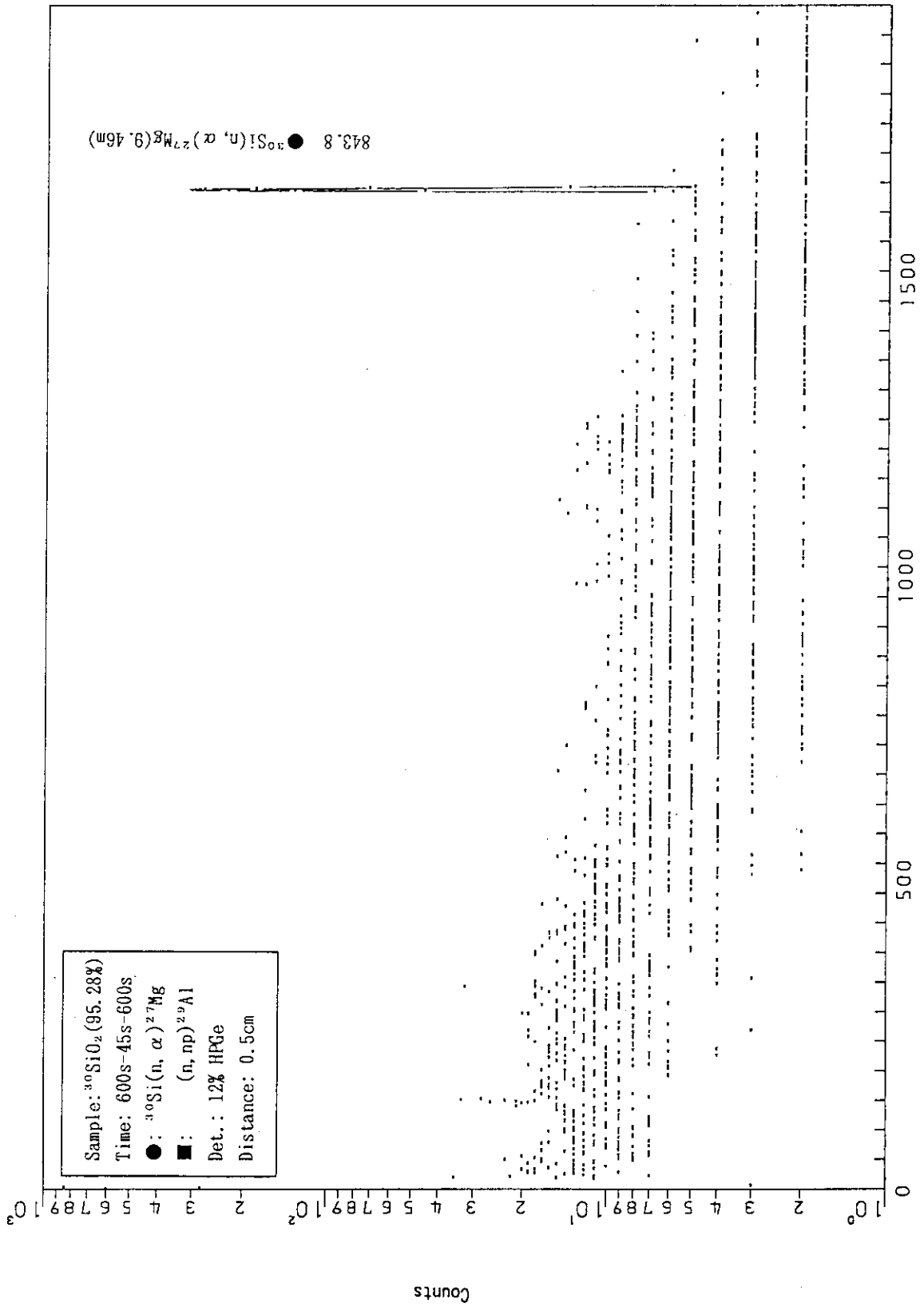
Sample: $^{30}SiO_2$(95.28%)
Time: 600s-45s-600s
●: $^{30}Si(n,\alpha)^{27}Mg$
■: $(n,np)^{29}Al$
Det.: 12% HPGe
Distance: 0.5cm
843.8 ●$^{30}Si(n,\alpha)^{27}Mg$(9.45m)
Counts
Channel Number
0
500
1000
1500
10^0
10^1
10^2
10^3

Fig. A.3.4

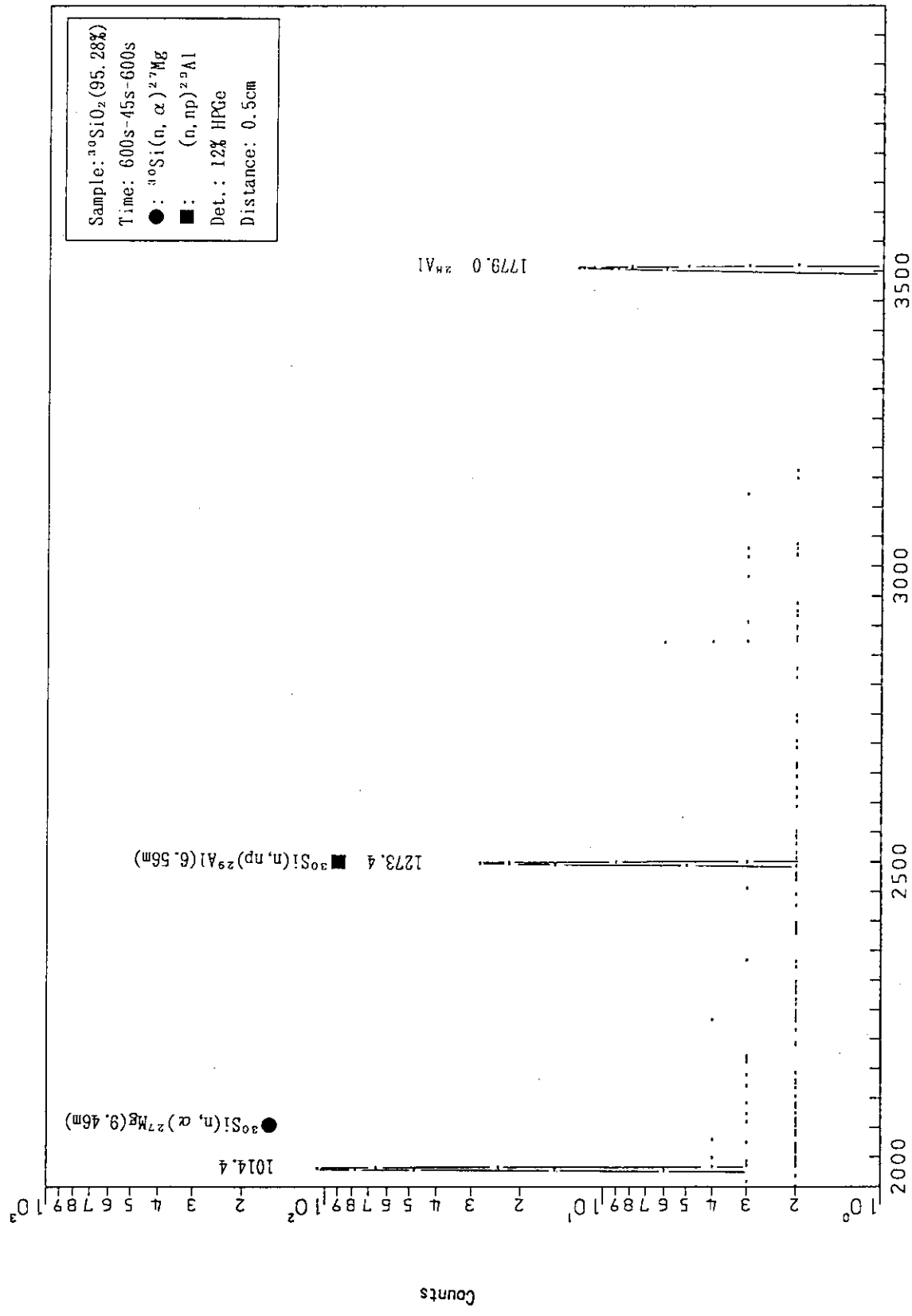
Sample: $^{30}SiO_2$(95.28%)
Time: 600s-45s-600s
●: $^{30}Si(n,\alpha)^{27}Mg$
■: $(n,np)^{29}Al$
Det.: 12% HPGe
Distance: 0.5cm
1014.4
●$^{30}Si(n,\alpha)^{27}Mg$(9.46m)
1273.4 ■$^{30}Si(n,np)^{29}Al$(6.56m)
1779.0 ^{28m}Al
Counts
Channel Number

Fig. A.3.5

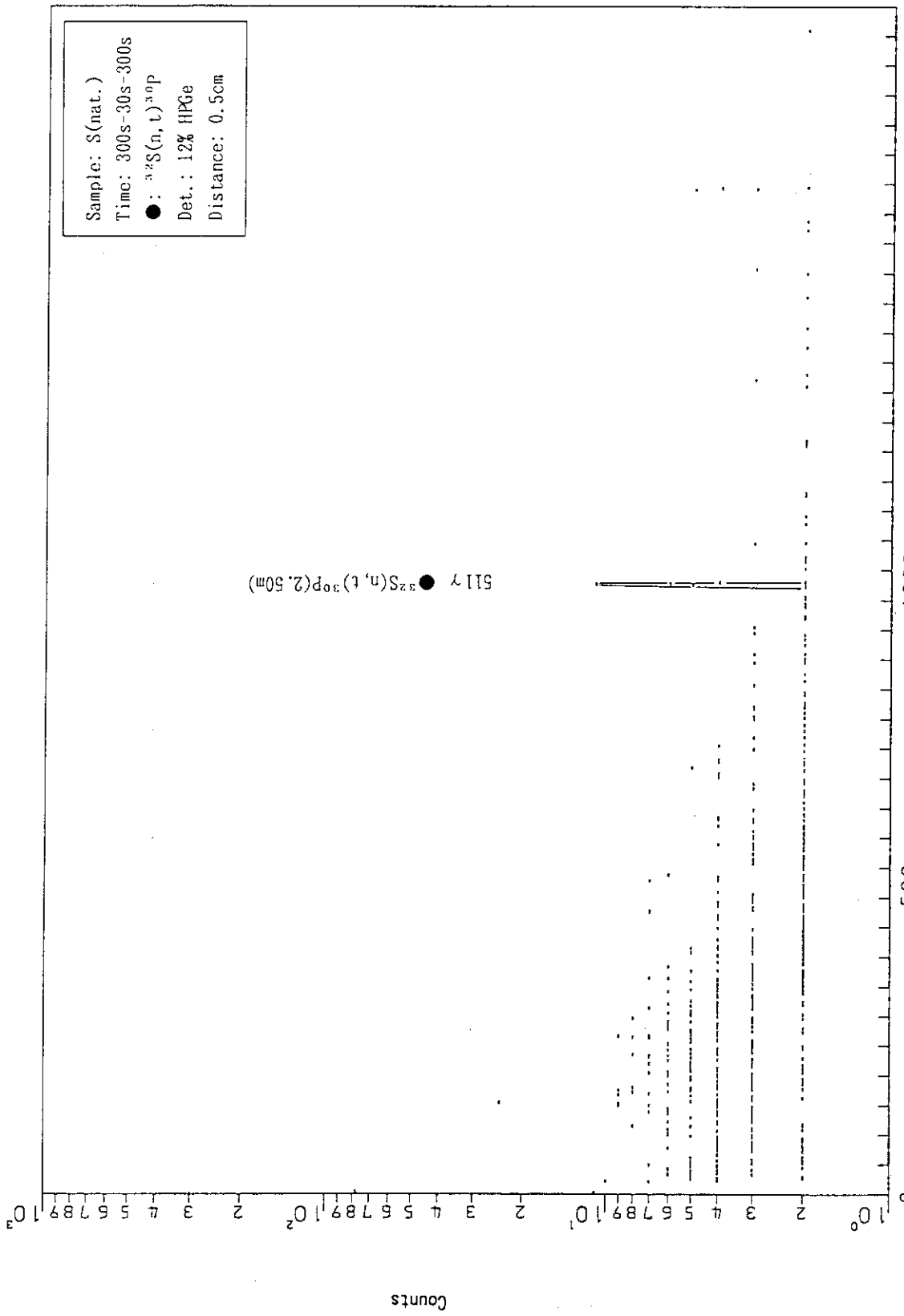
Sample: S(nat.)
Time: 300s-30s-300s
●: $^{32}S(n,t)^{30}P$
Det.: 12% HPGe
Distance: 0.5cm
511γ ●$^{32}S(n,t)^{30}P(2.50m)$
Counts
Channel Number
0
500
1000
1500
10^0
10^1
10^2
10^3

Fig. A.3.6

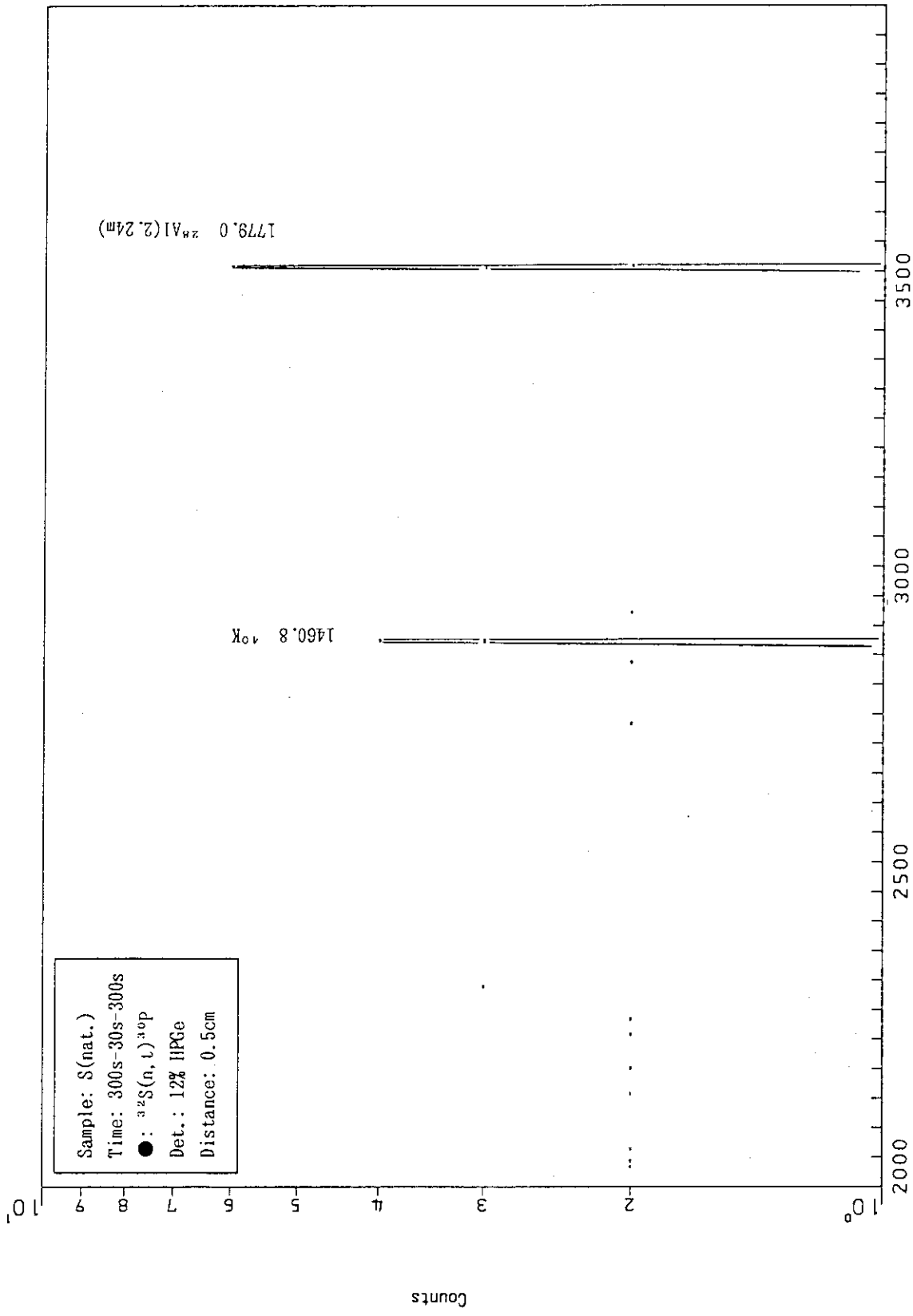
Sample: S(nat.)
Time: 300s-30s-300s
●: $^{32}S(n,t)^{30}P$
Det.: 12% HPGe
Distance: 0.5cm
1460.8 ^{40}K
1779.0 $^{28}Al(2.24m)$
Counts
Channel Number

Fig. A.3.7

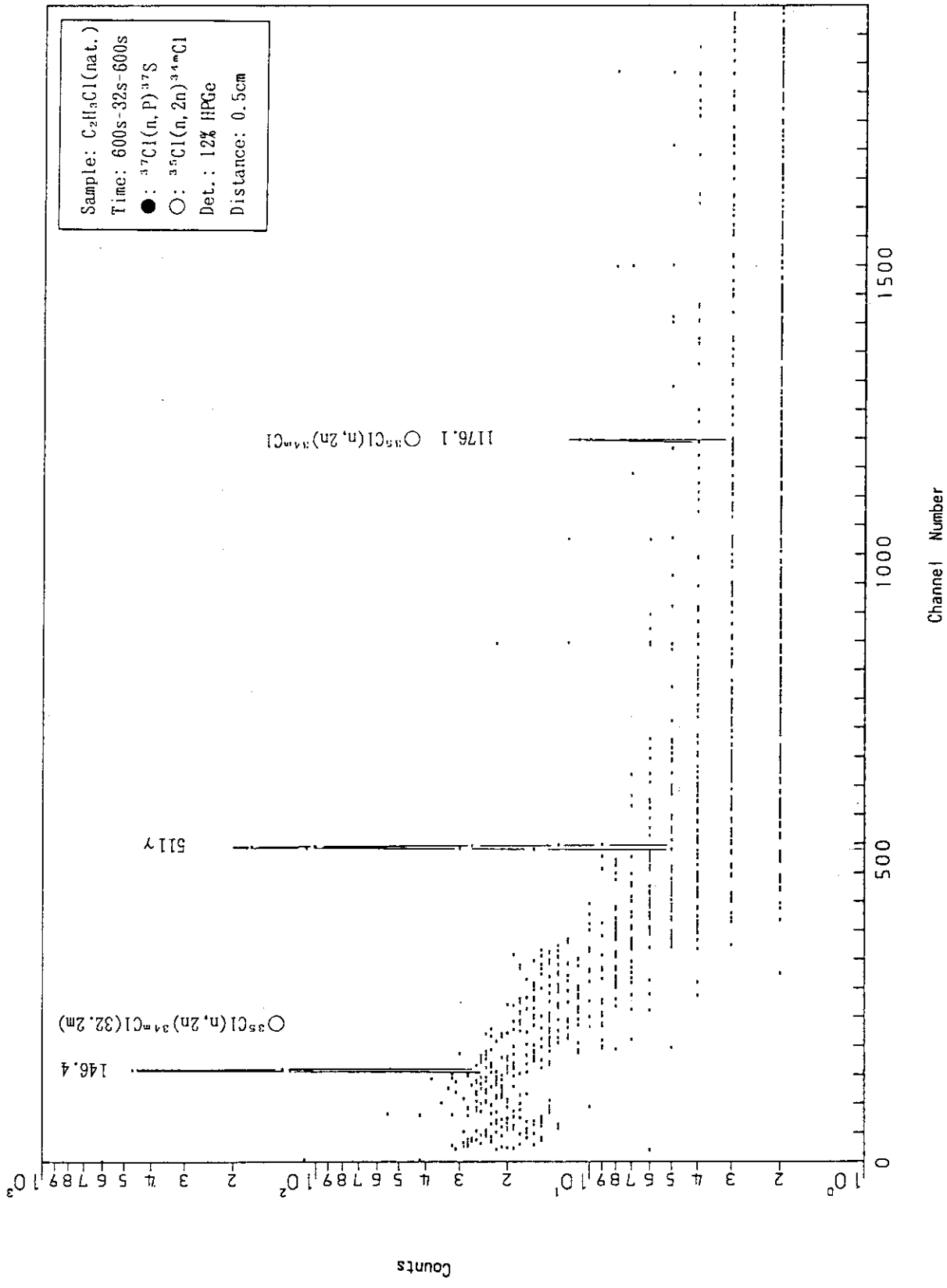
Sample: C_2H_3Cl(nat.)
Time: 600s-32s-600s
●: $^{37}Cl(n,P)^{37}S$
○: $^{35}Cl(n,2n)^{34m}Cl$
Det.: 12% HPGe
Distance: 0.5cm
146.4
○$^{35}Cl(n,2n)^{34m}Cl$(32.2m)
511γ
1176.1 ○$^{35}Cl(n,2n)^{34m}Cl$
Counts
Channel Number
0
500
1000
1500

Fig. A.3.8

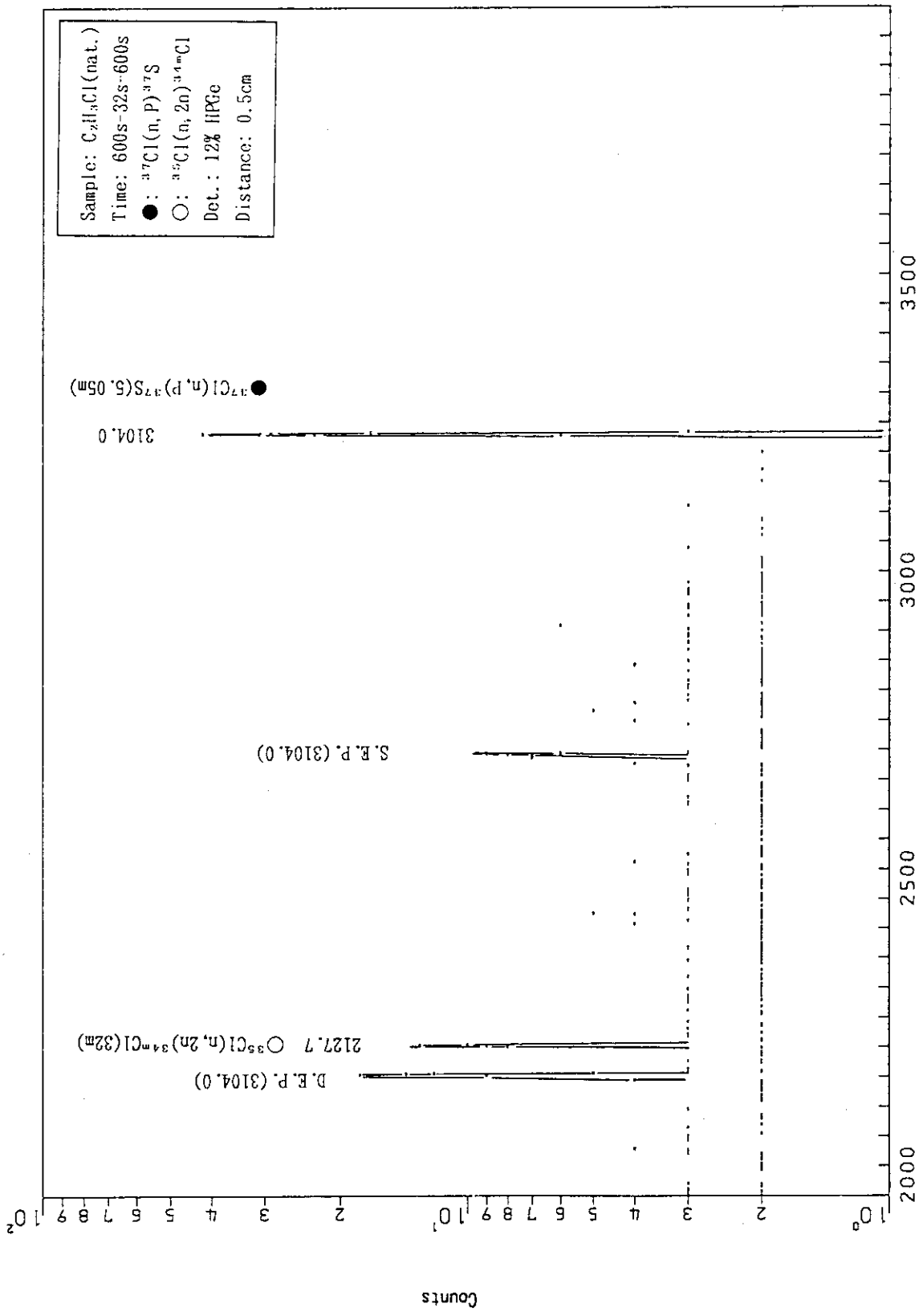
Sample: C_2H_3Cl(nat.)
Time: 600s-32s-600s
●: $^{37}Cl(n,P)^{37}S$
○: $^{35}Cl(n,2n)^{34m}Cl$
Det.: 12% HPGe
Distance: 0.5cm
●$^{37}Cl(n,p)^{37}S(5.05m)$
3104.0
S.E.P.(3104.0)
D.E.P.(3104.0)
2127.7 ○$^{35}Cl(n,2n)^{34m}Cl(32m)$
Counts
Channel Number

Fig. A.3.9

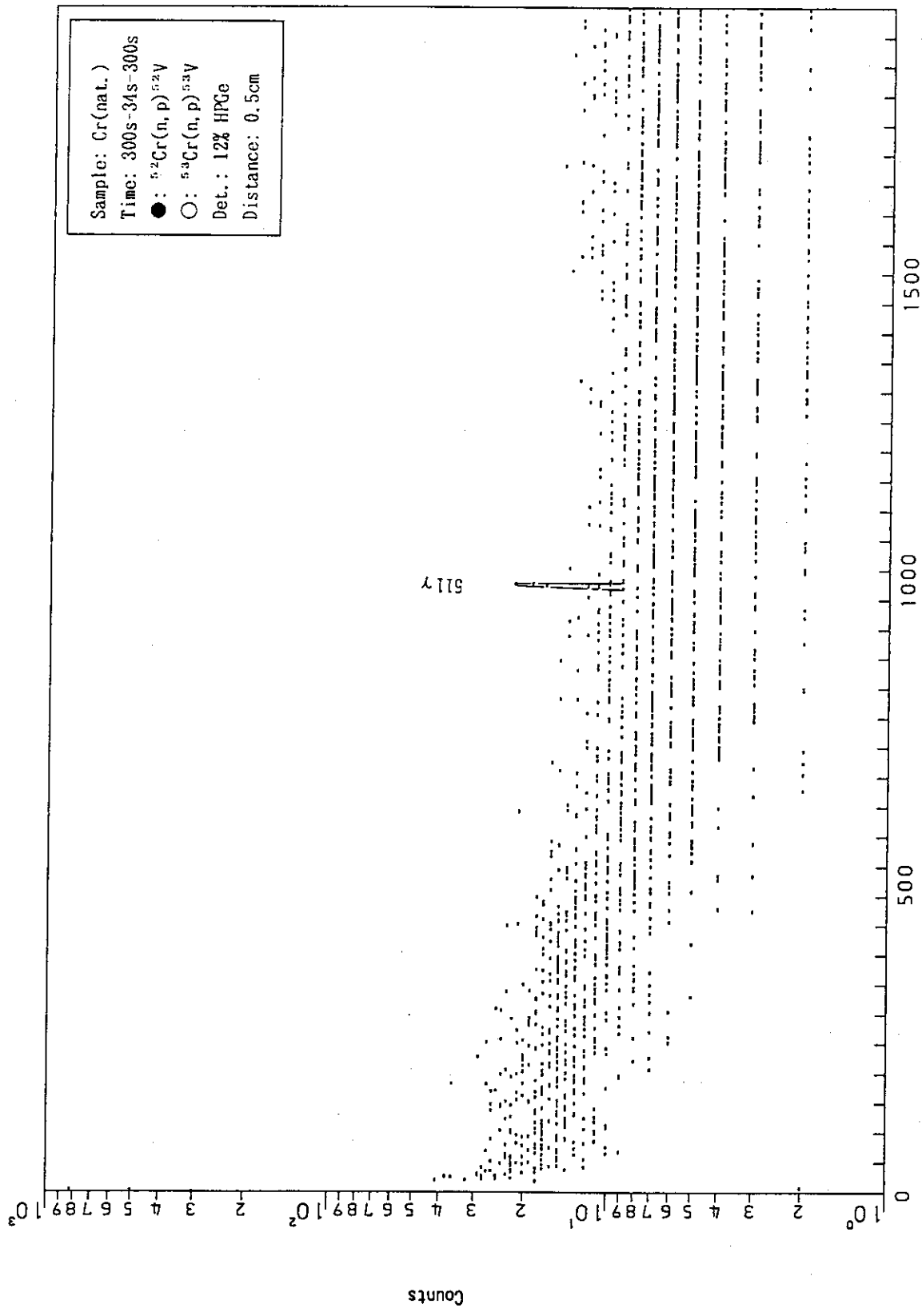
Sample: Cr(nat.)
Time: 300s-34s-300s
●: $^{52}Cr(n,p)^{52}V$
○: $^{53}Cr(n,p)^{53}V$
Det.: 12% HPGe
Distance: 0.5cm
511γ
Counts
Channel Number
0
500
1000
1500

Fig. A.3.10

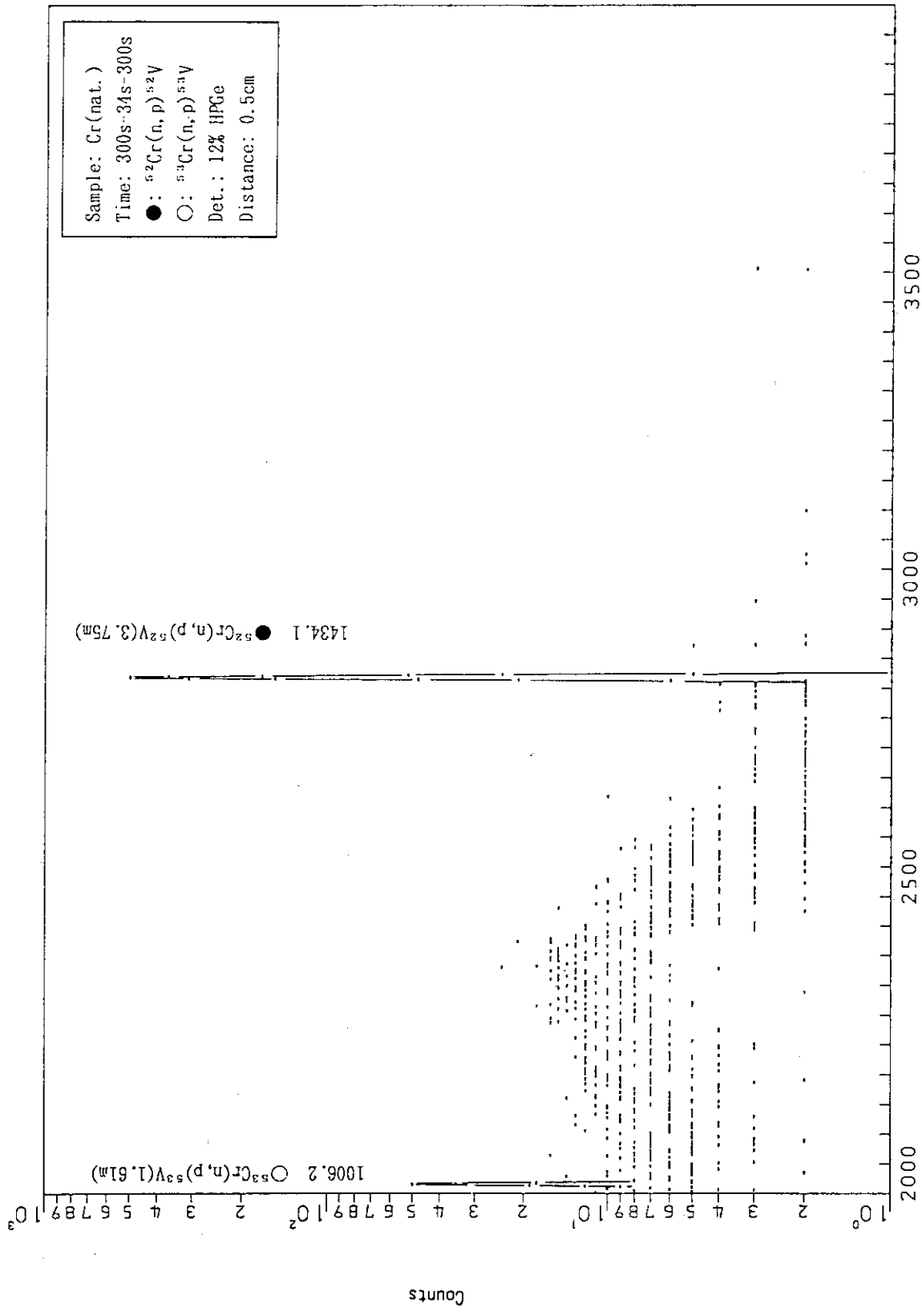
Sample: Cr(nat.)
Time: 300s-34s-300s
●: $^{52}Cr(n,p)^{52}V$
○: $^{53}Cr(n,p)^{53}V$
Det.: 12% HPGe
Distance: 0.5cm
1006.2 ○$^{53}Cr(n,p)^{53}V$(1.61m)
1434.1 ●$^{52}Cr(n,p)^{52}V$(3.75m)
Counts
Channel Number

Fig. A.3.11

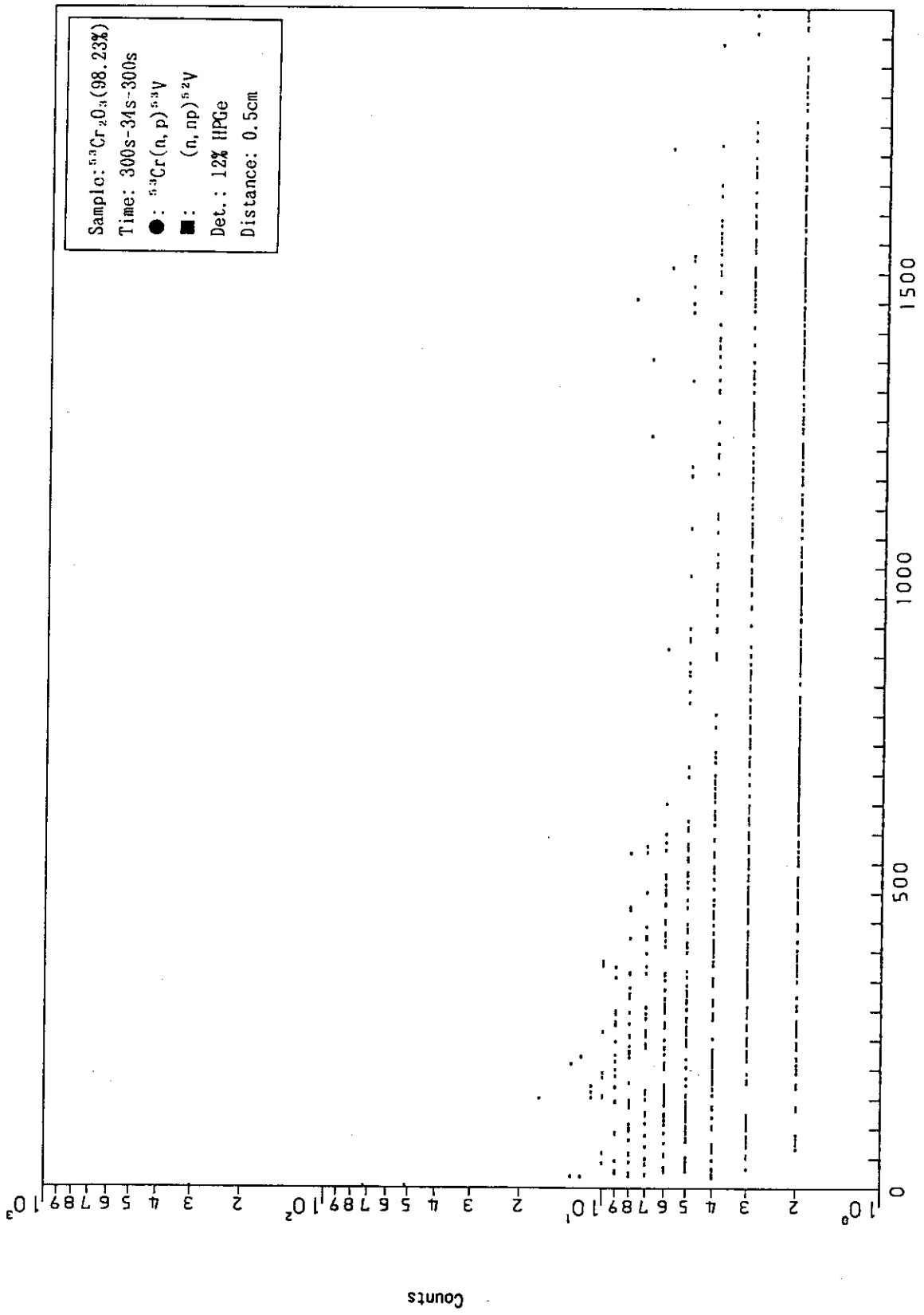
Sample: $^{53}Cr_2O_3$(98.23%)
Time: 300s-34s-300s
●: $^{53}Cr(n,p)^{53}V$
■: (n,np)^{52}V
Det.: 12% HPGe
Distance: 0.5cm
Counts
Channel Number
0
500
1000
1500

Fig. A.3.12

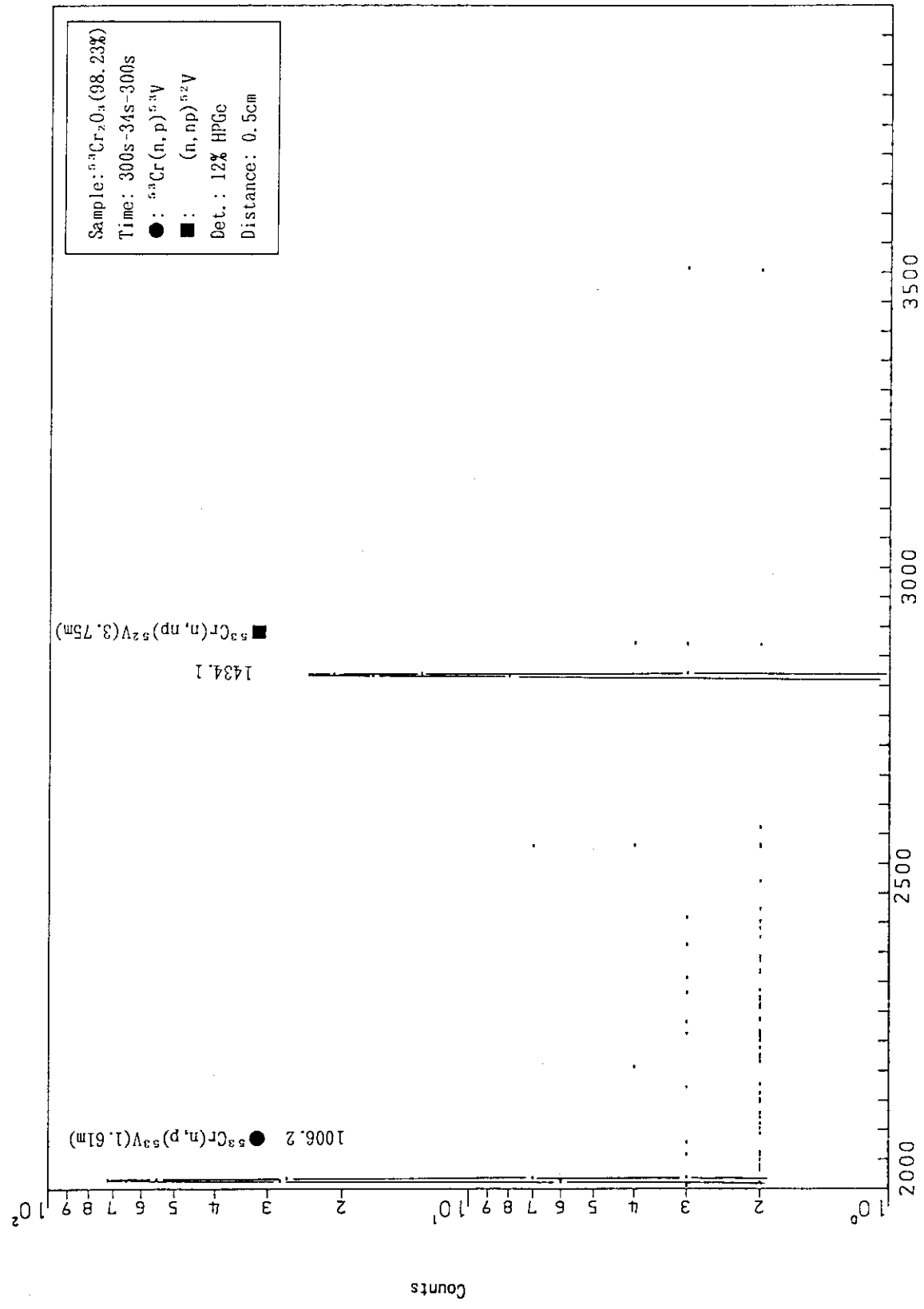
Sample: $^{53}Cr_2O_3$(98.23%)
Time: 300s-34s-300s
●: $^{53}Cr(n,p)^{53}V$
■: $(n,np)^{52}V$
Det.: 12% HPGe
Distance: 0.5cm
1006.2 ●$^{53}Cr(n,p)^{53}V$(1.61m)
1434.1
■$^{53}Cr(n,np)^{52}V$(3.75m)
Counts
Channel Number

Fig. A.3.13

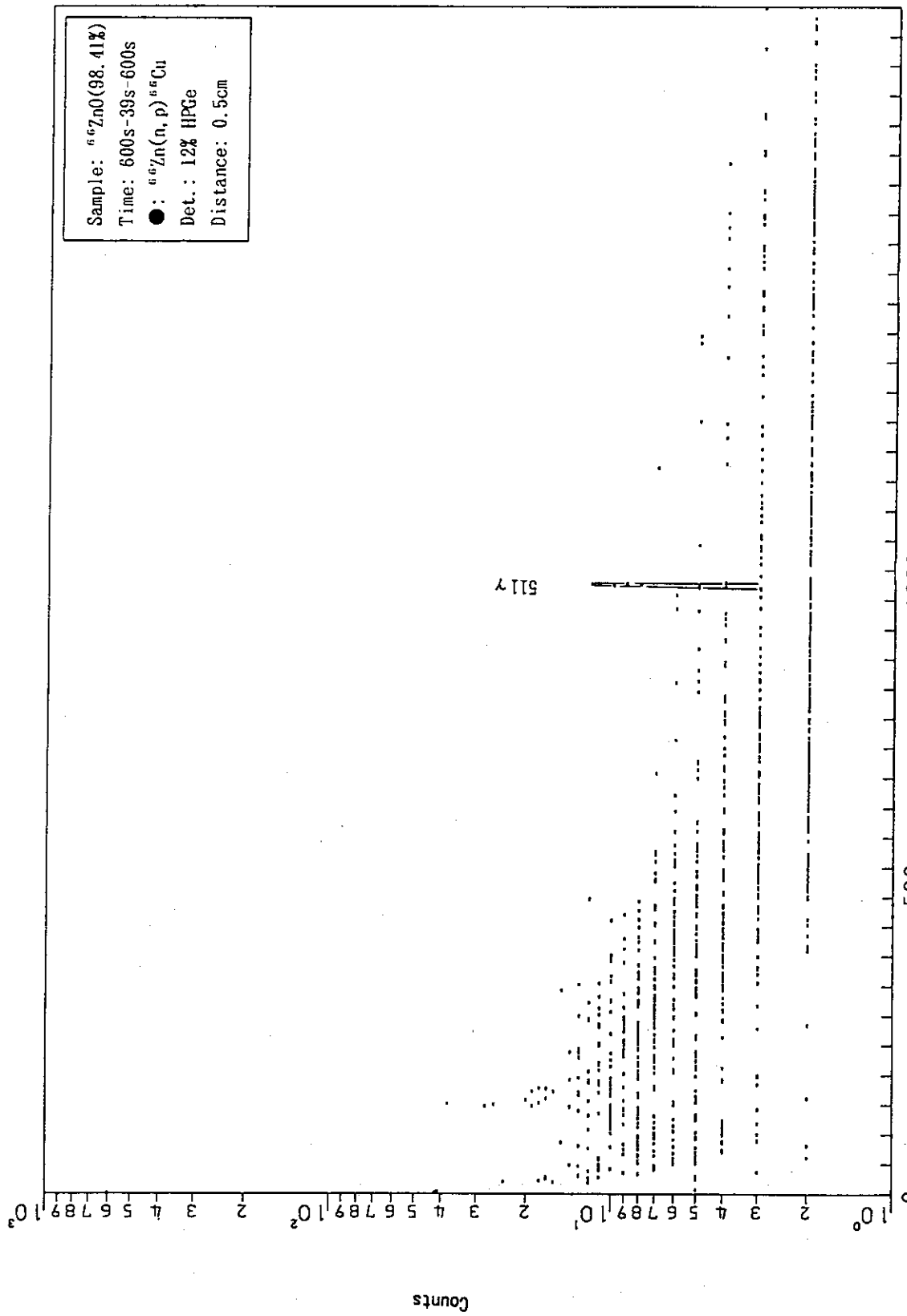
Sample: ^{66}ZnO(98.41%)
Time: 600s-39s-600s
●: ^{66}Zn(n,p)^{66}Cu
Det.: 12% HPGe
Distance: 0.5cm
511γ
Counts
Channel Number
0
500
1000
1500
10^{0}
10^{1}
10^{2}
10^{3}

Fig. A.3.14

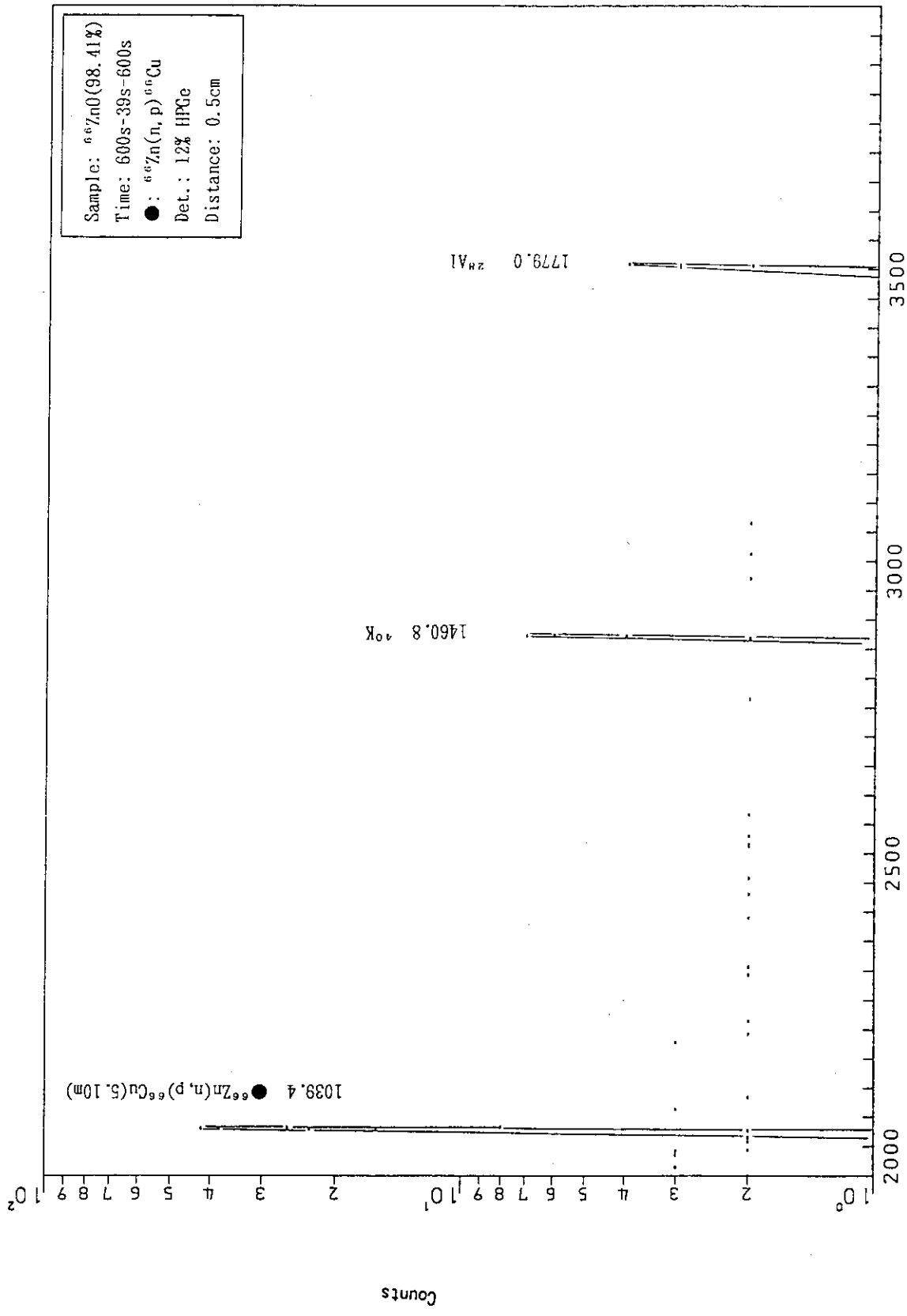
Sample: ^{66}ZnO(98.41%)
Time: 600s-39s-600s
●: ^{66}Zn(n,p)^{66}Cu
Det.: 12% HPGe
Distance: 0.5cm
1039.4 ●^{66}Zn(n,p)^{66}Cu(5.10m)
1460.8 ^{40}K
1779.0 ^{28}Al
Counts
Channel Number

Fig. A.3.15

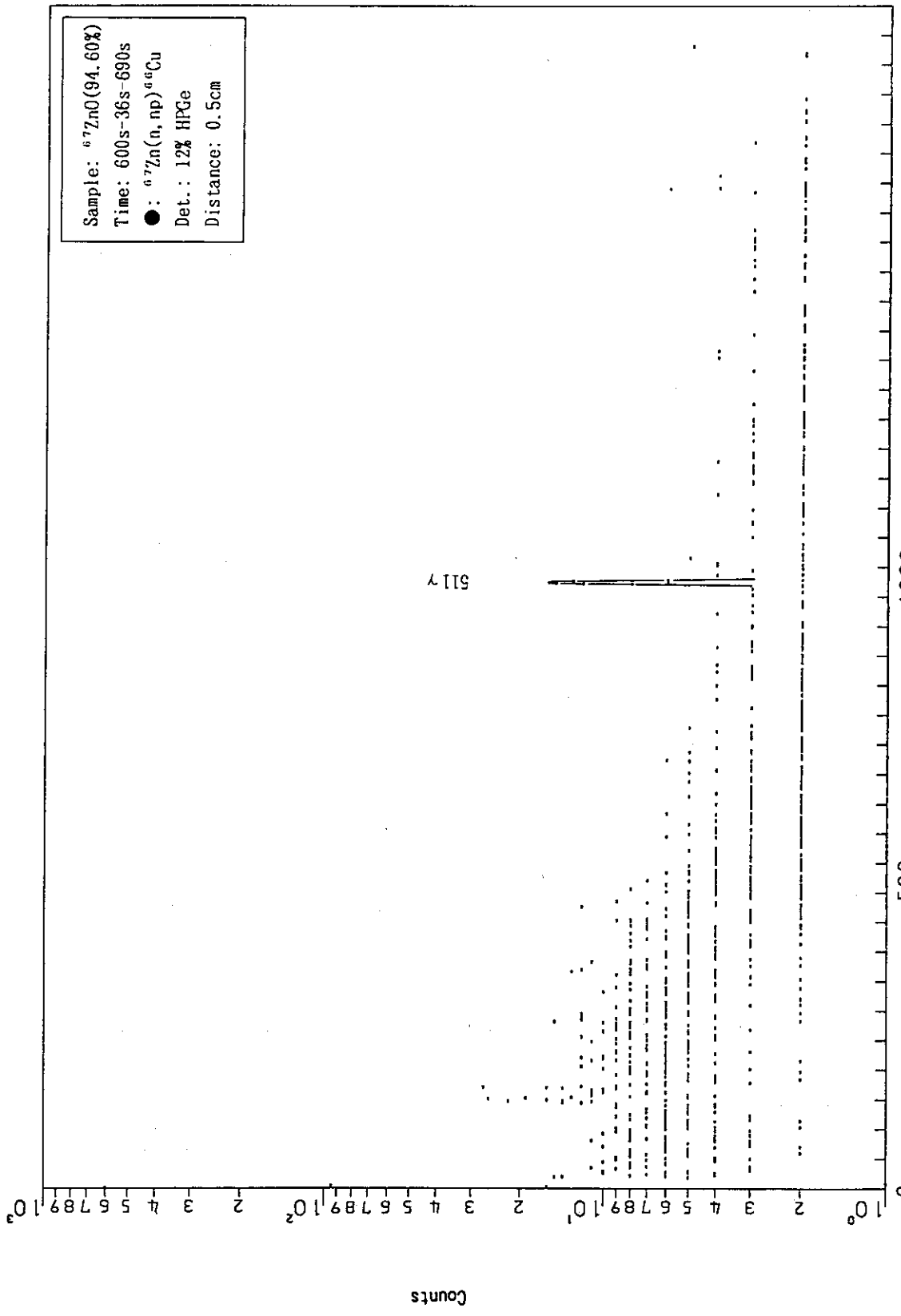
Sample: ^{67}ZnO(94.60%)
Time: 600s-36s-690s
●: ^{67}Zn(n,np)^{66}Cu
Det.: 12% HPGe
Distance: 0.5cm
511γ
Counts
Channel Number
0
500
1000
1500
10^0
10^1
10^2
10^3

Fig. A.3.16

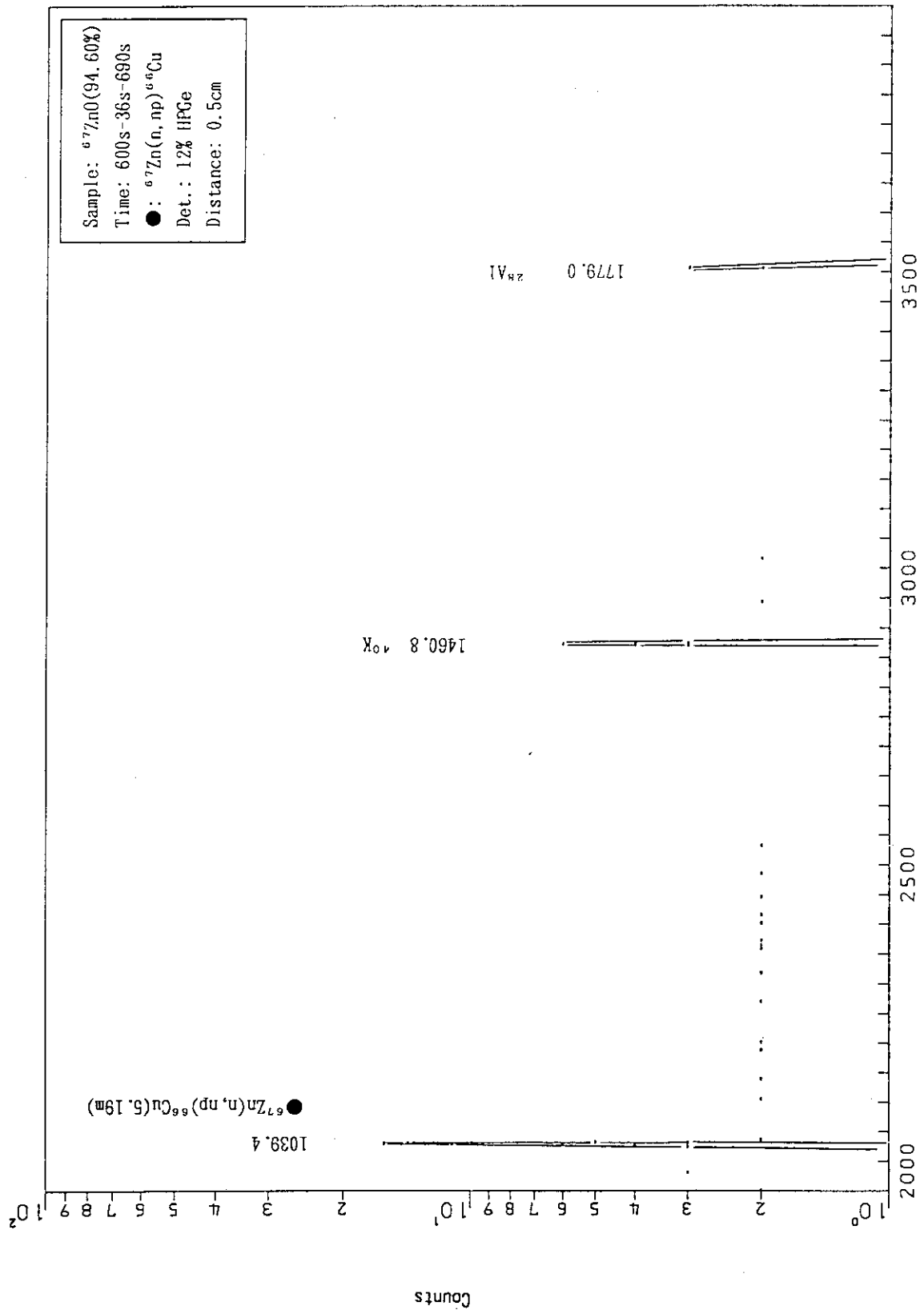
Sample: ^{67}ZnO(94.60%)
Time: 600s-36s-690s
●: ^{67}Zn(n,np)^{66}Cu
Det.: 12% HPGe
Distance: 0.5cm
1039.4
●^{67}Zn(n,np)^{66}Cu(5.19m)
1460.8 ^{40}K
1779.0 ^{28}Al
Counts
Channel Number

Fig. A.3.17

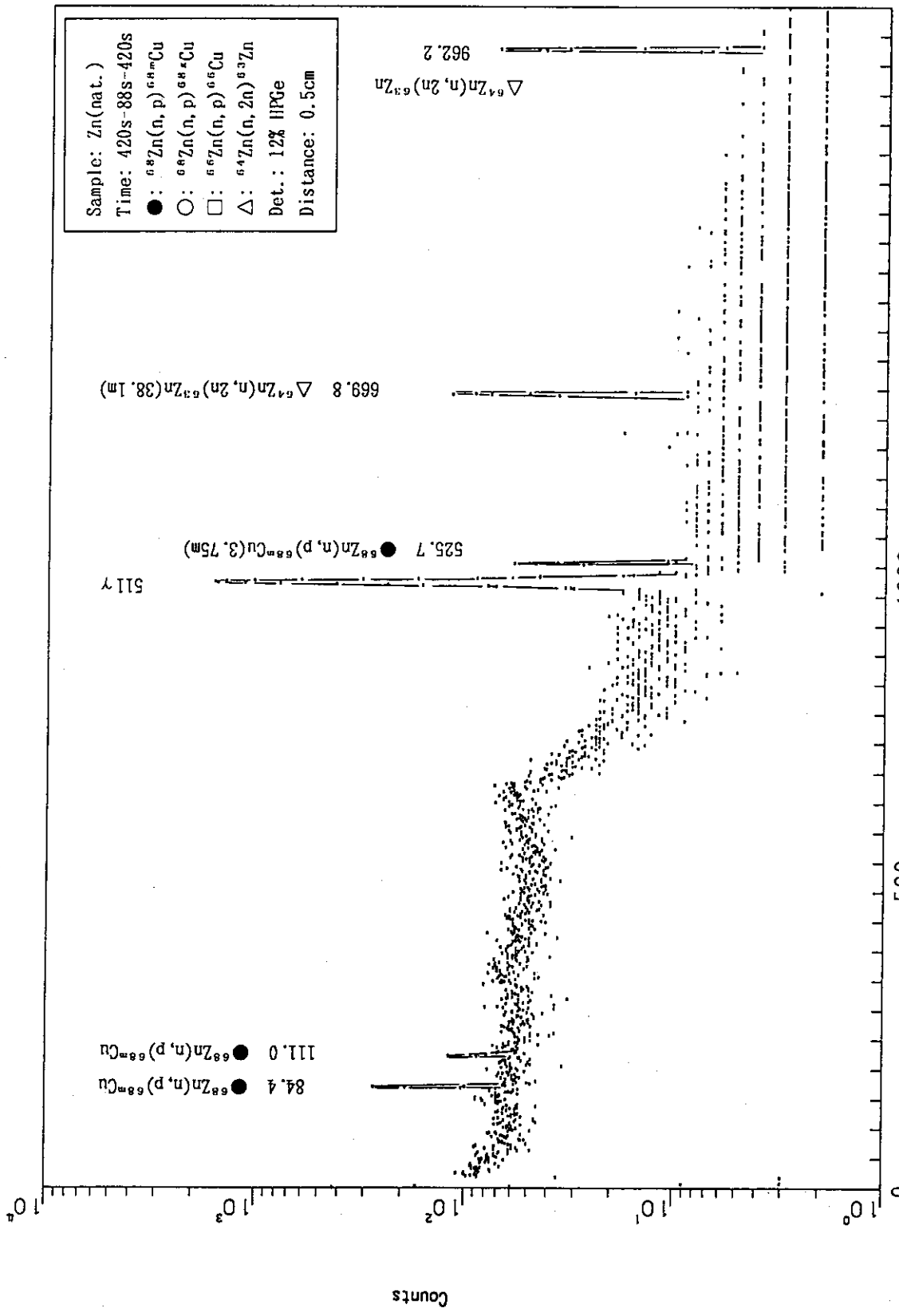
Sample: Zn(nat.)
Time: 420s-88s-420s
●: $^{68}Zn(n,p)^{68m}Cu$
○: $^{66}Zn(n,p)^{66}Cu$
□: $^{66}Zn(n,p)^{66}Cu$
△: $^{64}Zn(n,2n)^{63}Zn$
Det.: 12% HPGe
Distance: 0.5cm
962.2
△$^{64}Zn(n,2n)^{63}Zn$
669.8 △$^{64}Zn(n,2n)^{63}Zn(38.1m)$
525.7 ●$^{68}Zn(n,p)^{68m}Cu(3.75m)$
511γ
111.0 ●$^{68}Zn(n,p)^{68m}Cu$
84.4 ●$^{68}Zn(n,p)^{68m}Cu$
Counts
Channel Number

Fig. A.3.18

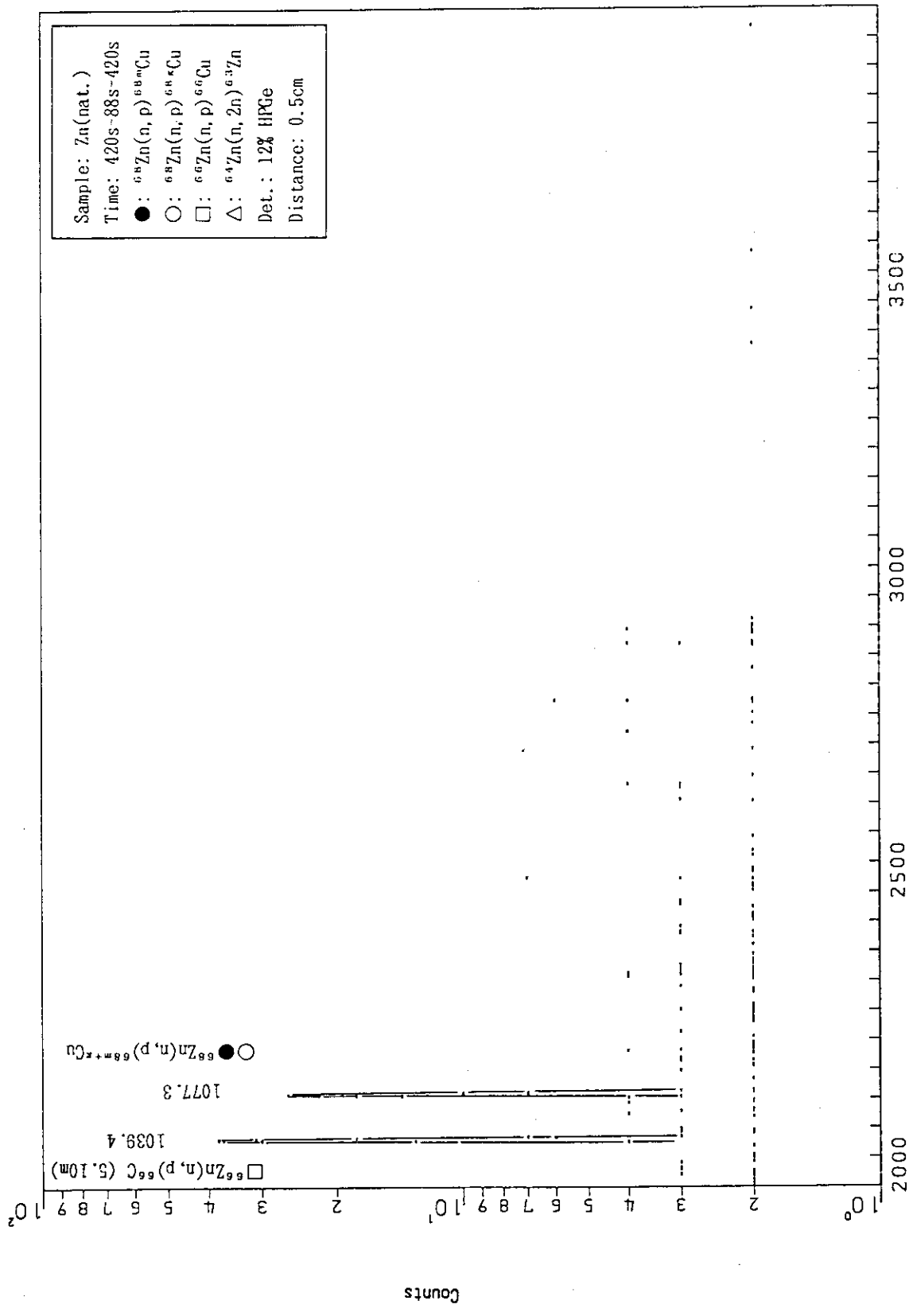
Sample: Zn(nat.)
Time: 420s-88s-420s
●: $^{68}Zn(n,p)^{68m}Cu$
○: $^{68}Zn(n,p)^{68+x}Cu$
□: $^{66}Zn(n,p)^{66}Cu$
△: $^{64}Zn(n,2n)^{63}Zn$
Det.: 12% HPGe
Distance: 0.5cm
□ $^{66}Zn(n,p)^{66}C$ (5.10m)
1039.4
1077.3
○● $^{68}Zn(n,p)^{68m+x}Cu$
Counts
Channel Number

Fig. A.3.19

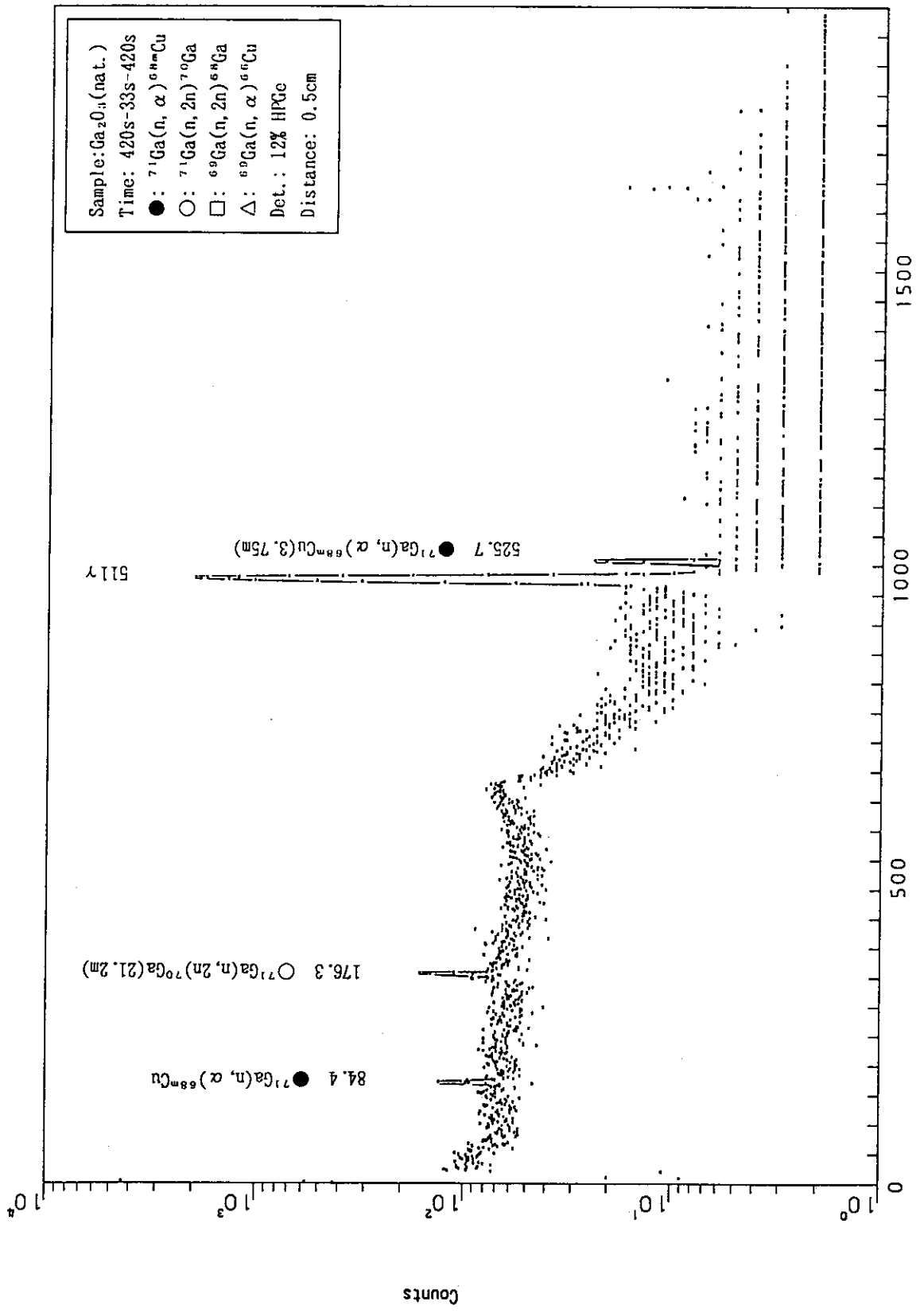
Sample:Ga2O3(nat.)
Time: 420s-33s-420s
●: 71Ga(n, α)68mCu
○: 71Ga(n, 2n)70Ga
□: 69Ga(n, 2n)68Ga
△: 69Ga(n, α)66Cu
Det.: 12% HPGe
Distance: 0.5cm
84.4 ●71Ga(n, α)68mCu
176.3 ○71Ga(n, 2n)70Ga(21.2m)
511γ
525.7 ●71Ga(n, α)68mCu(3.75m)
Counts
Channel Number
0
500
1000
1500

Fig. A.3.20

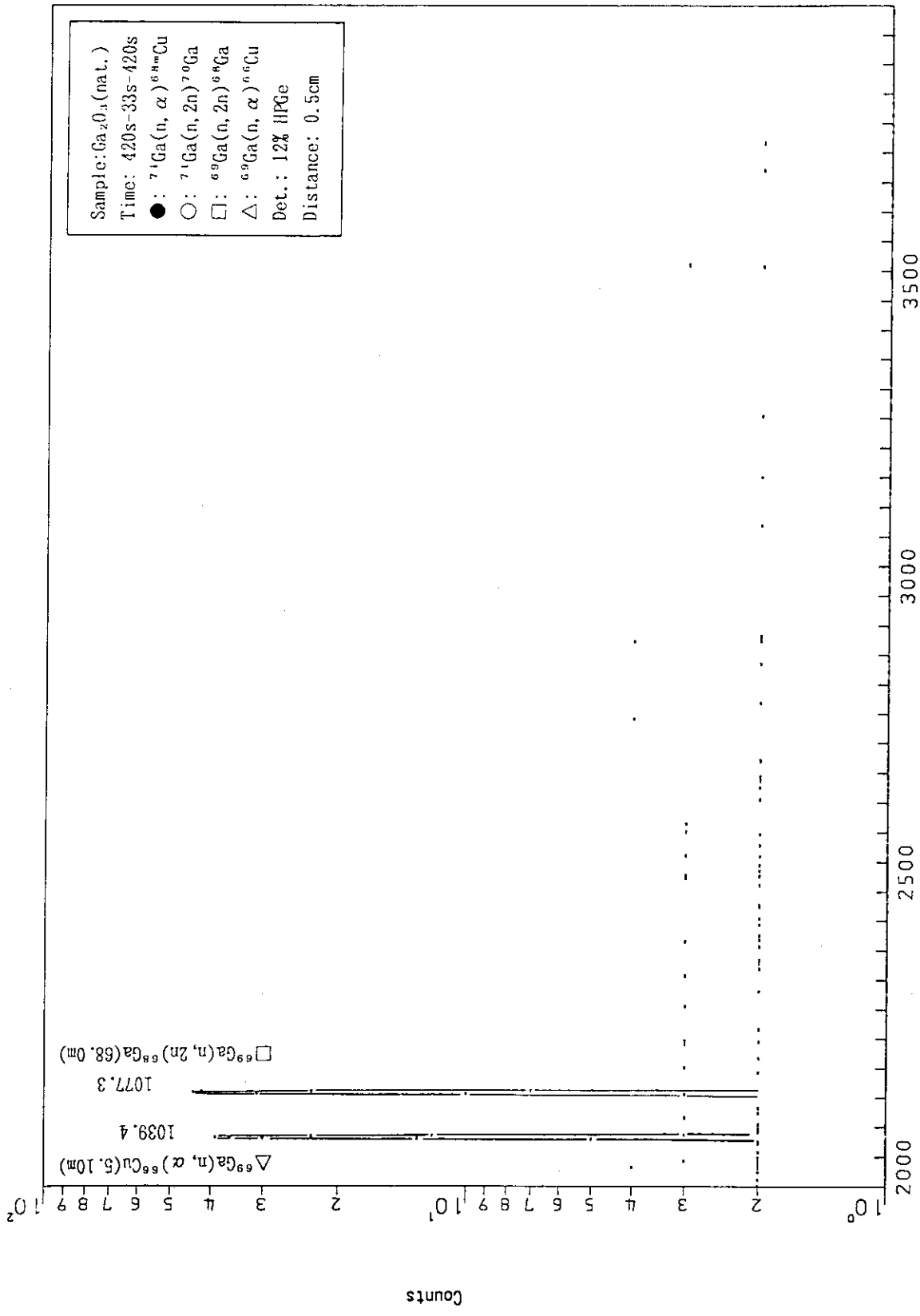
Sample: Ga_2O_3(nat.)
Time: 420s-33s-420s
●: $^{71}Ga(n,\alpha)^{68m}Cu$
○: $^{71}Ga(n,2n)^{70}Ga$
□: $^{69}Ga(n,2n)^{68}Ga$
△: $^{69}Ga(n,\alpha)^{66}Cu$
Det.: 12% HPGe
Distance: 0.5cm
△$^{69}Ga(n,\alpha)^{66}Cu(5.10m)$
1039.4
1077.3
□$^{69}Ga(n,2n)^{68}Ga(68.0m)$
Counts
Channel Number

Fig. A.3.21

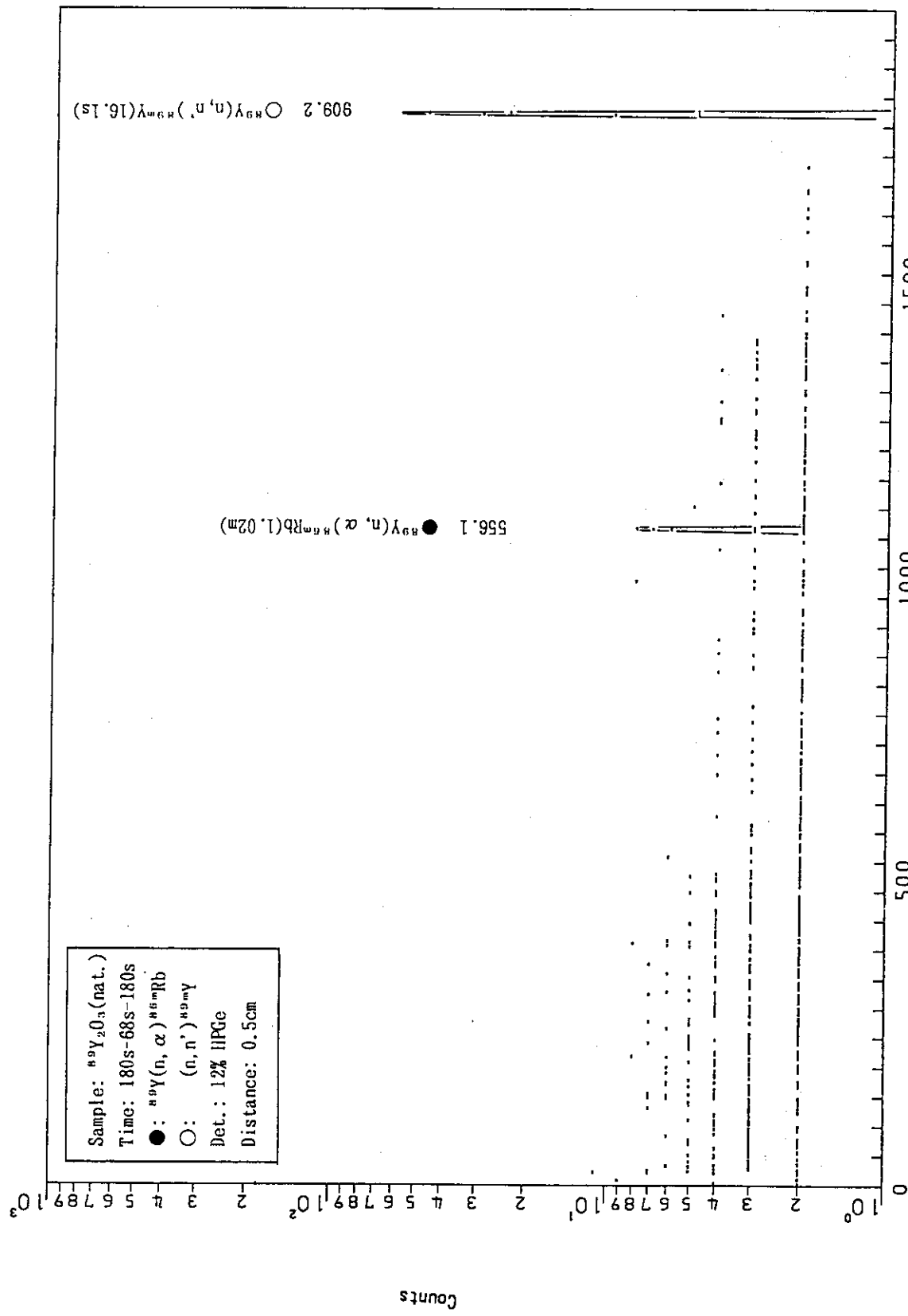
Sample: $^{89}Y_2O_3$(nat.)
Time: 180s-68s-180s
●: $^{89}Y(n,\alpha)^{86m}Rb$
○: $(n,n')^{89m}Y$
Det.: 12% HPGe
Distance: 0.5cm
556.1 ●$^{89}Y(n,\alpha)^{86m}Rb$(1.02m)
909.2 ○$^{89}Y(n,n')^{89m}Y$(16.1s)
Counts
Channel Number
0
500
1000
1500
10^0
10^1
10^2
10^3

Fig. A.3.22

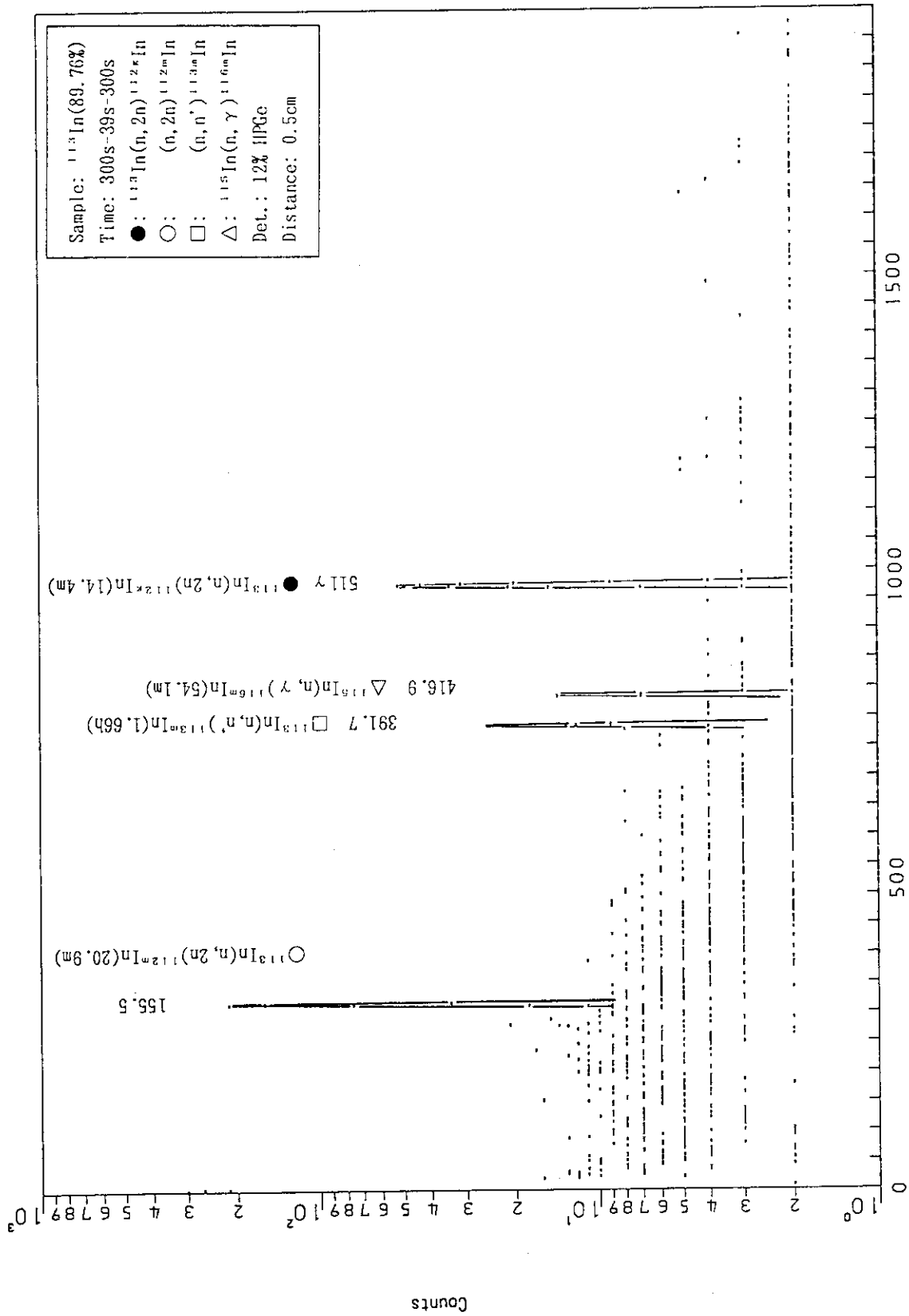
Sample: ^{113}In(89.76%)
Time: 300s-39s-300s
●: ^{113}In(n,2n)^{112*}In
○: (n,2n)^{112m}In
□: (n,n')^{113m}In
△: ^{115}In(n,γ)^{116m}In
Det.: 12% HPGe
Distance: 0.5cm
511γ ●^{113}In(n,2n)^{112*}In(14.4m)
416.9 △^{115}In(n,γ)^{116m}In(54.1m)
391.7 □^{113}In(n,n')^{113m}In(1.66h)
155.5
○^{113}In(n,2n)^{112m}In(20.9m)
Counts
Channel Number

Fig. A.3.23

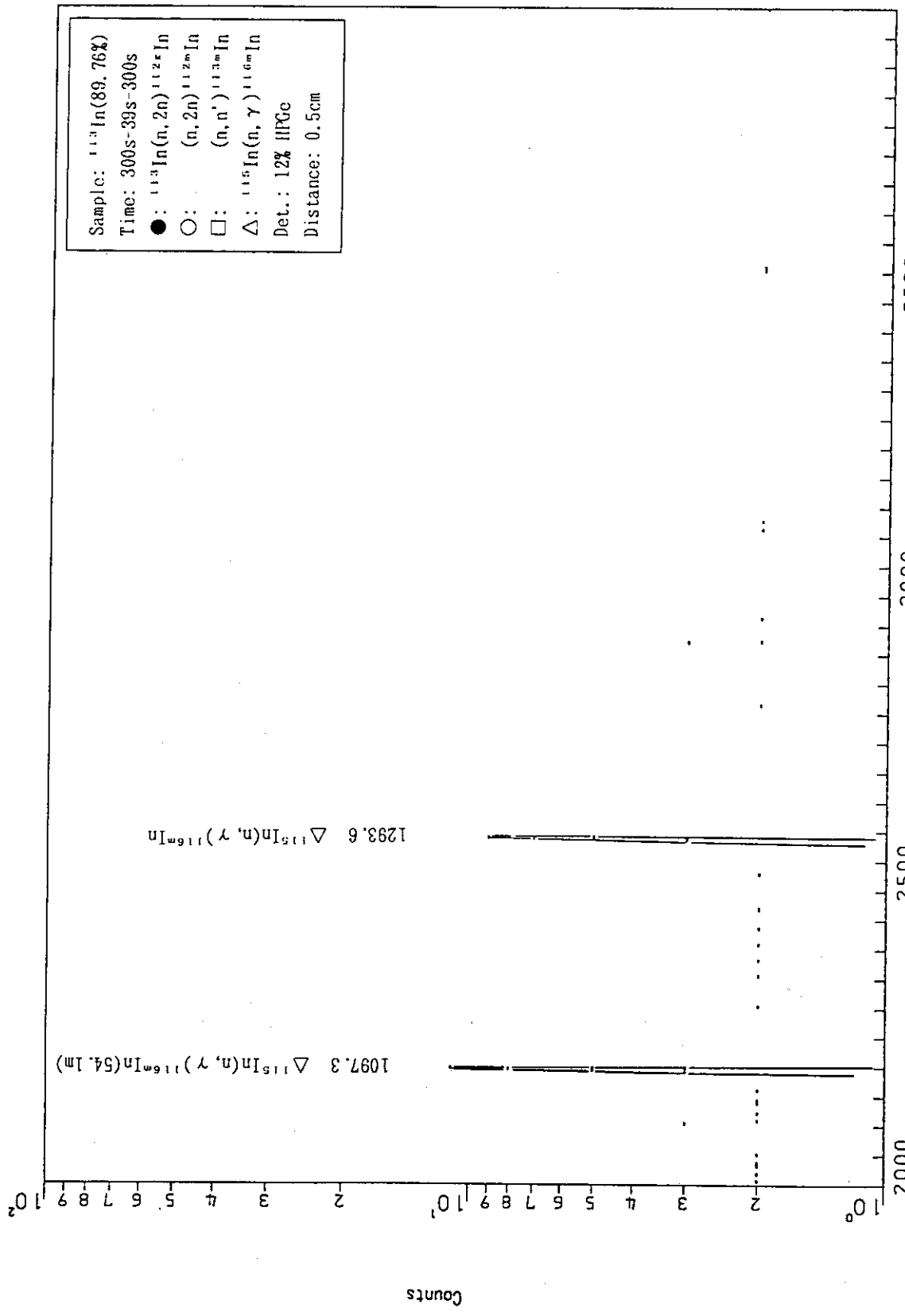
Sample: ^{113}In(89.76%)
Time: 300s-39s-300s
●: ^{113}In(n,2n)^{112g}In
○: (n,2n)^{112m}In
□: (n,n')^{113m}In
△: ^{115}In(n,γ)^{116m}In
Det.: 12% HPGe
Distance: 0.5cm
1097.3 △^{115}In(n,γ)^{116m}In(54.1m)
1293.6 △^{115}In(n,γ)^{116m}In
Counts
Channel Number

Fig. A.3.24

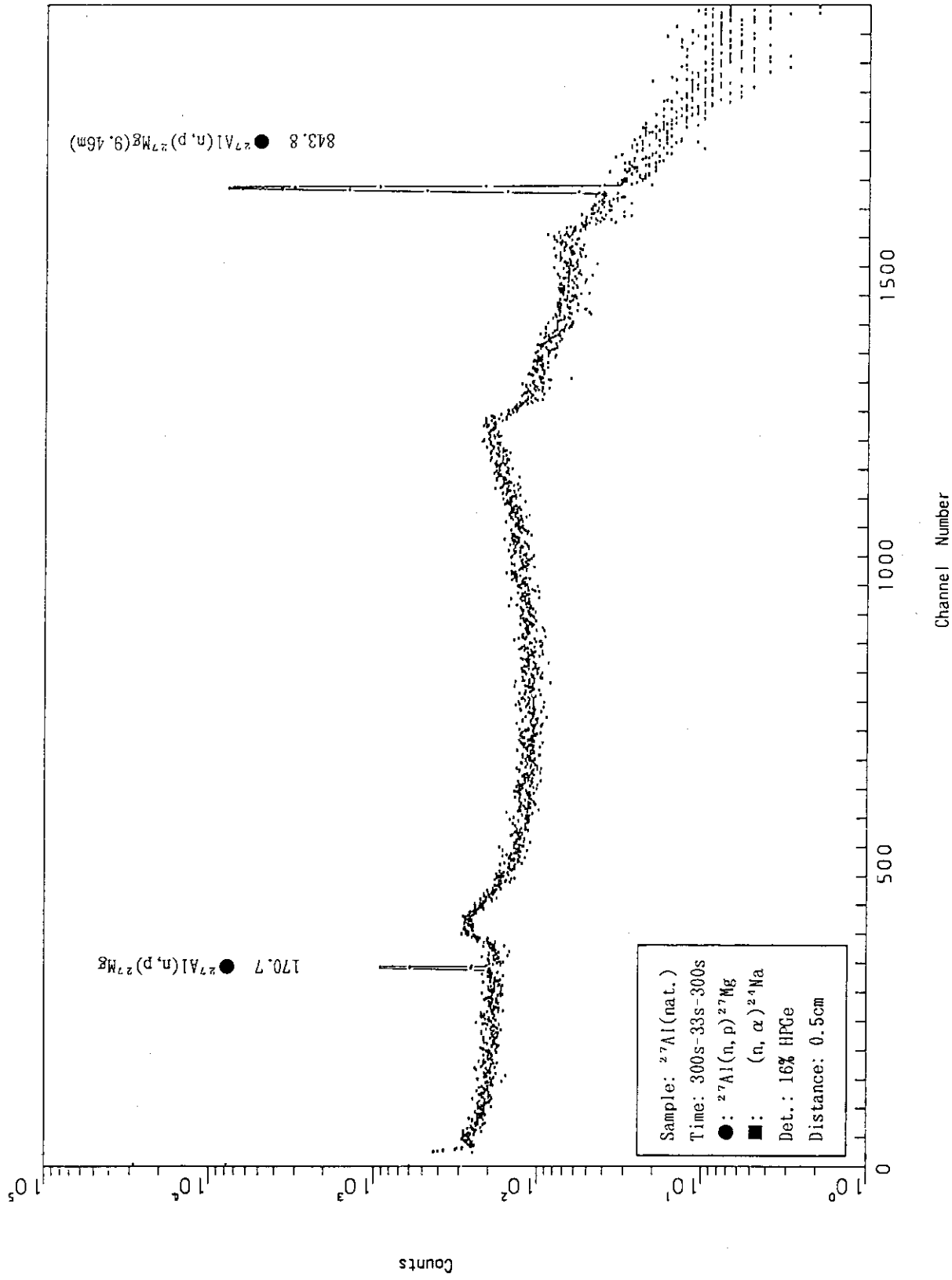
Counts
Channel Number
Sample: ^{27}Al(nat.)
Time: 300s-33s-300s
●: ^{27}Al(n,p)^{27}Mg
■: (n,α)^{24}Na
Det.: 16% HPGe
Distance: 0.5cm
170.7 ●^{27}Al(n,p)^{27}Mg
843.8 ●^{27}Al(n,p)^{27}Mg(9.45m)

Fig. A.3.25

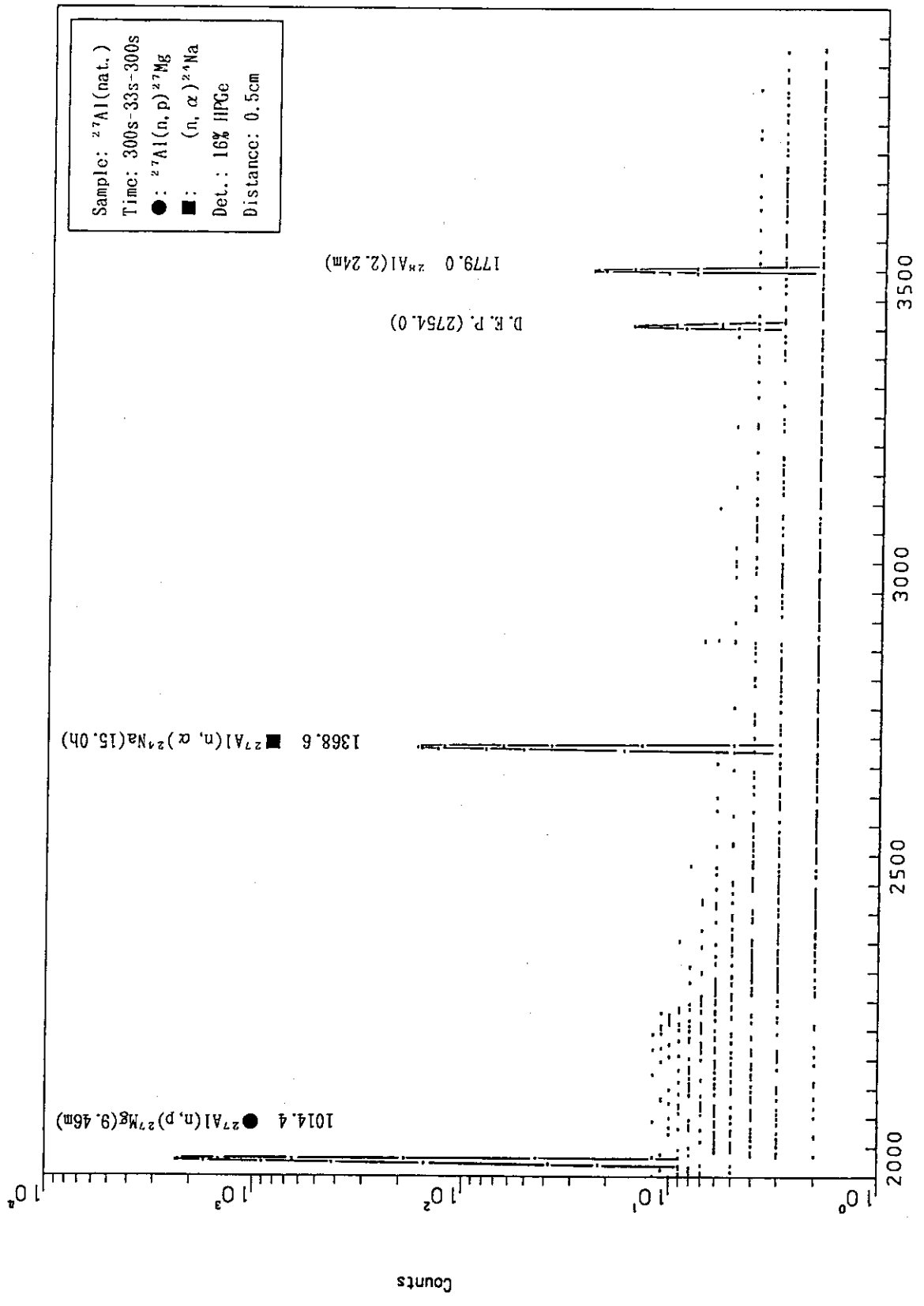
Sample: ^{27}Al(nat.)
Time: 300s-33s-300s
●: ^{27}Al(n,p)^{27}Mg
■: (n,α)^{24}Na
Det.: 16% HPGe
Distance: 0.5cm
1014.4 ●^{27}Al(n,p)^{27}Mg(9.46m)
1368.6 ■^{27}Al(n,α)^{24}Na(15.0h)
D.E.P.(2754.0)
1779.0 ^{28}Al(2.24m)
Counts
Channel Number

Fig. A.3.26

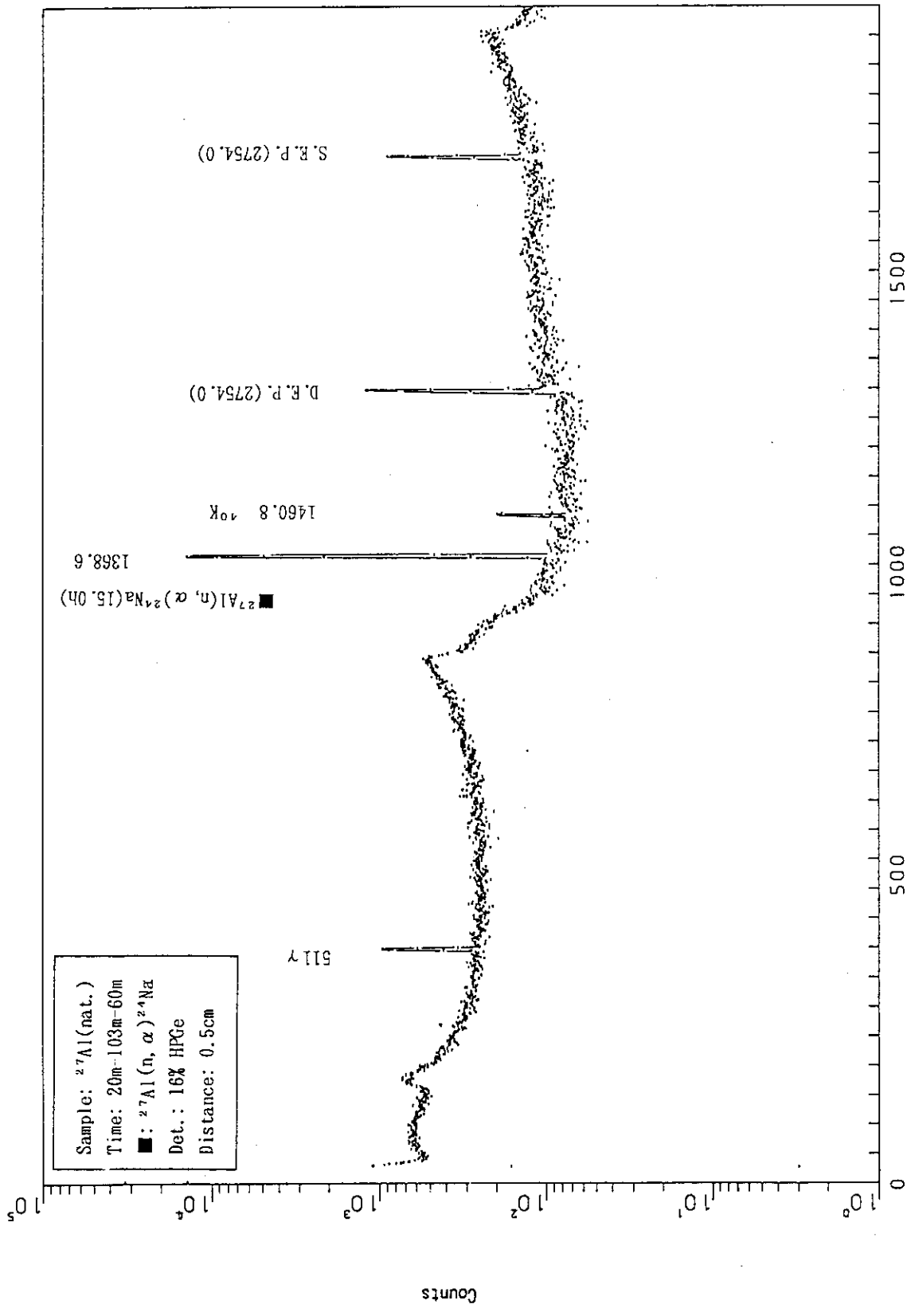
Sample: ^{27}Al(nat.)
Time: 20m-103m-60m
■: ^{27}Al(n, α)^{24}Na
Det.: 16% HPGe
Distance: 0.5cm
511 γ
■^{27}Al(n, α)^{24}Na(15.0h)
1368.6
1460.8 ^{40}K
D.E.P.(2754.0)
S.E.P.(2754.0)
Counts
Channel Number
0
500
1000
1500
10^0
10^1
10^2
10^3
10^4
10^5

Fig. A.3.27

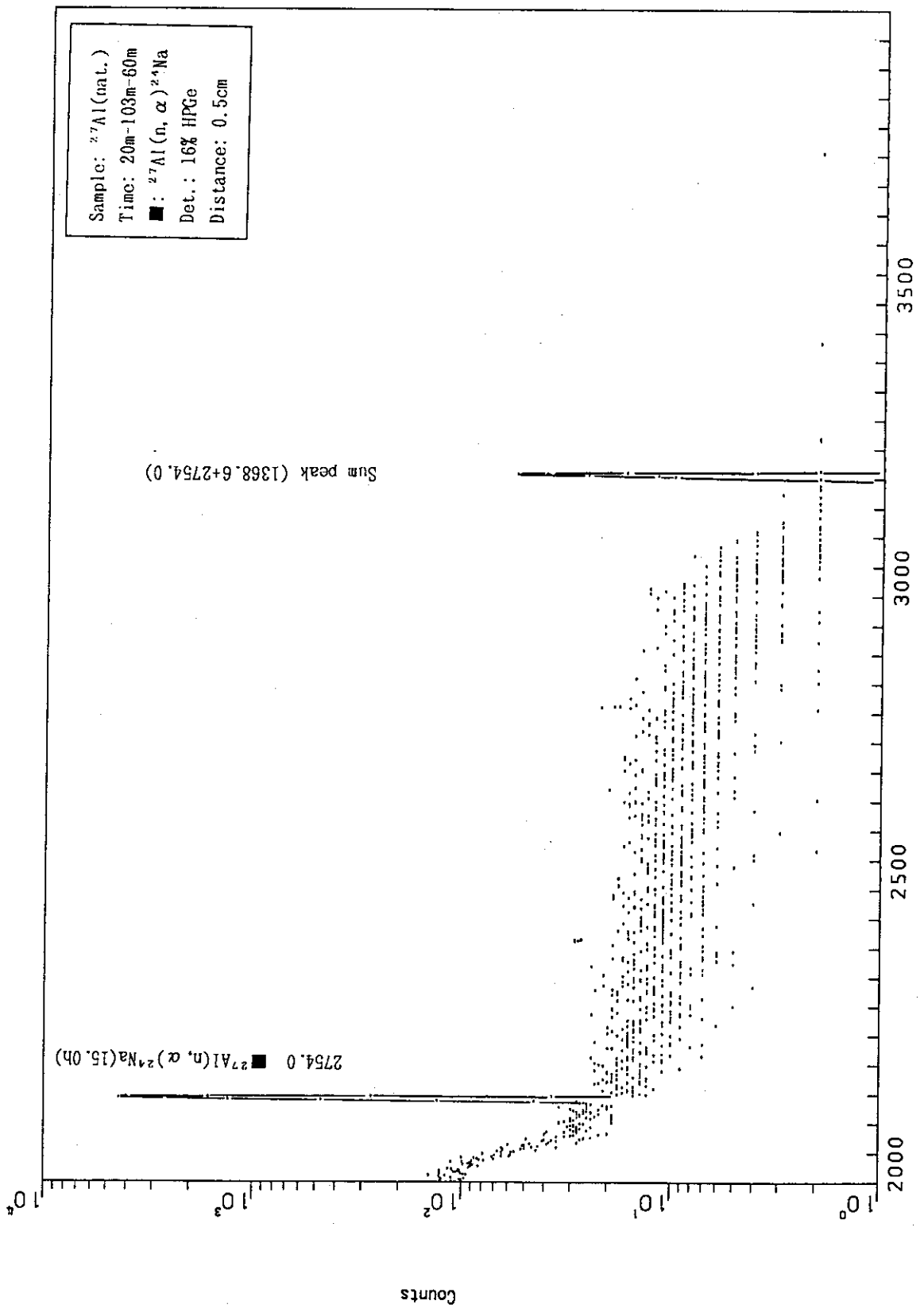
Sample: ^{27}Al(nat.)
Time: 20m-103m-60m
■: ^{27}Al(n, α)^{24}Na
Det.: 16% HPGe
Distance: 0.5cm
Sum peak (1368.6+2754.0)
2754.0 ■^{27}Al(n, α)^{24}Na(15.0h)
Counts
Channel Number

Fig. A.3.28

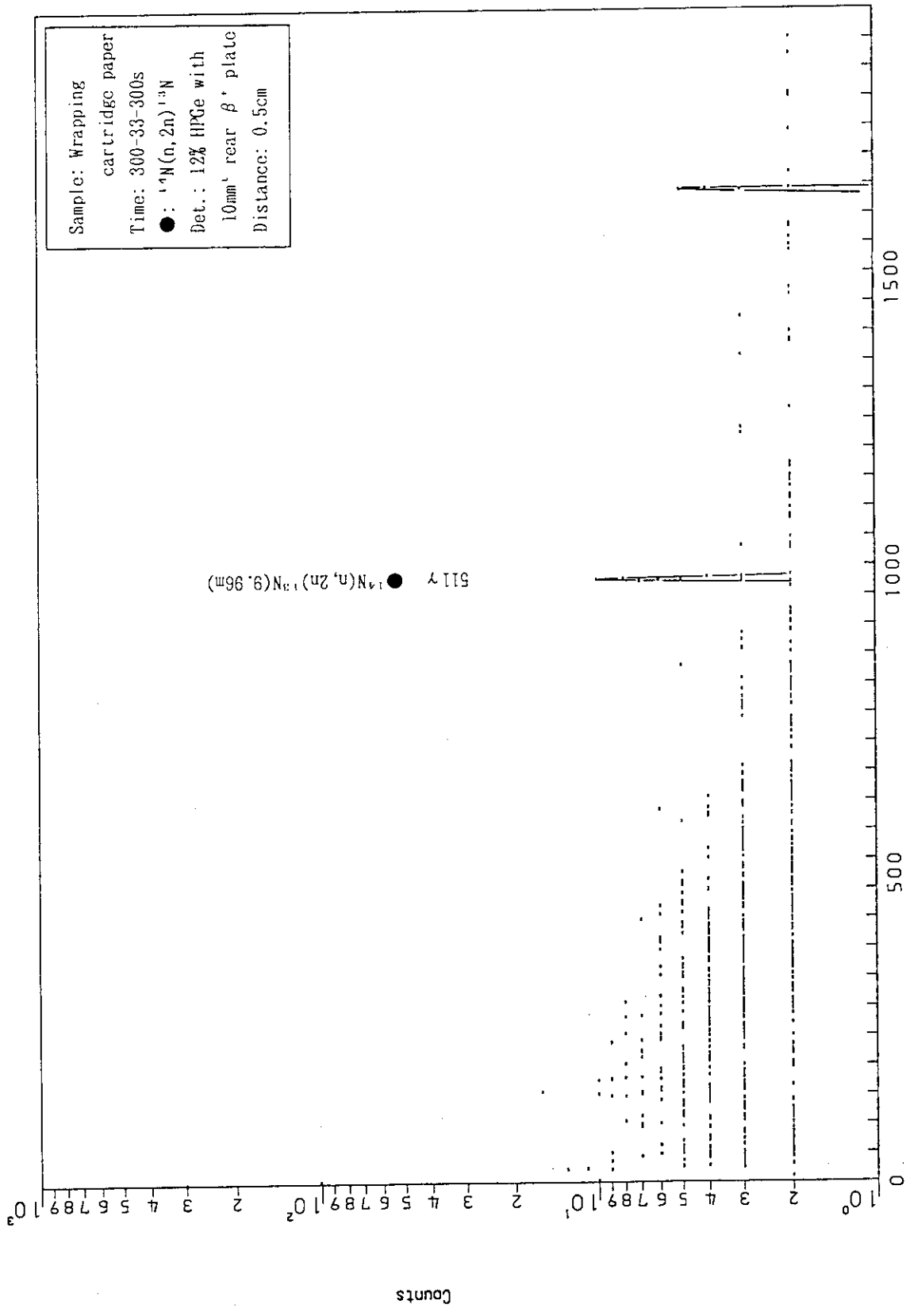
Sample: Wrapping
cartridge paper
Time: 300-33-300s
●: $^{14}N(n,2n)^{13}N$
Det.: 12% HPGe with
10mm' rear β' plate
Distance: 0.5cm
511γ
●$^{14}N(n,2n)^{13}N(9.98m)$
Counts
Channel Number
0
500
1000
1500
10^0
10^1
10^2
10^3

Fig. A.3.29

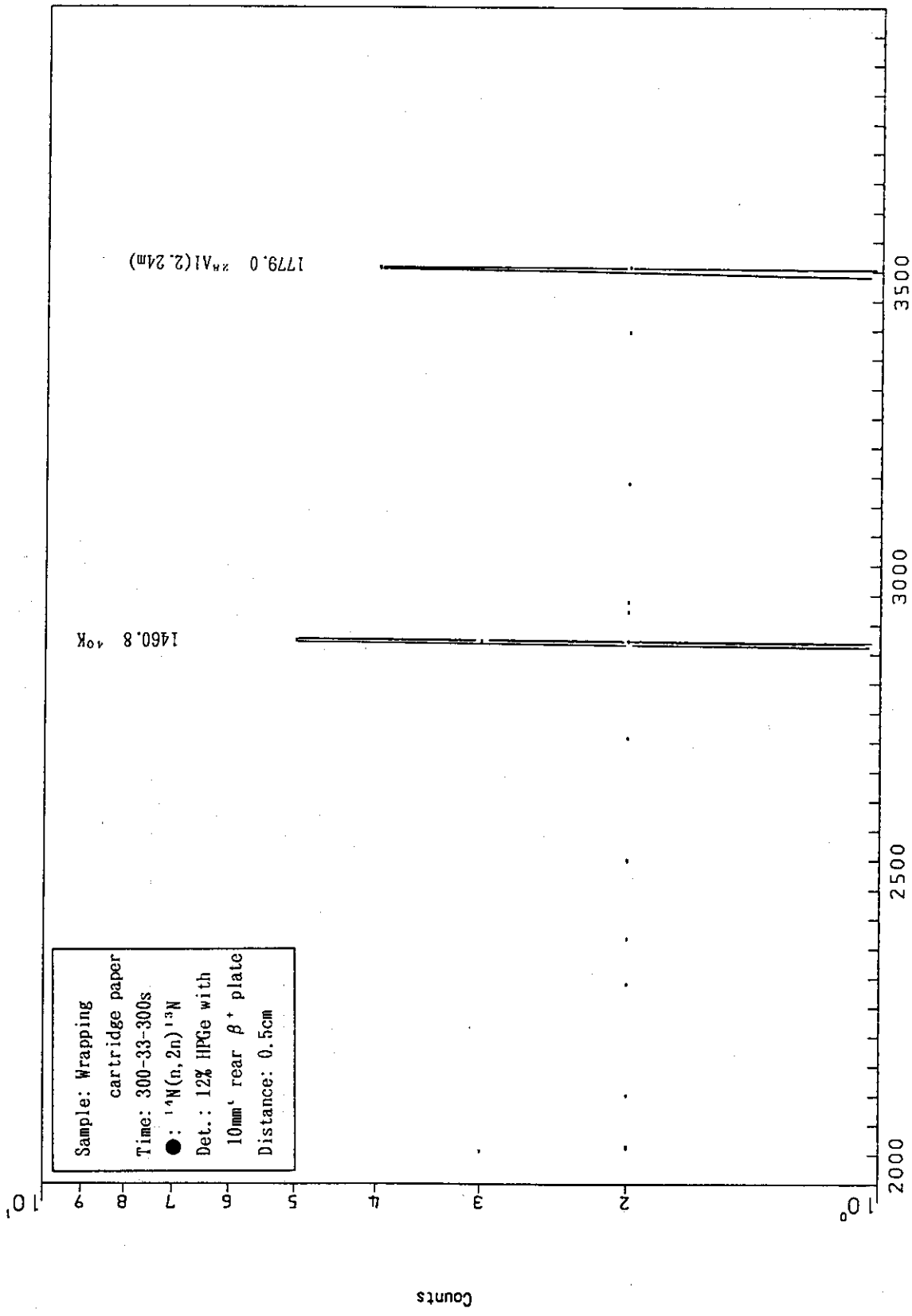
Sample: Wrapping
cartridge paper
Time: 300-33-300s
●: $^{14}N(n,2n)^{13}N$
Det.: 12% HPGe with
10mm' rear β^+ plate
Distance: 0.5cm
1460.8 ^{40}K
1779.0 $^{28}Al(2.24m)$
Counts
Channel Number

Fig. A.3.30